Nanoscale Probing of Modified Surfaces with Surface Plasmons

A Dissertation Presented for the

Doctor of Philosophy

Degree

The University of Tennessee, Knoxville

Vineet Kumar Khullar

August 2019

© by Vineet Kumar Khullar, 2019
All Rights Reserved.

To my family members

for their

support and encouragement

Acknowledgments

I would like to thank my advisors Dr. Gong Gu and Dr. Thomas Ferrell for their continuous support, I appreciate all their contributions of time and ideas. Besides my advisors, I would like to thank Dr. Ali Passian for his encouragement, insightful comments and hard questions.

I gratefully thank rest of my committee members Dr. Aly Fathy and Dr. Nicole McFarlane for their support. I appreciate members of Gu group who have been very kind and helpful at all times.

I acknowledge technical support of Mr. Mark Smith from AFM Services Inc. to help in customizing and troubleshooting the apparatus. Also, Mr. David Burkhead from Advanced Surface Microscopy Inc. helped in creating the software backup and installation. My acknowledgement would be incomplete without thanking Dr. John Dunlap (facility manager) at microscopy center in University of Tennessee (Knoxville), he was readily available to help users at all times.

Abstract

A material can be uniquely identified by its optical properties. Based on this principle, the Kretschmann configuration is widely used in chemical analysis to identify materials by determining optical properties of the sample material upon surface plasmon resonance. This conventional approach measures average optical properties within the diffraction-limited illumination beam spot, therefore is incapable of identifying or mapping samples that are inhomogeneous on the nanometer scale. On the other hand, near-field optical microscopy is capable of nanoscale imaging but quantitative optical property maps cannot be inferred from the obtained images. This work demonstrates the principles of surface plasmon scanning tunneling microscopy (SPSTM), a new method to map the optical properties of a material at the nanometer scale, thus providing the foundation of a novel approach towards nanoscale chemical mapping. In this demonstration of principles, surface plasmons are excited in a gold thin film that supports micrometer-size flakes of a two-dimensional (2D) layered material in some areas. The surface plamons are coupled to a gold-coated, nanometer-sized optical fiber tip, and the resulting optical signal is guided by the fiber to a detector. The nanoscale imaging capability stems from the exponential decay of the evanescent field of surface plasmon modes, resulting in the exponential decrease in plasmon coupling as the tip-substrate separation increases, as well as the sharpness of the probe tip. By fabricating Au-coated, sharp optical fiber tips and constructing an SPSTM setup, I have demonstrated exponential decrease in optical signal intensity with increasing probe height, with faster decay in the presence the 2D material flakes than on bare Au, consistent with theoretical prediction, laying down the groundwork for a future SPSTM prototype.

Table of Contents

1 Introduction **1**

1.1 Background . . . 1

1.1.1 History of Optical Microscopes . . . 1

1.1.2 Different Forms of Optical Microscopes . . . 2

1.1.3 Different Forms of Electron Microscopes . . . 3

1.1.4 Measurement of Optical Properties . . . 7

1.1.5 Ellipsometer . . . 8

1.2 Scanning Probe Microscopes (SPM) . . . 9

1.2.1 History of SPM . . . 9

1.2.2 Resolving Power of SPMs . . . 9

1.2.3 Types of SPMs . . . 11

1.3 Surface Plasmon Scanning Tunneling Microscope . . . 14

1.3.1 Motivation . . . 14

1.3.2 Operating Concept . . . 15

1.3.3 SPSTM Resolution . . . 18

1.3.4 SPSTM Spectroscopy . . . 19

1.3.5 SPSTM Compatible Samples . . . 20

2 Theory **21**

2.1 Overview . . . 21

2.2 Maxwell's Equations . . . 22

2.3 Boundary Conditions . . . 23

2.3.1 Boundary Conditions for Electric Field . . . 23

2.3.2 Boundary Condition for Magnetic Field . . . 24
2.4 Fresnel Equations . . . 25
2.4.1 S-Polarized Light . . . 25
2.4.2 P-Polarized Light . . . 27
2.4.3 Implications of Fresnel coefficients for an Air-Glass Interface . . . 28
2.4.4 Fresnel Coefficients for an Glass-Air Interface . . . 29
2.5 Interpretation of Signal Intensity . . . 30
2.5.1 Quantitative representation . . . 30
2.5.2 Interpretation of SPSTM Images . . . 31
2.5.3 Tip to Sample Distance Control . . . 32
2.6 Field Enhancement . . . 33

3 Design and construction of SPSTM 34
3.1 SPSTM: Apparatus and Design . . . 34
3.2 Fabrication of Plasmonic Probe . . . 39
3.3 Laser for Exciting Surface Plasmons . . . 42
3.4 Microscope Head . . . 45
3.4.1 Scanner head construction . . . 45
3.4.2 Nanoscope IIIA Controller . . . 49
3.5 Signal Detection Assembly . . . 50
3.5.1 Photomultiplier tube . . . 50
3.5.2 Current to Voltage Amplifier . . . 53
3.6 Apparatus Check: Step by step process to run Nanoscope Software . . . 55
3.7 Sample Preparation . . . 58
3.7.1 Gold film deposition by sputtering . . . 58
3.7.2 Plasma Glow Discharge . . . 59
3.7.3 MoS_2 Exfoliation and Transfer over Gold Film . . . 61

4 Results and Discussion 63
4.1 Plasmonic Probe tips . . . 63
4.2 Sample Flakes: Optical and AFM images . . . 69

4.3 Exponential Dependence of Probe Signal Intensity on Probe Height 72
4.4 Discussion 74

Bibliography **75**

Appendices **80**

Appendix A Tip Fabrication by Meniscus Etching **81**

Appendix B PMT Casing **84**

Appendix C Nanoscope Pin Connections **86**

Appendix D Optical Fiber Holder **90**

Appendix E Nanoscope Cards **92**

Appendix F Scanner Head Macor Drawings **94**

Vita **97**

List of Figures

1.1 Bright field vs phase contrast image 3
1.2 Working principle of confocal microscope. Source: www.sciencedirect.com . . 4
1.3 Schematic of Optical microscope, TEM and SEM 6
1.4 Ellipsometer schematic. Source: www.wikipedia.org 8
1.5 Comparison of resolving power of existing imaging modalities. Source: Zeiss microscopy website 10
1.6 Different forms of SPMs 12
1.7 Frustrated Total Internal Reflection(FTIR) 15
1.8 SPSTM operating concept 17
1.9 SPSTM spectroscopic setup 19

2.1 Interface of two dielectric mediums 23
2.2 Enclosed surface at the interface with zero net charge 24
2.3 Loop at the interface with infinitesimal small area 25
2.4 S-polarized electromagnetic wave at an interface 26
2.5 Fresnel reflection coefficient for air-glass interface 28
2.6 Fresnel reflection coefficient for glass-air interface 29
2.7 Field enhancement 33

3.1 SPSTM Schematic 35
3.2 Optical elements of SPSTM in Kretschmann configuration 37
3.3 Scanner head 38
3.4 Corning 50/125 multimode optical fiber configuration 39
3.5 Jonard JIC-375 optical fiber stripping tool 39

3.6 P-2000 Micropipette puller schematic. Source: Sutter Instruments 40
3.7 JDSU 1100 series HeNe laser and power supply 42
3.8 S and P polarization 43
3.9 Kretschmann configuration 44
3.10 Surface Plasmon Resonance angle (θ_{sp}) 44
3.11 Possible orientation of piezoelectric crystal domains 46
3.12 Piezoelectric tubes in scanner head 47
3.13 XY piezoelectric tube 48
3.14 Scan modes: a) Constant current mode b) Constant height mode 49
3.15 Photomultiplier tube schematic. Source: www.hamamatsu.com 51
3.16 Photomultiplier tube IP28 51
3.17 Current to voltage amplifier 54
3.18 Current to voltage amplifier schematic for higher sensitivity 55
3.19 Home page of nanoscope software 56
3.20 Signal strength vs distance plot 57
3.21 A test image of bare prism surface 58
3.22 RF sputtering schematic 60
3.23 MoS_2 exfoliation using Nitto tape. Source: Slideshare.net/mechanical exfoliation 62

4.1 An optical image of metal coated tip: geometry 1 64
4.2 An optical image of metal coated tip: geometry 2 65
4.3 An optical image of metal coated tip: geometry 3 65
4.4 An optical image of metal coated tip: geometry 4 66
4.5 Fiber holder for SEM 66
4.6 SEM image of the metal coated tip: view 1 67
4.7 SEM image of the metal coated tip: view 2 67
4.8 SEM image of the metal coated tip in metallic holder 68
4.9 Optical image of MoS_2 flake 1 69
4.10 An AFM scan of MoS_2 flake 1: Area 1 70

4.11 An AFM scan of MoS_2 flake 1: Area 2 70
4.12 An AFM scan of MoS_2 flake 2: Area 1 71
4.13 An AFM scan of MoS_2 flake 2: Area 2 71
4.14 Decaying surface plasmons over modified surfaces: Modified by MoS_2 73
4.15 Log plot of exponential region 73

A.1 HF etching setup 82
A.2 Meniscus etching. Source: www.researchgate.net 83

B.1 PMT casing 85
B.2 PMT power supply socket 85

C.1 37 pin connector on Nanoscope controller 86
C.2 Nanoscope front panel: pin connections for microscope 87
C.3 Nanoscope rear panel: slot for computer cable 87
C.4 37 pin connector: pin labels 88
C.5 Top view of center macor and interface pins embedded within 89

D.1 Fiber holder for coating 91

E.1 xy cards 92
E.2 z card 93
E.3 P88 high voltage low current power amplifier in NS xy and z cards 93

F.1 Center macor 94
F.2 Nose cone 95
F.3 Ring holder 96

Chapter 1

Introduction

1.1 Background

1.1.1 History of Optical Microscopes

Lenses for simple optical magnification were being produced long before sixteenth century. Microscopes with multiple lenses started appearing in sixteenth century but they had poor performance because of enhanced distortions due to multiple lens, where distortions got compounded. It was Anton van Leeuwenhoek (1623-1723) [39] who designed a microscope with better resolution and least distortion. Primary reason being that he used a single lens that was powerful enough to provide detailed amplified images. His idea was accepted by Biologists who were widely using microscopes at that time. Hence, Anton van Leeuwenhoek is known as the father of microscopy.

Compound microscopes [13] have been around for centuries and several technological limitation arising from lens design, beam alignment, optical abberations etc. have now been resolved due to advances in technology but still best optical microscopes are limited by their resolution (about 200 nm) due to a fundamental principal called 'Abbe diffraction limit' [8] which defines the nearest distance by which two objects can be identified when examined by an optical system and this distance d is defined as

$$d = \frac{\lambda}{2 \times \mathrm{NA}} \tag{1.1}$$

As defined in above equation, this distance or diffraction limit depends on the numerical aperture of an optical system (NA) and the wavelength (λ) of the light being used. If we use oil as a medium [26] and green light to illuminate a sample then best possible resolution would be

$$d = \frac{532 \text{ nm}}{2 \times 1.5} = 200 \text{ nm} \tag{1.2}$$

1.1.2 Different Forms of Optical Microscopes

As light passes through a sample [21] it gets reflected, refracted, transmitted, scattered, absorbed or phase shifted. In order to view a magnified image of an object with high resolution, one or combination of the above signatures are used. Some forms of technique might also involve modifying the sample itself so as to get more information about it e.g. making sample fluorescent. Brightfield, phase shifted and fluorescent microscopy are some of the most commonly used techniques.

Brightfield microscopes [30] are based on a simple phenomenon of light absorption and works on the principle that areas in a sample having varying optical intensity will have varying light absorption i.e. areas that absorb more light will appear darker than the one absorbing less light. This method work for some materials which have varying optical density but fails for the samples with uniform optical density.

Light also shifts in phase [20] when passing through a material. In phase contrast microscopes (Figure 1.1) this technique was used to image the samples as phase contrast microscopes can measure shift in phase after light passes through a sample. This method helped to overcome limitation of brightfield microscopes which failed to provide good contrast in case of samples with uniform optical density.

Another imaging methodology used is based on Fluorescence where material is excited by a light of specific wavelength, after absorbing that light specimen emits light of a longer wavelength. In fluorescence microscope [22] magnified image is produced by the emission of a secondary light of longer wavelength. It is important to separate secondary light from the primary light as sample information for imaging is present in fluorescent light.

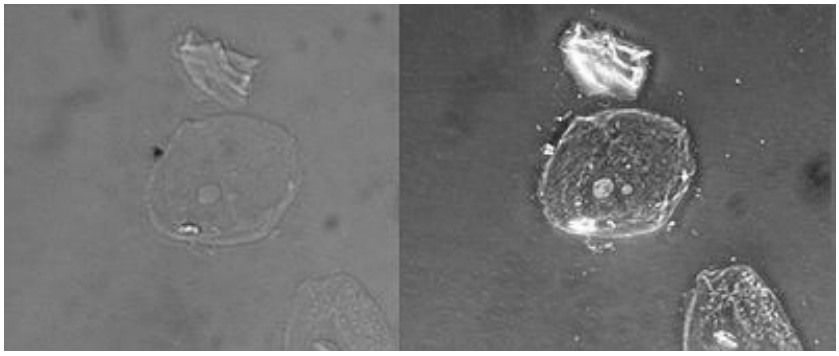

Figure 1.1: Bright field vs phase contrast image

Confocal Microscopy [36] is another imaging methodology where Abbe limit can be transcended and it helps to see fine structure of three dimensional samples. In this case field of illumination and depth of sample detection are restricted using pair of pinholes (Figure 1.2). Size of first pinhole aperture restricts illumination of sample and second pinhole placed in front of detector restricts light reaching the detector to only the focal plane. Hence, image with desired field of view can be created, raster scan is performed to get composite image.

1.1.3 Different Forms of Electron Microscopes

Light waves are commonly used for imaging, electrons also have a wave nature associated with them as they exhibit wave particle duality. Wavelength associated with electrons depends on the energy of the electrons i.e. it depends on the accelerating voltage used to accelerate electrons. This relationship between wavelength (λ) and momentum (p) of electrons (as electrons accelerate) is known as DeBroglie relationship

$$\lambda = \frac{h}{p} = \frac{h}{2 \times m \times e \times V} \tag{1.3}$$

where

h = Planck's constant (6.626×10^{-34} Joule second)

p = momentum of the particle

m = mass of electron (9.1×10^{-31} Kg)

e = charge on electron (1.6×10^{-19} C)

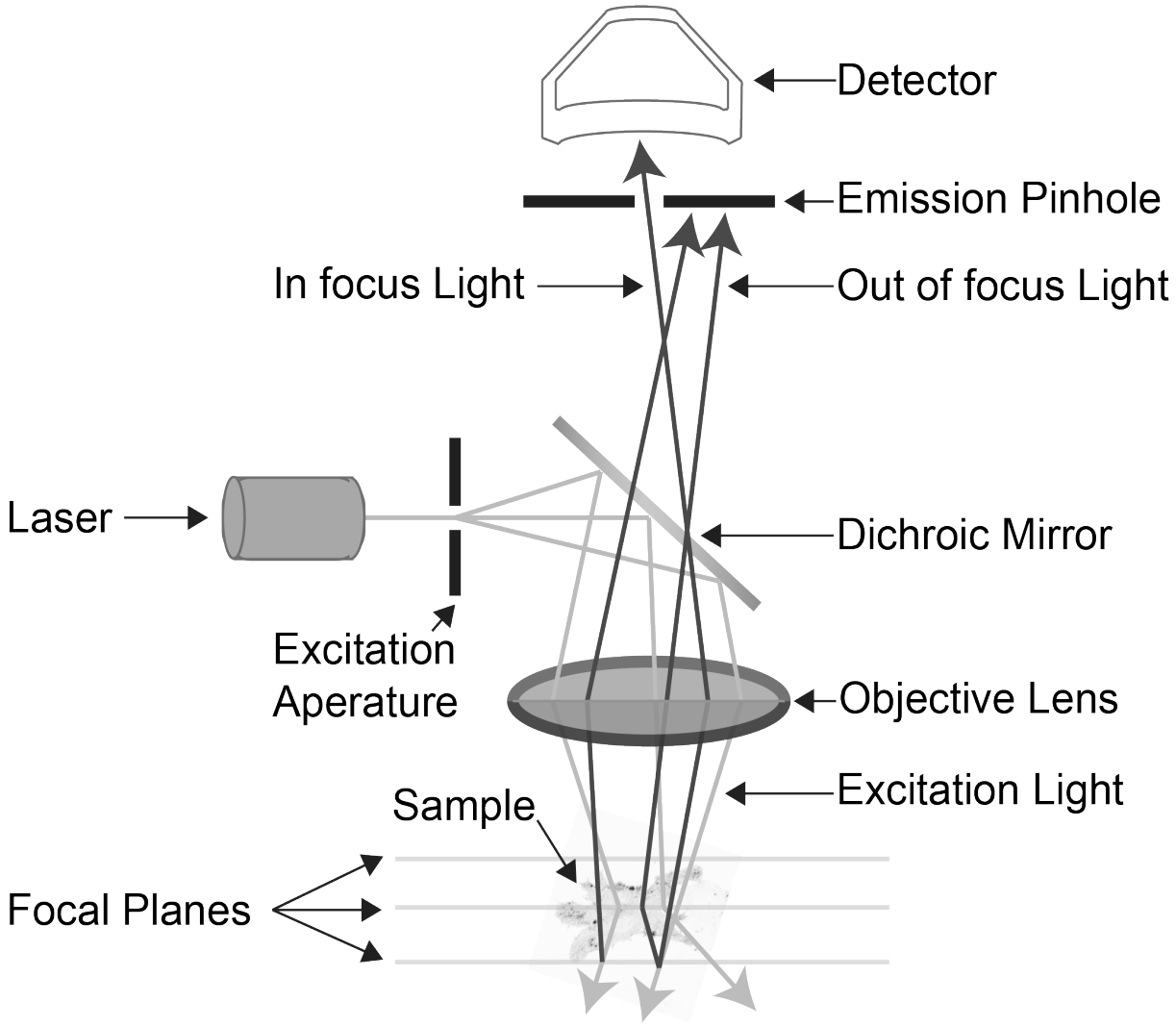

Figure 1.2: Working principle of confocal microscope. Source: www.sciencedirect.com

V = accelerating potential

If an electron microscope operates at 100 keV then wavelength (λ) of electron is 3.88 picometers.

As we know that lower is the λ of light (or particle) used for imaging, higher will be the resolution of a microscope. Since accelerated electrons can have λ much smaller than that of visible light, electrons are widely used for high resolution imaging.

Electron microscopes [16] can be broadly split in two categories, scanning electron microscopes (SEM) and transmission electron microscopes (TEM) (Figure 1.3). These have an electron gun that acts as a source of electrons which are then accelerated to form a beam. Similar to optical lenses in optical microscope there are electromagnetic lenses which are used to focus and direct electron beam to a specific path. SEM [35] for example detects secondary electrons emitted by a sample, number secondary electrons emitted depends upon topography of the sample, its physical and chemical properties. Primary electron beam scans sample in a raster scan mode and an image is formed depending upon intensity of the signal at various positions over sample. Scanning electron microscopes can achieve resolution better than 1 nm. SEM is mainly used to obtain high resolution images of an electrically conductive surface and can perform some crude spectroscopy.

As opposed to SEM where electron beam scans scans a sample, in TEM [45] there is a static beam being focused on a thin sample. Transmitted electron beam is focused by electromagnetic lenses onto sample and is then projected on a phosphor screen or a charged coupled device (CCD). TEM is mainly used to obtain material structure of a sample e.g crystal structure, structures like dislocations, grain boundaries etc. A TEM sample must be thin enough to allow electrons to pass with least energy loss hence, special sample preparation techniques are used to thin down sample. Electron microscopes usually requires high vacuum to operate which introduces some limitations on type of samples than can be used e.g. it will be very challenging to image biological samples in high vacuum sue to presence of high water content.

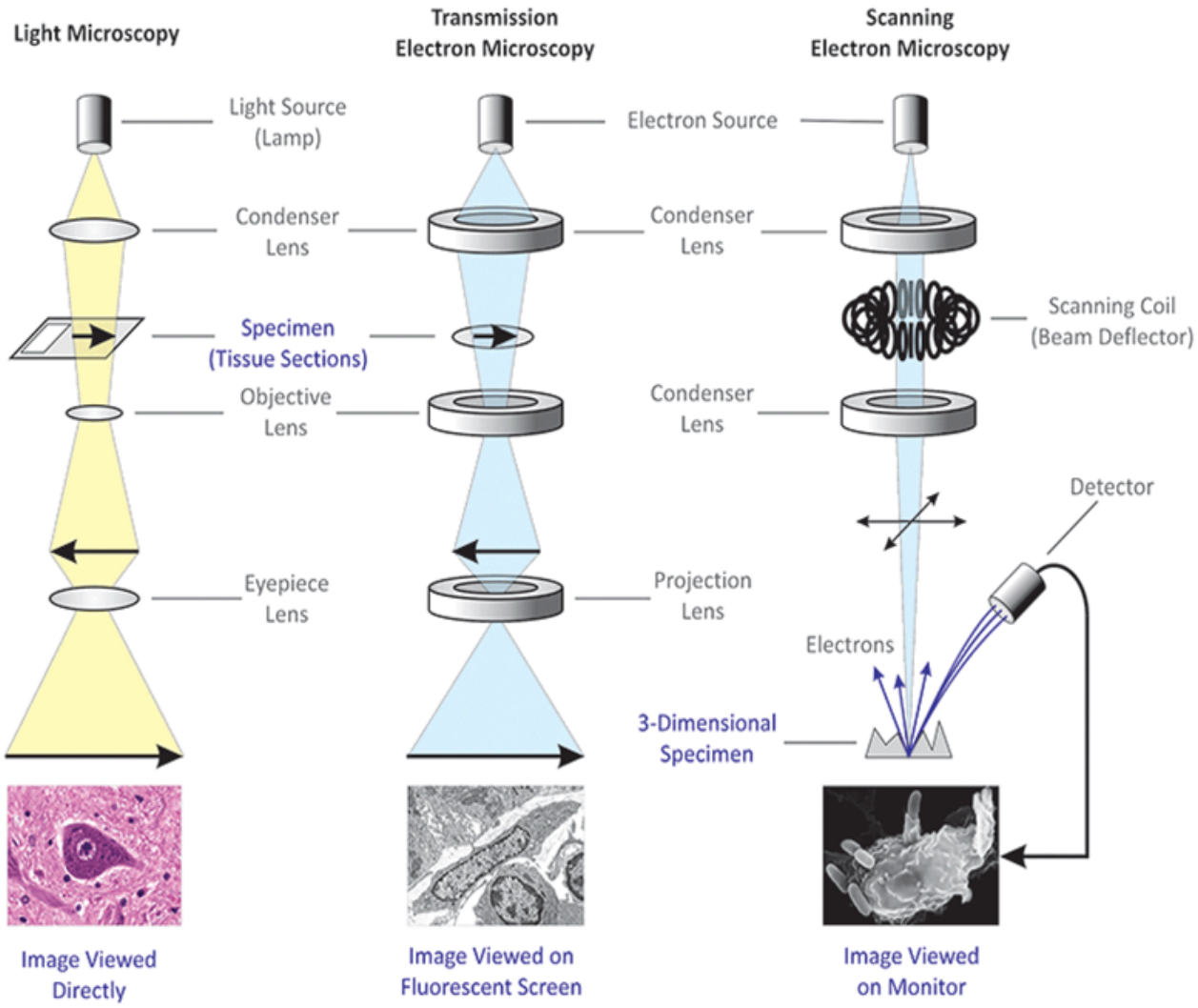

Figure 1.3: Schematic of Optical microscope, TEM and SEM

1.1.4 Measurement of Optical Properties

Measuring optical properties [23] of materials helps us to understand its chemical and physical structure which can lead to identification of the material uniquely. Refractive index (η) is one of the optical property that helps in understanding response of a material to the incident light. Refractive index (η^*) [9] is usually a complex number with real part and imaginary part defined as:

$$\eta^* = \eta + i\mathrm{k} \tag{1.4}$$

where η represents the real part of the refractive index and k represents the imaginary part called extinction coefficient. These two parameters helps to understand how a material/sample will respond to the incident light. η implies the speed at which light will pass through the material

$$\eta = \frac{c}{v} \tag{1.5}$$

where

c = speed of light

v = velocity at which light will travel in a material/sample.

k = extinction coefficient i.e. the amount of light that will be attenuated/absorbed as light passes through material/sample

In most circumstances $k > 0$ (light is absorbed) or $k = 0$ (light travels without loss). In some situations e.g. gain medium of laser it is also possible that $k < 0$, which implies amplification of light.

There are different measurement modalities which can measure refractive indices and their underlying principle is to measure deviation in angle of the incident beam when it passes through a material. Some of the techniques use a theoretical model to estimate value of complex refractive index. All the existing technologies provides an average value of any optical property over an area and are not capable of measuring values on a nanoscale dimension. This is broadly due to the fact that either the beam spot is very large or the detector is too big to collect light at nanometer scale.

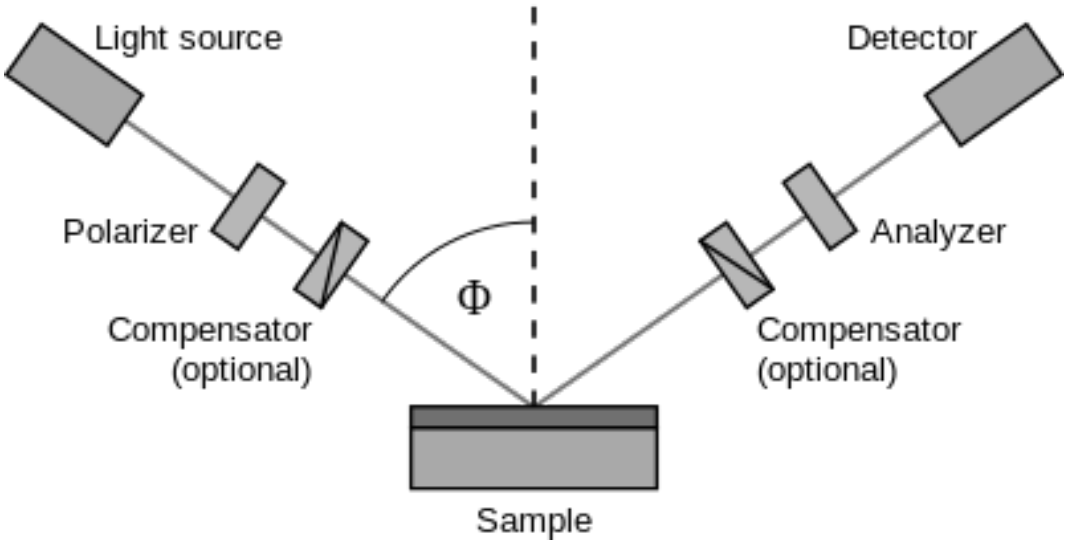

Figure 1.4: Ellipsometer schematic. Source: www.wikipedia.org

1.1.5 Ellipsometer

Ellipsometry [2] measures the change in polarization as light reflects or transmits (Figure 1.4) from material structure and compares it to a model. A polarizer and a quarter wave plate provides a state of polarization which varies incident beam from linearly polarized light to elliptically polarized light to circularly polarized light by varying the angle of the polarizer. The beam is reflected off the layer of interest and then analyzed with an analyzer. Modeling and parameter fitting for the actual structure are required to extract the thickness and the refractive indices values as ellipsometry is an indirect metrology technique.

The polarization change is represented as an amplitude ratio ψ and the phase difference δ. The measured response depends on optical properties and thickness of the individual material. Thus, ellipsometry is primarily used to determine film thickness and optical constants. However, it is also applied to characterize composition, crystallinity, roughness, doping concentration, and other material properties associated with a change in optical response. Ellipsometer [34] performs model based analysis over large area (several micrometers) as beam spot is large. Hence, all measurements done by this technique represents an average response of the sample over the beam spot.

1.2 Scanning Probe Microscopes (SPM)

1.2.1 History of SPM

Theoretical description of near field optical microscope was given by EH Synge much before invention of Scanning Tunneling Microscope (STM) and his idea was brought into practice only after advent of piezoelectric scanners and computer controlled data acquisition systems. EH Synge [38] was first to apply principle of scanning to imaging.

Unlike optical microscopes, Scanning Probe Microscopes (SPM) [43] do not see sample surface directly instead they see an image that represents surface of the sample [27]. Advent of scanning probe microscopes brought significant improvement in imaging as they moved away from conventional diffraction limited microscopy. All forms of SPMs had a tip held by cantilever moving very close to the sample in a raster scan to construct an image. Scanning Tunneling Microscope (STM) developed at IBM Research Lab, Zurich in 1982 was first addition in SPM family and it had atomic resolution [37].

1.2.2 Resolving Power of SPMs

Resolving power of an optical system (Figure 1.5) is defined as its ability to separate central peaks in diffracted image of two point sources. However, this definition must be redefined for SPMs as these optical microscopes are fundamentally different. Unlike diffraction limit and Abbe's criteria which were used to calculate resolution of optical microscopes, one needs to consider several parameters like probe size, probe shape, sample type, sample roughness, response time of piezoelectric tubes and feedback loop to define resolving power of SPMs. Resolving power [42] in this case must be defined separately in two different directions, one normal to the surface called normal resolution and another lateral to the surface called lateral resolution. Normal and lateral resolution varies differently depending upon different parameters of equipment being used e.g. lateral resolution in SPMs mainly depends on the size of tip/probe being used. A wider (blunt) tip leads to lower lateral resolution and normal resolution mainly depends on ability of the equipment to bring tip close to sample without crashing it.

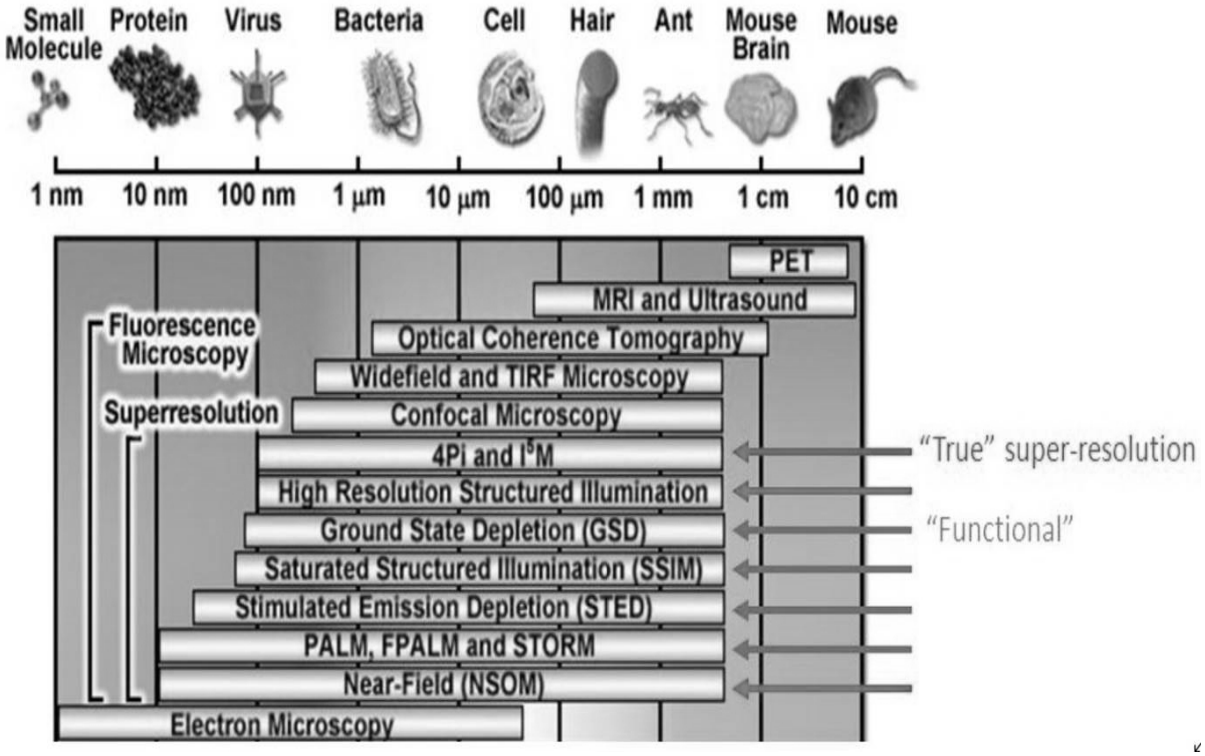

Figure 1.5: Comparison of resolving power of existing imaging modalities. Source: Zeiss microscopy website

1.2.3 Types of SPMs

Scanning Probe Microscopes (Figure 1.6) can be categorized based upon their working type. Generally, there exists three working modalities. First are the ones using electron called Scanning Tunneling Electron Microscope (STEM) [19] and are capable of obtaining sub-atomic resolution images of electrically conductive samples via electron tunneling. There exists a sharp metallic probe over the sample [17] and a voltage bias is applied between probe tip and sample, current tunnels across the gap and amount of tunneling current is measured which gives high resolution images of electron distribution over sample [5]. Resolution in this case is limited by the size of tip through which tunneling occurs. Their disadvantage being that it becomes challenging when using non-conductive samples [6].

Second commonly used type of SPM is Atomic Force Microscope (AFM) [4] in which probe is maintained in close contact with sample using a feedback mechanism as it scans over surface. Shear force between probe and sample is used to gauge probe-sample gap. There are mainly two modes AFM operates in, contact mode (static mode) where tip maintains a constant gap from sample and non-contact mode (dynamic mode) where a piezoelectric tubes oscillates at 5-400 kHz as it is attached to cantilever holder, in this mode tip of probe actually touches the sample as it oscillates. The probe is attached to a cantilever that acts as a spring and maintains constant gap between sample and probe(if operated in constant height mode). A reflected laser beam from the cantilever gets projected over a detector and height variation of probe-cantilever is recorded by laser detector. AFM can also be used to measure temperature gradients and magnetic forces. Although it is a versatile tool for getting topographical details and can provide atomic level resolution however, it had limited spectroscopic resolution.

Third commonly used SPM is Scanning Near-field Optical Microscope (SNOM) [29] which is a versatile tool for imaging and light manipulation at nanometer scale, it gives high resolution images by collecting near-field light and allows to study surface and sub-surface phenomenon. This methodology was theoretically proposed by Synge in 1928 and were demonstrated experimentally in 1984.

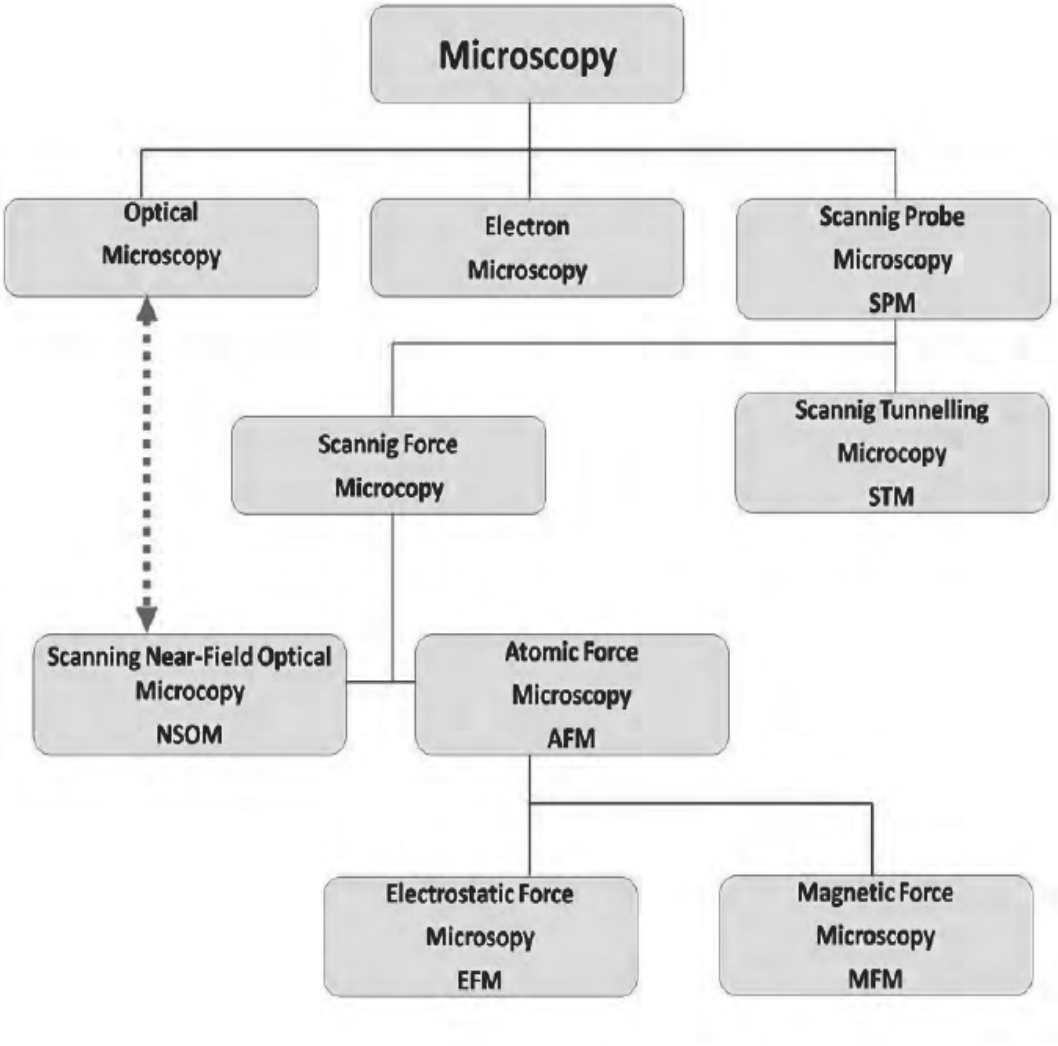

Figure 1.6: Different forms of SPMs

In general, design of a SNOM consists of a light beam illuminating the sample and a waveguide over the sample to collect light in near field region, where apex of the waveguide in much smaller then the wavelength of light used for illumination. Amount of optical signal is measured and is used in feedback mechanism to prevent tip from crashing into the sample. Resolution in this case depends upon size of the aperture, small aperture acts as a dipole antenna and converts electric field in near zone to radiated signal. SNOM is limited by its inability to accurately determine probe sample difference [3] and additional methods are used to gauge this distance e.g. shear force method.

Current optical scanning probe microscopes include near-field scanning optical microscope and photon scanning-tunneling microscope (PSTM) [32]. The latter form of scanning-probe microscope uses no apertured probe, but rather photon tunneling in much the same way that the electron scanning-tunneling microscope (STM) uses electrons. The PSTM resolution, while better than the Rayleigh limit, is not sufficient for many important samples. Several improvements have been made to the PSTM, but work has concentrated in the past few years on using it to image biological samples such as human and mouse chromosomes and liposomes. The technology is inherently limited by the long decay length of evanescent photons [10] in the visible-to-ultraviolet regions. A barrier exists due to the diminishing index of refraction and to the absorption properties of materials as the photon energy increases. This barrier is not faced by the completely different principle of the atomic-force microscope (AFM), but the AFM [14] cannot be used for optical spectroscopy as can the PSTM. Use of the AFM does not permit high-resolution spectroscopic identification of local sample regions, although some crude spectroscopy can be performed using other physical properties. In order to attain both high-resolution imaging and high-resolution spectroscopy a new concept in microscopy/spectroscopy must be obtained. The technique needs to be photonic in order to take advantage of the superior form of spectroscopy. But it should simultaneously.

Almost every analytical chemistry laboratory in the world utilizes an instrument based upon surface plasmons, the quanta of waves in an electron gas in conducting media. Surface plasmon excitation in a gold film on a prism can be obtained at only a single angle within one milliiradian for a given incident wavelength of light. The presence of any material on the films surface alters this angle and the alteration is determined by the optical properties

of the material. Sensitivity to submonolayers of an adsorbate is routinely obtained. But the measurements are averaged over the optical spot size. By using a scanned optical probe it is possible to perform these same measurements on the scale of nanometers and to determine the influence of the sample topography.

1.3 Surface Plasmon Scanning Tunneling Microscope

1.3.1 Motivation

Conventional forms of optical SPMs that identifies a material optically uses an optical beam to illuminate the sample in Kretschmann configuration. Optical beam is launched at first angle such that it totally internally reflected and the material is then placed on the prism so as to determine the second angle at which beam gets totally internally reflected. Difference between these two angles helps in determining optical properties of the sample. However, reflected beam's angle is an average effect of the optical beam's light spot area illuminating the sample and this technique is not capable of identifying properties upto nanometer size of sample. Also, the material might have empty spaces or chemical structure varying at nanometer scale and conventional techniques will not be able to take these effects into considerations and will respond to an an averaged area of the sample.

SPSTM not only circumvents diffraction limits that plagues conventional optical microscopes but is also capable of imaging and chemically mapping samples at nanometer scale with high resolution. As opposed to other NSOM techniques, SPSTM does not collect light in far-field region. A plasmonic tip captures surface plasmon enhanced evanescent field, this help plasmonic tip to stay within sub-wavelength region of the sample surface. In addition to that, it can provide more information about how sample's properties are modified when surface plasmons are excited on its surface. Combination of high resolution imaging, chemical mapping and capability of exciting surface plasmons in samples makes this equipment a versatile tool.

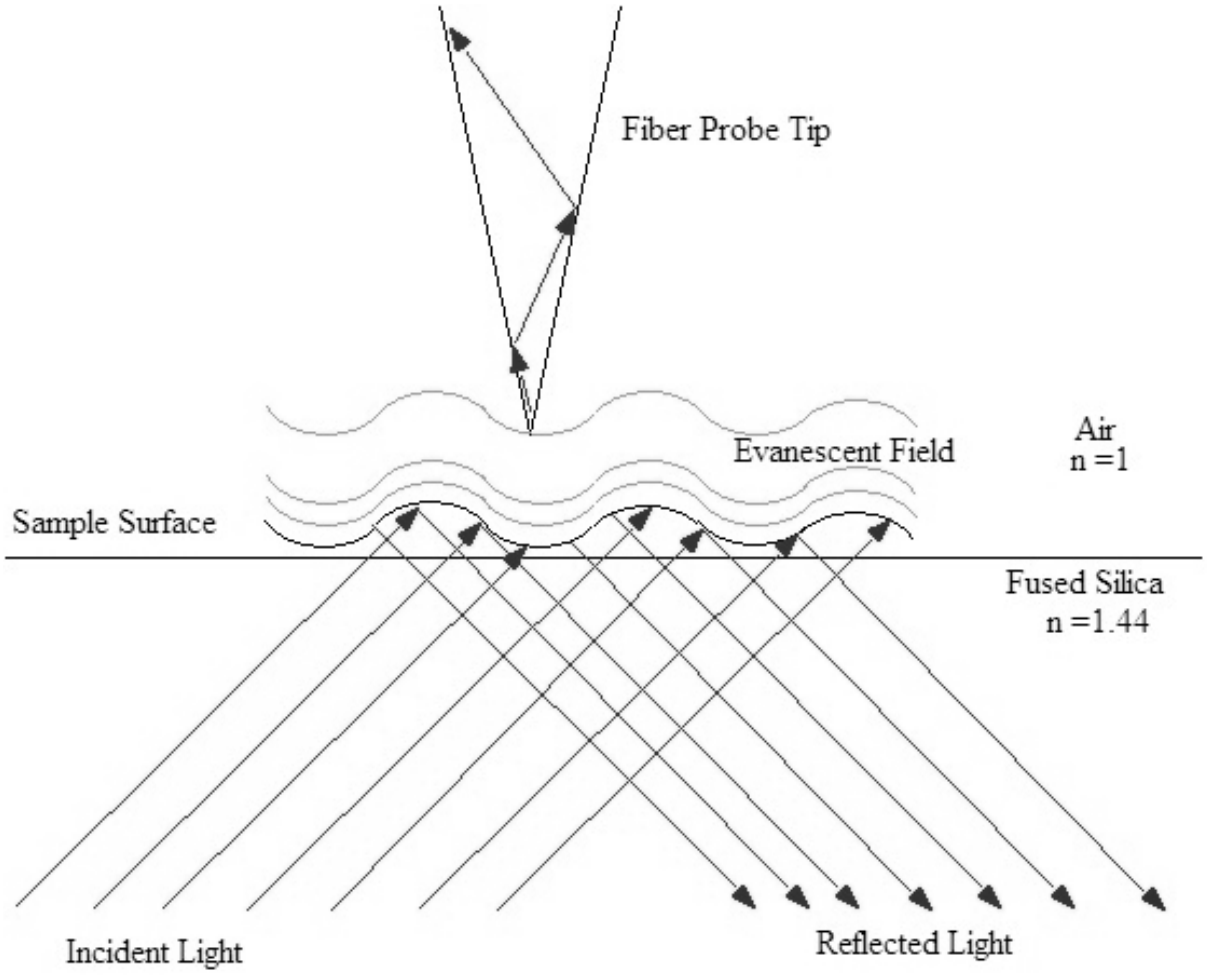

Figure 1.7: Frustrated Total Internal Reflection(FTIR)

1.3.2 Operating Concept

SPSTM works fundamentally different from existing near-field optical imaging technologies. It operates by collecting surface plasmons coupled exponentially decaying signal [48]. When angle of the incident laser beam is greater than the critical angle, the beam is totally reflected back to the incident medium. However, if there is another medium at the boundary of glass air interface then part of beam gets tunneled to that medium (Figure 1.7) this is called Frustrated total internal reflection (FTIR) [28].

In SPSTM surface plasmons are excited in Kretchmans configuration. If a thin material is placed on the metal layer surface plasmons on the metal layer then gets coupled to thin material and may exhibit unique optical properties which are then measured by the system.

SPSTM can measure optical properties at nanometer scale by measuring exponential signal (Figure 1.8). This exponential signal (photons) tunnel from the surface of the material to the plasmonic tip, this tip is an extension of the optical fiber which acts as a waveguide to transmit photons to photomultiplier tube, which converts light to electrical signal. This electrical signal is unique signature of nanoscale area of sample over which tip is present.

Measuring refractive index at nanometer scale level can help in determining chemical structure of a sample. Also, a material may exhibit unique characteristics when surface plasmons are excited on its surface and its detection can provide additional information about light matter interaction. Moreover, decay length of exponential signal will vary depending upon the chemical structure of the material. All these signatures which are unique to a material can be measured at nanometer scale.

Conventional approaches can also measure such properties but they measure an average value over a region and the region may have non-uniform chemical structure or may even have empty spaces and average value of optical property over a region may lead to inaccurate identification of the sample. Apart from collected signal being exponential in nature, dimensions of the plasmonic tip also helps to get nanometer scale accuracy as the plasmonic tip has a tapered geometry and it collects exponential signal only from the very end of the tip and nature of the exponential signal prevents it from interacting with rest of the probe.

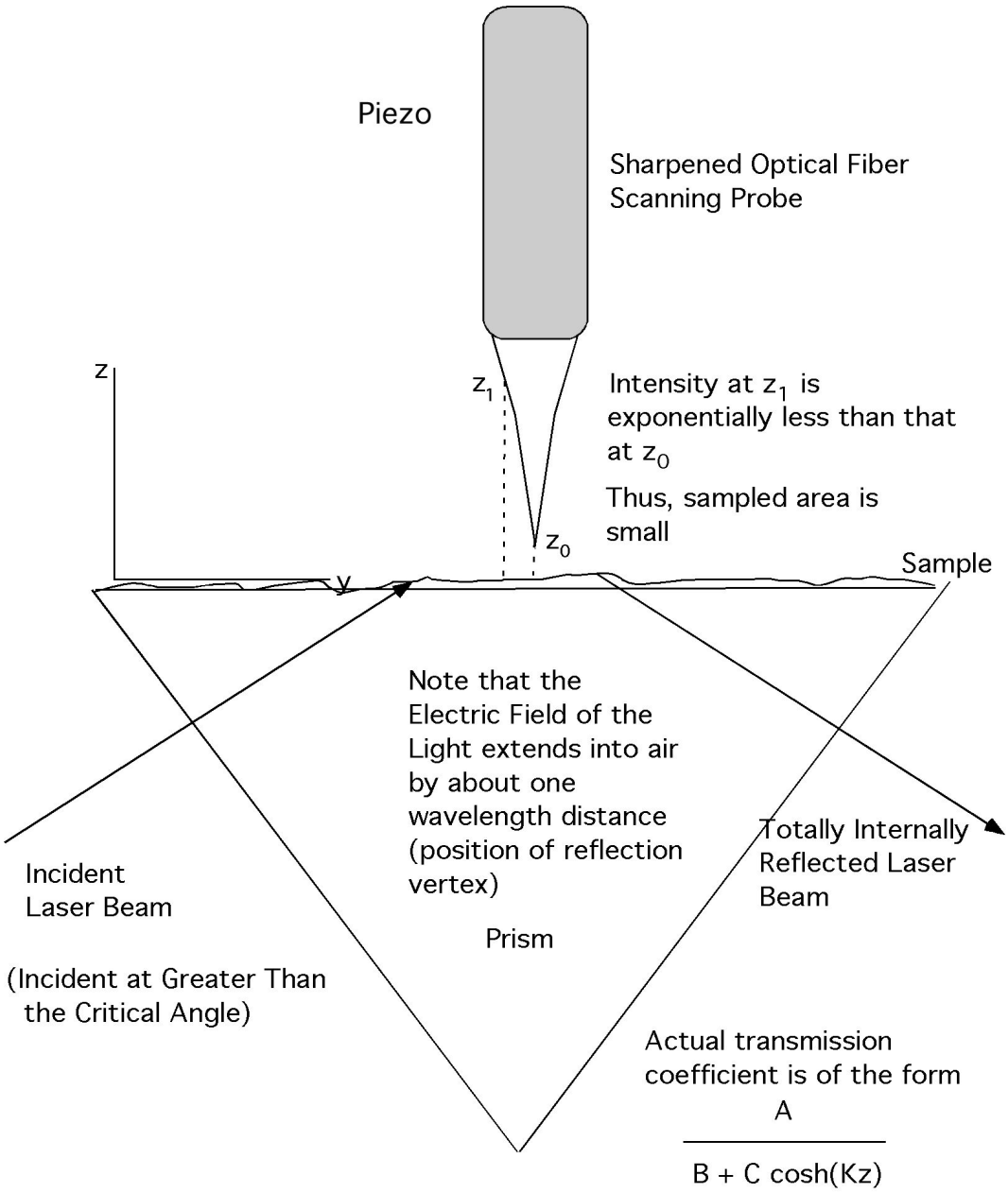

Figure 1.8: SPSTM operating concept

1.3.3 SPSTM Resolution

Conventional forms of optical microscopy were diffraction limited and it was not possible to detect an object with dimensions smaller than the λ of light being used. Some of the microscopes based on near field optics were able to circumvent diffraction limit by using the microscopic tip and fabricating a nanoscale channel that is much smaller than the λ of the light being used. This channel collects and acts as a waveguide to transmit the light collected. However, there is no way to accurately control the distance between the tip and the sample in case of near field microscopes. Such microscopes usually have an indirect method of measuring the distance between the tip and the sample.

SPSTM, on the other hand works by collecting the signal which decays exponentially in z direction i.e. direction perpendicular to the sample and intensity of signal collected is a direct measure of distance from the sample. Hence, resolution in z direction is only limited by the resolution of the controller that extends and retracts the tip. Lateral resolution depends on the size of tip, sharper the tip better the resolution. It has been demonstrated that tip as sharp as a few (2-3) nm can be produced therefore it is possible to achieve resolution of below 5 nm with SPSTM.

Change in the perpendicular distance for each corresponding nanometer-sized region may trigger an exponential change in signal intensity resulting in an increased sensitivity of the spatial resolution of the sample image. The increased sensitivity of the exponential signal may enable the resulting spatial resolution of the sample image to not be diffraction limited to the wavelength of the optical beam and/or to the aperture of the nanometer-sized tip of the optical probe.

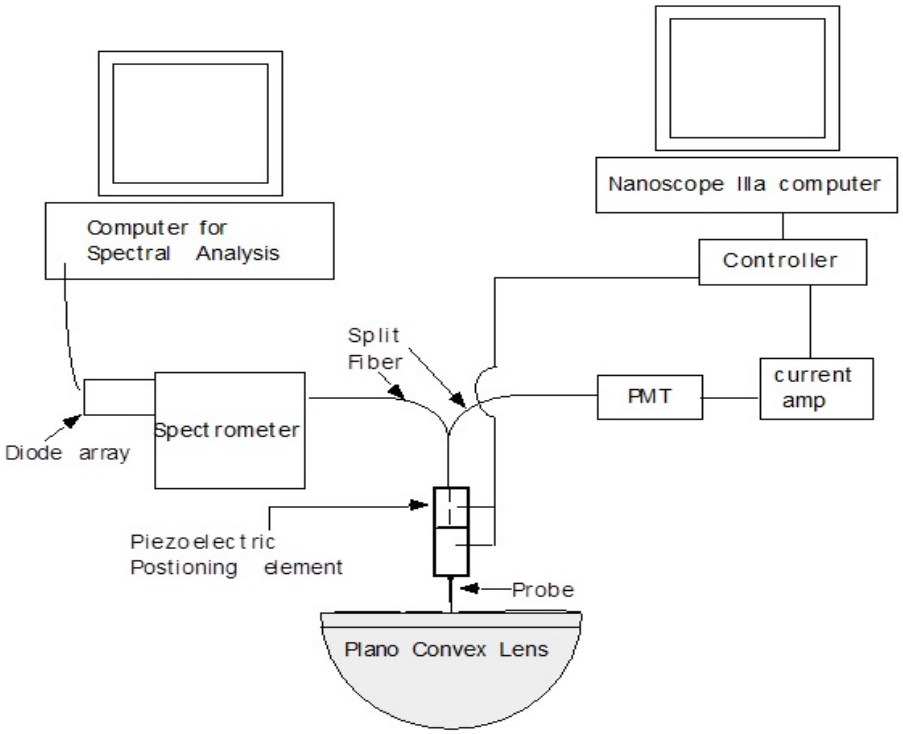

Figure 1.9: SPSTM spectroscopic setup

1.3.4 SPSTM Spectroscopy

SPSTM can also be used to perform spectroscopy. Typically, light from a source can consist of a continuous spectrum, an emission spectrum (bright lines), or an absorption spectrum (dark lines). Because each element leaves its spectral signature in the pattern of lines observed, a spectral analysis can reveal the composition of the sample being analyzed. Optical fiber terminating in photomultiplier tube can be split (Figure 1.9) such that signal is partially transmitted to a spectrometer and it can analyze chemical shifts when a material is illuminated by the laser beam. Laser beams of different wavelengths can be used, one at a time to not only get high resolution optical image but to also perform spectroscopic measurements.

Size of a plasmonic tip is complimentary to spectroscopic signal. A sharper tip will have better resolution but at the same time it will collect significantly less signal (as compared to a broad tip) and the tip would need to be localized to a particular region for a longer time

to collect spectroscopic data. A broad tip will have high signal intensity but signal will be collected over large area and lateral resolution will be compromised.

1.3.5 SPSTM Compatible Samples

SPSTM has the potential to provide identification characteristics of materials to the nanometer scale and has direct feedback for tip to sample distance control. Since its operation is based on detection of exponential signal and exponential signal extends in space to about a wavelength, it introduces a limit on maximum thickness of a sample whose optical properties can be accurately measured. Typically, thickness of the sample should be less than the wavelength of light being used to excite and detect surface plasmons.

SPSTM offer a great advantage in terms of sample preparation as compared to it's electron counterparts with nanometer scale resolution (e.g. SEM, TEM, STEM) by working in the ambient. This is especially advantageous for the biological samples and the samples with high water content. Since energetic electrons will have smaller mean free path in the ambient, high vacuum is always required for optimum operation of any electron microscope to minimize scattering of an electron beam by the air molecules. Typically, mean free path should be larger than the length electron column in microscope. Moreover, ultra-thin samples are likely to get contaminated in ambient hence, vacuum help to keep samples clean.

SEM samples have to be electrically conductive so as to avoid charge accumulation and TEM works on thin slices of samples loaded after extensive sample preparation. SPSTM on the other hand does not need elaborate sample preparation and can operate in the ambient avoiding use of the vacuum chambers. Since SPSTM is an optical microscope, electrical conduction no more puts a limit on type of samples compatible.

Chapter 2

Theory

2.1 Overview

When light waves strike an interface of two optical mediums of different refractive indices it may undergo many phenomenons depending upon the type of boundary, light may transmit, reflect, refract, scatter or might get absorbed. Also, there are phase shifts as electromagnetic waves strikes boundary of optical mediums. If an optical medium in low absorbing, isotropic and if interface of two optical mediums is flat then absorption and scattering is negligible as compared to transmission, reflection and refraction. No matter which phenomenon/s does an electromegnetic wave undergoes it always satisfies some boundary conditions and it is possible to compute amount of light that may be reflected and transmitted. These amplitudes are given by set of equations called 'Fresnel equations'. Fresnel equations are complex ratios of amplitudes and phases of reflected and transmitted wave's electric field to that of incident electric field.

Fresnel equations for single interface can be derived using Maxwell's equations and by applying boundary conditions. Fresnel equations for multiple interfaces can be derived by extending the case of single interface.

2.2 Maxwell's Equations

Consider two dielectric mediums of permittivity ϵ_1, ϵ_2 and permeability μ_1, μ_2. If an electromagnetic wave propagates at the interface of these two mediums then Maxwell's equations [46] must be satisfied at interface as well as in bulk. Maxwell's equations in integral form are given by Equations 2.1 to 2.4.

$$\text{Gauss' law for electricity:} \quad \oint_{\substack{\text{closed}\\\text{surface}}} \vec{E} \cdot d\vec{A} = \frac{Q_{enc}}{\epsilon_0} \tag{2.1}$$

$$\text{Gauss' law for magnetism:} \quad \oint_{\substack{\text{closed}\\\text{surface}}} \vec{B} \cdot d\vec{A} = 0 \tag{2.2}$$

$$\text{Faraday's law:} \quad \oint \vec{E} \cdot d\vec{s} = -\frac{d\phi_B}{dt} \tag{2.3}$$

$$\text{Ampere-Maxwell law:} \quad \oint \vec{B} \cdot d\vec{s} = \mu_0\epsilon_0\frac{d\phi_E}{dt} + \mu_0 i_{enc} \tag{2.4}$$

In general, electric and magnetic flux densities $\vec{D}, \vec{B}$ are related to the field intensities $\vec{E}, \vec{H}$ as Eq. 2.5 and Eq. 2.6. Their exact form depends on the material in which field exists.

$$\vec{D} = \epsilon_0\vec{E} \tag{2.5}$$

$$\vec{B} = \mu_0\vec{H} \tag{2.6}$$

Where

$$\epsilon_o = 8.854 \times 10^{-12} \text{ farad/m} \tag{2.7}$$

$$\mu_o = 4\pi \times 10^{-7} \text{ henry/m} \tag{2.8}$$

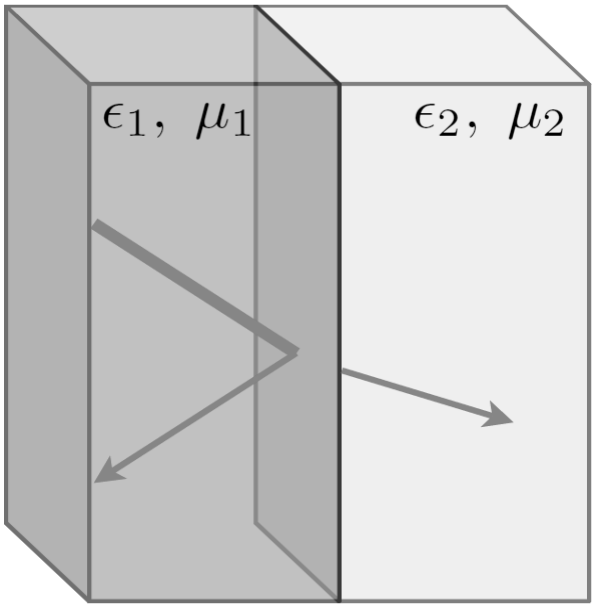

Figure 2.1: Interface of two dielectric mediums

2.3 Boundary Conditions

When an electromagnetic wave is incident on a boundary of two mediums (Figure 2.1) with different refractive indices, Maxwell's equations must be valid at the interface as well as in bulk of both the mediums. There are some conditions that must be satisfied for Maxwell's equation to be valid, these constraints are called boundary conditions. These conditions [7] can be derived from Maxwell's equation for electric field and magnetic field components. It will turn out that normal component of $\vec{D}, \vec{B}$ are continuous across the dielectric interface and tangential component of $\vec{E}, \vec{H}$ are continuous across the dielectric interface.

2.3.1 Boundary Conditions for Electric Field

Gauss's law can be used to find boundary condition for the component of electric field perpendicular to the interface. Since both mediums are dielectric, net charge enclosed within a surface is zero, Eq. 2.10 represents a boundary condition for perpendicular component of the electric field.

$$\epsilon_1 \vec{E}_{1\perp} - \epsilon_2 \vec{E}_{2\perp} = 0 \tag{2.9}$$

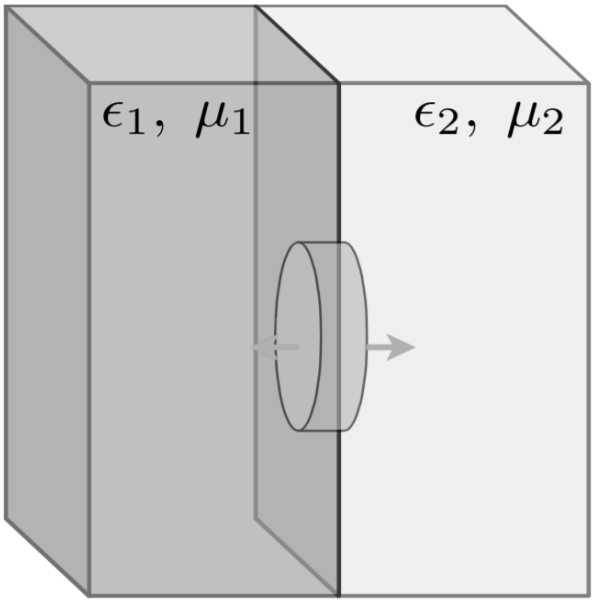

Figure 2.2: Enclosed surface at the interface with zero net charge

$$\epsilon_1 \vec{E}_{1\perp} = \epsilon_2 \vec{E}_{2\perp} \tag{2.10}$$

Faraday's law can be used to find boundary condition for component of electric field parallel to the interface. If the loop around which electric field is computed is made to have infinitesimally small area then $d\vec{s} = 0$ and equation 2.3 will yield

$$\vec{E}_{2\parallel} - \vec{E}_{1\parallel} = 0 \tag{2.11}$$

2.3.2 Boundary Condition for Magnetic Field

Ampere's law will yield boundary condition for parallel component of the magnetic field along the interface.

$$\frac{\vec{B}_{1\parallel}}{\mu_1} = \frac{\vec{B}_{2\parallel}}{\mu_2} \tag{2.12}$$

Gauss's law for magnetism yields boundary condition for perpendicular component of the magnetic field

$$\vec{B}_{1\perp} A - \vec{B}_{2\perp} A = 0 \tag{2.13}$$

$$\vec{B}_{1\perp} A = \vec{B}_{2\perp} A \tag{2.14}$$

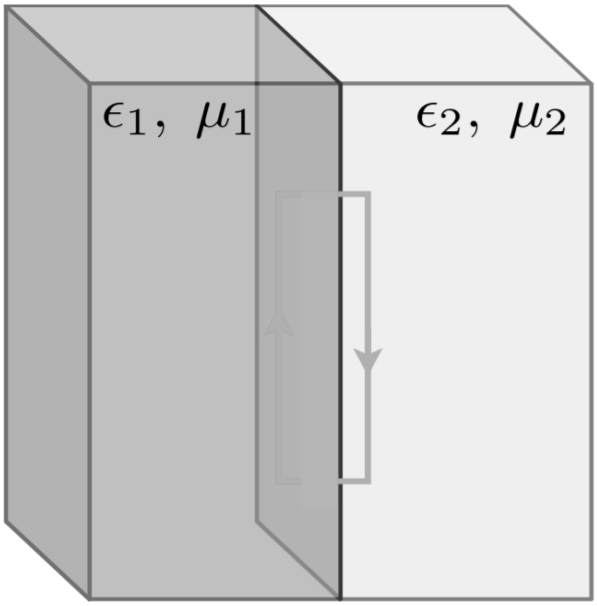

Figure 2.3: Loop at the interface with infinitesimal small area

2.4 Fresnel Equations

Fresnel equations [31] gives fraction of light reflected and transmitted by interface between two dielectric mediums with different refractive indices. These reflection and transmission amplitudes depends on the polarization of the incident light. Figure 2.4 represents s-polarized electromagnetic wave as electric field is in z direction which is the place of interface and is perpendicular to plane of incidence.

Fresnel equations depends on polarization of incident electromagnetic wave and are derived separately for s and p polarized light. It is assumed that both the mediums are homogeneous and isotropic and incident wave is considered as plane wave.

2.4.1 S-Polarized Light

For s polarized light at the interface tangential component of the electric field is continuous

$$\vec{E}_{\mathrm{i(y=0)}} + \vec{E}_{\mathrm{r(y=o)}} = \vec{E}_{\mathrm{t(y=0)}} \tag{2.15}$$

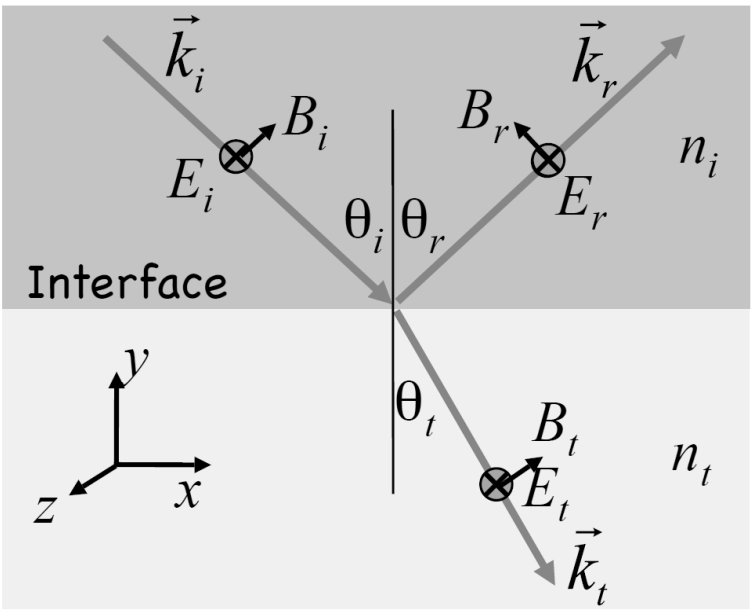

Figure 2.4: S-polarized electromagnetic wave at an interface

Similarly, for s-polarized light at the interface tangential component of the magnetic field is continuous

$$\vec{B}_{\mathrm{i(y=0)}} \cos\theta_{\mathrm{i}} + \vec{B}_{\mathrm{r(y=o)}} \cos\theta_{\mathrm{i}} = \vec{B}_{\mathrm{t(y=0)}} \cos\theta_{\mathrm{t}} \tag{2.16}$$

Considering only amplitude of waves at the boundary and considering $\theta_{\mathrm{i}} = \theta_{\mathrm{r}}$ with $B = \frac{nE}{C}$ gives

$$\eta_{\mathrm{i}}(\vec{E}_{\mathrm{or}} - \vec{E}_{\mathrm{oi}}) \cos\theta_{\mathrm{i}} = -\eta_{\mathrm{t}}(\vec{E}_{\mathrm{or}} + \vec{E}_{\mathrm{oi}}) \cos\theta_{\mathrm{t}} \tag{2.17}$$

Fresnel reflection coefficient is then found to be

$$r_{\perp} = \frac{\vec{E}_{\mathrm{or}}}{\vec{E}_{\mathrm{oi}}} = \frac{\eta_{\mathrm{i}} \cos\theta_{\mathrm{i}} - \eta_{\mathrm{t}} \cos\theta_{\mathrm{t}}}{\eta_{\mathrm{t}} \cos\theta_{\mathrm{t}} + \eta_{\mathrm{t}} \cos\theta_{\mathrm{t}}} \tag{2.18}$$

Similarly, Fresnel transmission coefficient would be

$$t_{\perp} = \frac{\vec{E}_{\mathrm{ot}}}{\vec{E}_{\mathrm{oi}}} = \frac{2\eta_{\mathrm{i}} \cos\theta_{\mathrm{i}}}{\eta_{\mathrm{i}} \cos\theta_{\mathrm{i}} + \eta_{\mathrm{t}} \cos\theta_{t}} \tag{2.19}$$

2.4.2 P-Polarized Light

Boundary conditions for an electromagnetic wave depends on polarization. For p-polarized light tangential component of electric field and tangential component of magnetic field is continuous this yields to following equations

$$\vec{E}_{\mathrm{i(y=0)}} \cos\theta_{\mathrm{i}} + \vec{E}_{\mathrm{r(y=o)}} \cos\theta_{\mathrm{i}} = \vec{E}_{\mathrm{t(y=0)}} \cos\theta_{\mathrm{t}} \tag{2.20}$$

$$\vec{B}_{\mathrm{i(y=0)}} + \vec{B}_{\mathrm{r(y=o)}} = \vec{B}_{\mathrm{t(y=0)}} \tag{2.21}$$

Considering only amplitude of waves at the boundary and using the fact that $\theta_{\mathrm{i}} = \theta_{\mathrm{r}}$ and $E = \frac{cB}{n}$ gives

$$\eta_{\mathrm{t}}(\vec{E}_{\mathrm{or}} - \vec{E}_{\mathrm{oi}}) \cos\theta_{\mathrm{i}} = \eta_{\mathrm{i}}(\vec{E}_{\mathrm{or}} + \vec{E}_{\mathrm{oi}}) \cos\theta_{\mathrm{t}} \tag{2.22}$$

Fresnel reflection coefficient is then given as

$$r_{\parallel} = \frac{\vec{E}_{\mathrm{or}}}{\vec{E}_{\mathrm{oi}}} = \frac{\eta_{\mathrm{t}} \cos\theta_{\mathrm{t}} - \eta_i \cos\theta_{\mathrm{t}}}{\eta_{\mathrm{i}} \cos\theta_{\mathrm{t}} + \eta_{\mathrm{t}} \cos\theta_{\mathrm{i}}} \tag{2.23}$$

Similarly, Fresnel transmission coefficient would be

$$t_{\parallel} = \frac{\vec{E}_{\mathrm{ot}}}{\vec{E}_{\mathrm{oi}}} = \frac{2\eta_{\mathrm{i}} \cos\theta_{\mathrm{i}}}{\eta_i \cos\theta_{\mathrm{t}} + \eta_{\mathrm{t}} \cos\theta_{\mathrm{i}}} \tag{2.24}$$

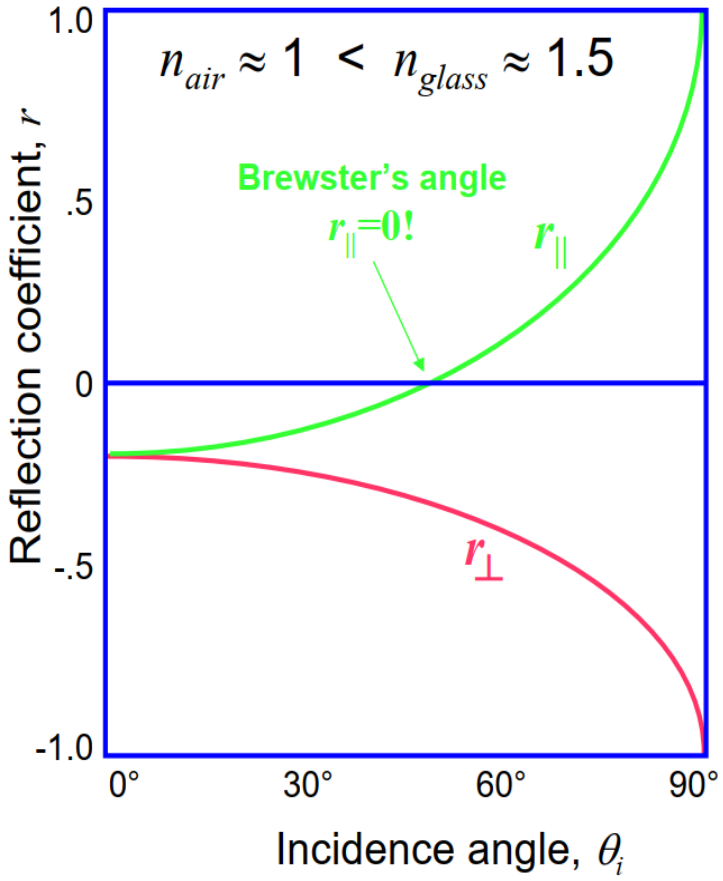

Figure 2.5: Fresnel reflection coefficient for air-glass interface

2.4.3 Implications of Fresnel coefficients for an Air-Glass Interface

Figure 2.5 shows reflectively vs incidence angle for s and p polarized light at an air-glass interface. It turns out that when light in incident normally i.e. $\theta_{\mathrm{i}} = \theta_{\mathrm{r}} = 0^{\mathrm{o}}$, Fresnel coefficients are same for both polarization. If light is incident at $\theta_{\mathrm{i}} = 90^{\mathrm{o}}$ then total reflection occurs for both polarizations. It is also evident that there is significant amount of reflection from the interface for any polarization. This becomes important for an optical system with multiple optical components e.g. microscopes, telescopes etc. and there could be significant loss of light from reflection alone, further calculation will yield that about 4% light gets reflected from each air-glass interface. Hence, anti-reflection coatings are used to minimize reflection and index matching gel or fluid is used if incident beam is to pass through multiple interfaces.

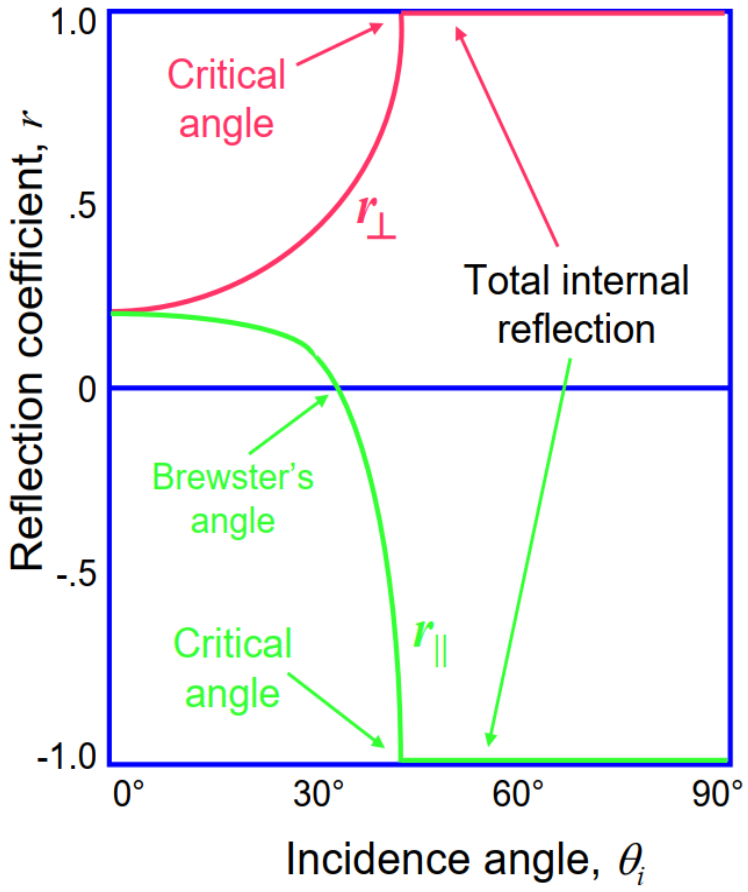

Figure 2.6: Fresnel reflection coefficient for glass-air interface

2.4.4 Fresnel Coefficients for an Glass-Air Interface

For glass to air interface there is an angle at which light gets totally reflected (Figure 2.6) to the medium of incidence. This condition is called 'total internal reflection', the angle at which total internal reflection occurs depends upon the refractive indices of both the mediums i.e. η_{t}, η_{i} and it is given as

$$\theta_{\mathrm{crit}} = \sin^{-1} \frac{n_{\mathrm{t}}}{n_{\mathrm{i}}} \tag{2.25}$$

2.5 Interpretation of Signal Intensity

2.5.1 Quantitative representation

The exponential signal as measured by the plasmonic tip for each nanometer-sized region can be represented as Eq. 2.26. In general, the optical properties and thickness of each nanometer-sized region may be obtained by fitting the measured dependence of the intensity level, I, of the exponential signal on the position z. For each nanometer-sized region of the sample, there is a range of z, where the model of Eq. 2.26 may be expressed as

$$I = I_0 e^{-ankz} \tag{2.26}$$

where

I = the intensity level of the exponential signal,

I_0 = a pre-factor,

n = the real part of the index of refraction of the target material in the nanometer-sized region,

$k = 2\pi/\lambda$ is the free-space wavelength of the optical beam with λ being the free-space wavelength,

a = a parameter that depends on the materials and geometry of the transparent optical element, the material layer, the target material, and the plasmonic tip of the optical probe,

z = the perpendicular distance of the optical probe from the nanometer-sized region

In the range of the position z of the plasmonic tip where Eq. 2.26 is valid any change in the position z may result in a significant change in the intensity level I of the exponential signal. For regions with homogeneous optical properties and differences in thickness of the target material the maintaining of the intensity level I of the exponential signal the position z of the plasmonic tip from the top surface of the nanometer-sized region to be constant. Therefore, raster scanning with a constant intensity level of the exponential signal may result in a topography image of the sample. For a more general sample with in-homogeneous optical properties, the contrast of an image acquired by constant intensity raster scanning

is due to the variations in both the thickness and the optical properties, such as the η as the real part of the index of refraction. Such a constant intensity raster scanned image may indicate degrees of in-homogeneity of the sample, while the exact values of the optical properties and thickness of each nanometer-sized region of the sample, may be obtained from the intensity level of the exponential signal as function of the relative position z of the plasmonic tip from the sample surface. The wave vector k of the optical beam launched into the transparent optical element by the optical beam source is known, thus, the product of ank in Eq. 2.26 may be determined. The parameter a may be inferred from the materials and geometry of the configuration and therefore the real part of the index of refraction, η, may be determined. More generally, the intensity level of the exponential signal as a function of the position z of the plasmonic tip may be measured by scanning the plasmonic tip in the direction perpendicular to the top surface of the target material the nanometer-sized region of the sample in a range of position z beyond where Eq. 2.26 is valid. The optical properties and thickness of each probed nanometer-sized region may then be determined by fitting the measured intensity level of the exponential signal as function of the relative position z to the model provided in Eq. 2.26. The dependence of intensity on z can also be measured using lock-in techniques at specific frequencies.

2.5.2 Interpretation of SPSTM Images

An image is formed by integration of several pixels. SPSTM, like any other microscope will generate an image as plasmonic tip measures variation in intensity of exponential signal. Contrast in this image will represent variation in thickness of the sample if functional dependence of the intensity level of the probe signal is based on the relative position z that indicates homogeneity in the optical properties i.e. if intensity level is same over lateral scan and intensity differs only because of shift in z. This would represent a sample which is optically homogeneous. However, if the product $a \times n \times k$ in Eq. 2.26 differs during a lateral scan and the difference is not only due to variation in z then sample is optically in-homogeneous and SPSTM my determine optical properties and variation in thickness (if present) by fitting intensity level as a function of tip position as in Eq. 2.26

$$I = I(z) \tag{2.27}$$

where

$I =$ is the intensity level of the probe signal, and

$z =$ is the perpendicular distance of the nanometer-sized tip to top surface.

2.5.3 Tip to Sample Distance Control

The probe position controller may monitor the intensity level of the exponential signal of each corresponding nanometer-sized region via the intensity level signal to determine whether the intensity level of the exponential signal of each corresponding nanometer-sized region deviates from the intensity level threshold. The exponential signal is an exponential where the power of the exponential is a function of the perpendicular distance (z) that the plasmonic tip is from a top surface of the sample. A change in the perpendicular distance of the plasmonic tip from the top surface of the sample may result in an increased sensitivity to the intensity level of the exponential signal in that any change in the perpendicular distance may result in a significant change in the intensity level of the exponential signal. Nanoscope controller may monitor the intensity level of the exponential signal via the intensity level signal for any change in the intensity level. A change in the intensity level of the exponential signal may likely be the result of a change in the perpendicular distance of the plasmonic tip from the top surface of the sample. Nanoscope controller may then adjust the perpendicular distance such that the plasmonic tip is positioned within exponential region from the top surface of the nanometer-sized region when the intensity level of the exponential signal deviates from the intensity level threshold as any deviation of the intensity level of the exponential signal that is outside of the intensity level threshold is likely the result of a change in the perpendicular distance of the sample from the plasmonic tip. Nanoscope controller may adjust the perpendicular distance when the intensity level of the exponential signal is outside of the intensity level threshold to maintain the intensity level of the exponential signal within the intensity level threshold.

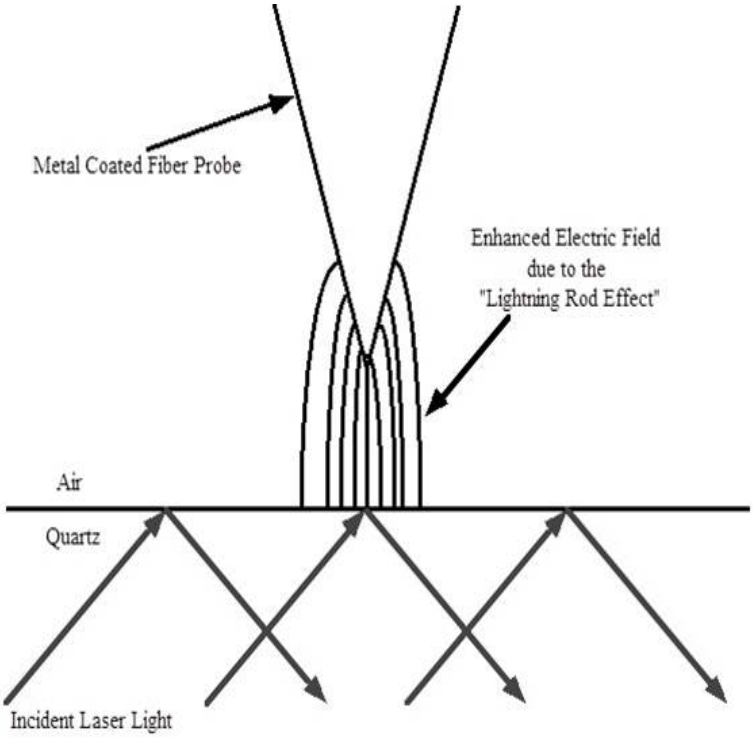

Figure 2.7: Field enhancement

2.6 Field Enhancement

Surface plasmons are coupled oscillations that arise from the interaction between light and the conduction electrons in a metal or semiconductor. It is possible that charge density distribution over a metal [41] varies on a scale smaller than the wavelength of incident light. This can happen as surface plasmons [11] can couple to incident electric field on a sub-wavelength regime i.e. light absorption by surface plasmons can occur on scale much smaller than the wavelength of incident light. In that case optical fields are enhanced strongly over sub-wavelength regions and their collective effect leads to overall field enhancement. Hence, light-matter interaction (Figure 2.7) is amplified significantly by this effect. Since plasmonic tip in SPSTM is a few nanometers sharp and is also metal coated, field enhancement effect can be exploited and by leveraging surface enhancement, performance of SPSTM is improved.

Chapter 3

Design and construction of SPSTM

3.1 SPSTM: Apparatus and Design

SPSTM apparatus consists of several electrical and optical components which enables it to measure optical properties of thin materials by exciting and detecting tunneled surface plasmons [24]. HeNe laser acts as an excitation beam which interacts with thin metal layer and the sample, signal from the sample tunnels to plasmonic tip (which is one end of optical fiber), optical fiber acts as a wave guide and transmits optical signal to photomultiplier tube which amplifies and converts optical signal to electrical signal. Photomultiplier is a current source, current amplifier amplifies and converts it to voltage before feeding it to Nanoscope controller. IP-128 photomultiplier tube's sensitivity varies with the input voltage and its important to keep input voltage in the region of maximum sensitivity. Nanoscope controller not only collects signal but also acts as a feedback controller by providing high voltage (150V) to piezo tubes in scanner head (Figure 3.12). Nanascope controller also interacts with PC via Nanoscope cards which are A/D converter cards installed in PC.

In schematic diagram of SPSTM, optical fiber is split, part of the signal is directed to photomultiplier tube for imaging and part of the signal is directed to spectrophotometer.

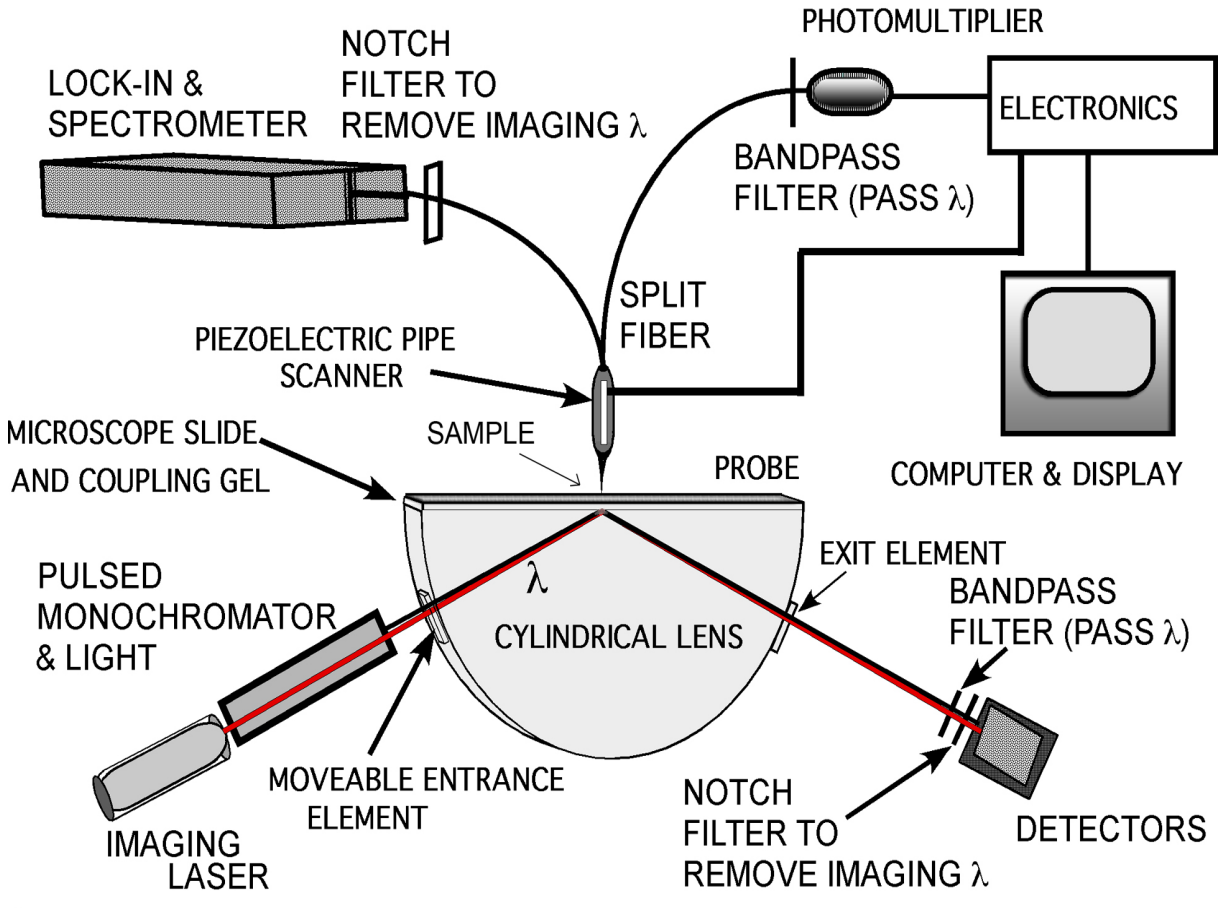

Figure 3.1: SPSTM Schematic

Surface plasmon excitation by kretchman configuration is vital component of this setup. Metal layer in this case is on top of a (Total Internal Reflection) TIR surface which enables coupling of electric field to electron gas on surface of thin metal film. Semi-cylindrical lens whose flat surface holds a microscopic slide is coupled to lens by coupling gel whose refractive index matches closely with that of BK-7 glass. Top surface of a microscopic slide is coated with 50 nm thick gold and acts as a stage to hold samples. Laser is coupled to the sample as it passes through entrance element, lens, coupling gel and microscopic slide. It is important to incident the laser beam at a certain angle with specific polarization for successful excitation of surface plasmons, for that to happen angle of incidence must be greater than the critical angle, in this case most of the beam gets reflected from the plane of incidence. If the angle of incidence is increased further (Figure 3.10), laser beam then gets coupled to the electron gas at the surface of a gold film and there is almost no reflected beam.

Microscopic head is designed to control the motion of plasmonic tip over the sample and to collect signal from the sample, it is placed on top of the cylindrical lens and consists of metal casing to hold piezoelectric tubes with optical fiber being present along the axis of piezoelectric tubes. Optical fiber is held in a steel tubing (called hypo-tubing Figure 3.12). It is important that hypo-tubing holds the fiber firmly especially near the plasmonic end of the fiber. A loosely held fiber can be a source of noise and is also more prone to mechanical damage. In order to hold it firmly, small amount of bee was is melted and applied at the very end of hypo-tubing, wax will hold the optical fiber firmly once its temperature returns to room temperature. Microscopic head rests on the casing which holds cylindrical lens, it is in contact with the casing via finely moving bolts which allows coarse movement of the microscopic head in vertical direction. Sample loading stage is raised so as to allow laser beam to be incident at desired angles. Ideally, reflected beam's intensity should be minimum at surface plasmon angle and reflected beam should be dumped otherwise.

Figure 3.2 shows different optical elements used in SPSTM to excite and detect surface plasmons. It important to keep surface of thin metal clean as little contamination will cause scattering and absorption of light causing surface plasmons to deplete.

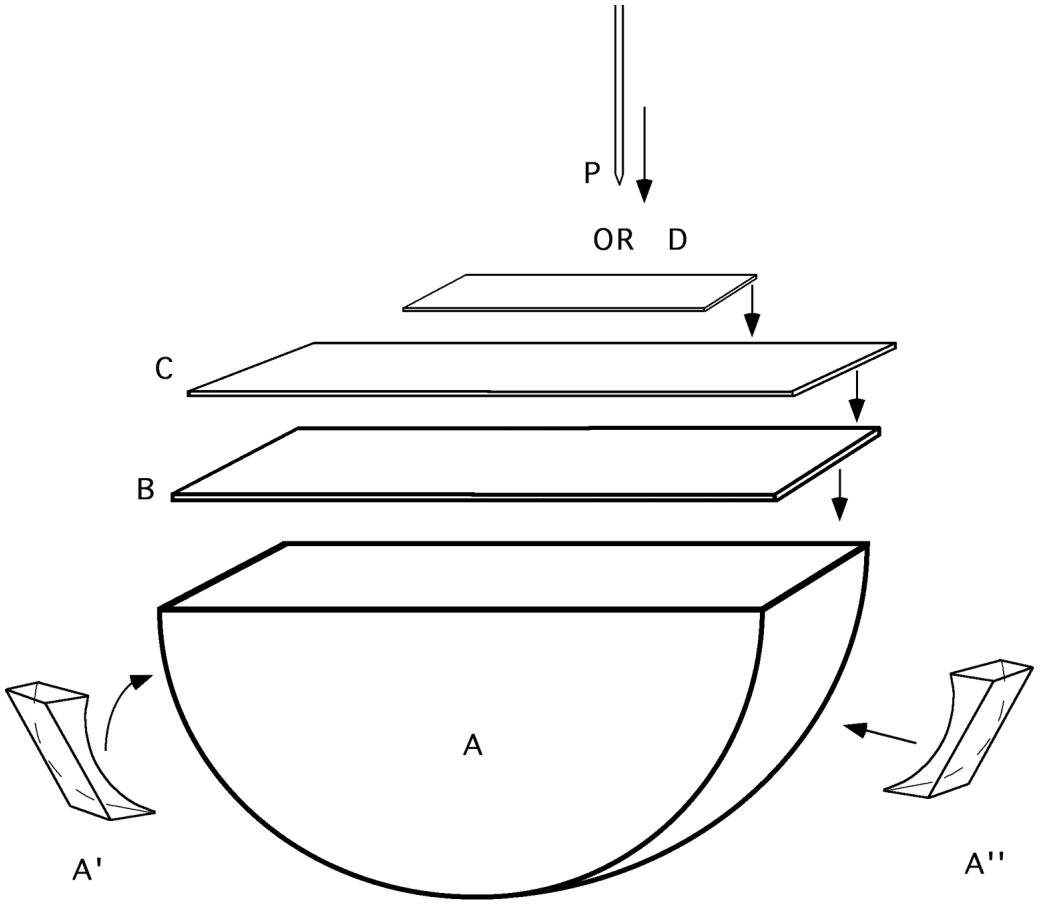

A. Transparent Plano-Convex Cylindrical Lens
A'. Movable Entrance Element (Optional) To Prevent Focusing of Entering Photons
A''. Movable Exit Element (Optional) To Prevent Defocusing of Exiting Photons

Elements A, A', A'', B Typically are of the same material such as fused silica.

B. Slide (Such As a Microscope Slide) To Be Mated To The Surface of Element A Using a Photonic Gel That Matches the Index of Refraction of the Slide and Element A

C. Thin Metal (Typically Aluminum, Silver. or Gold) Foil Evaporated at Nanoscale Thickness by Vacuum Evaporation Onto the Surface of Element B.

D. Detector Array or P. Optical Fiber Probe

Figure 3.2: Optical elements of SPSTM in Kretschmann configuration

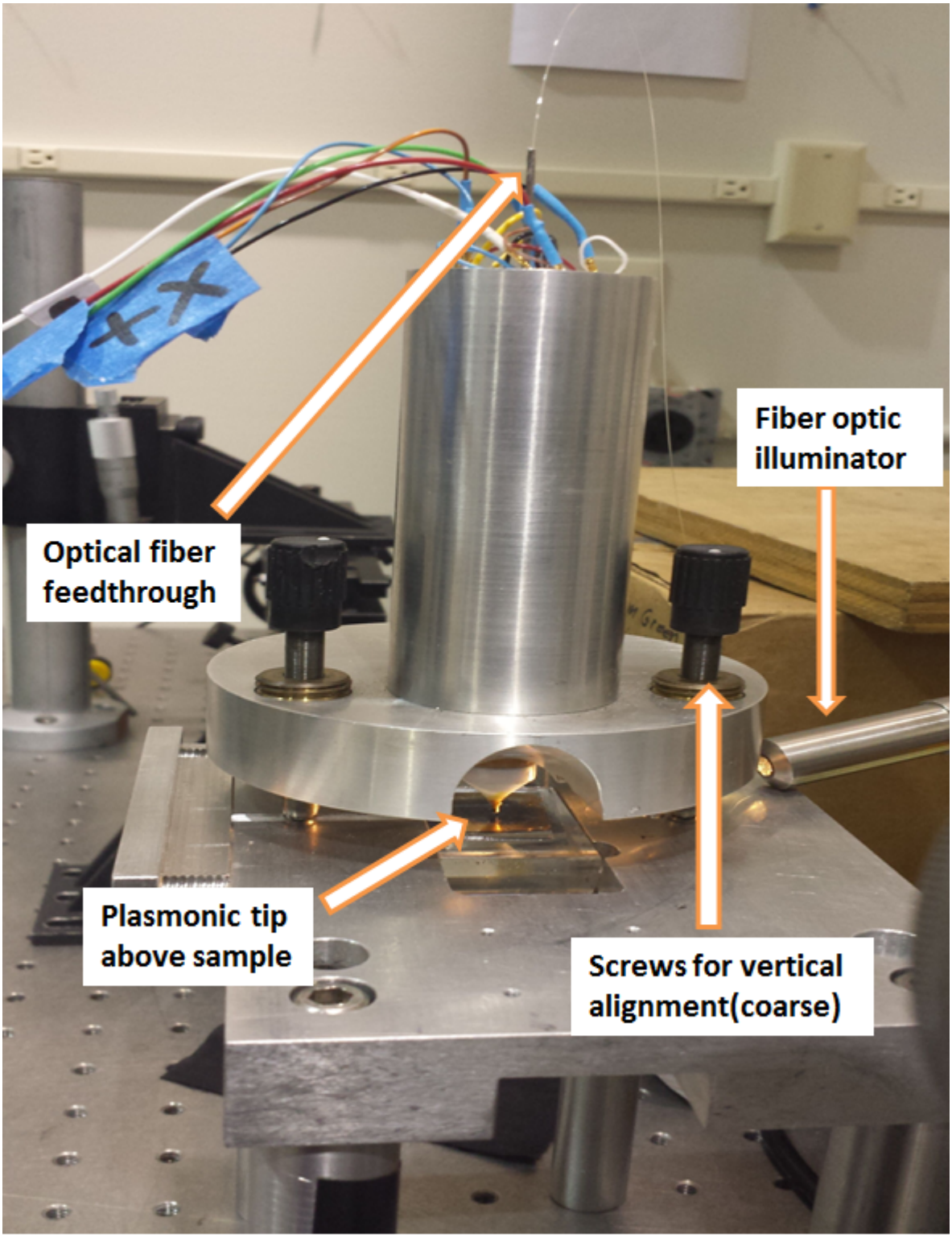

Figure 3.3: Scanner head

3.2 Fabrication of Plasmonic Probe

Plasmonic probe plays very important role in the collection and transmission of the signal to waveguide. Dimensions of the probe tip are crucial as lateral resolution of scan depends on geometry of the tip. Fabrication of a plasmonic probe is a two step process. In first step, cladding and the buffer is removed and core of the optical fiber (quartz) is made sharp to the nanometer scale using a micropipette tip puller (Figure 3.6). In second step, sharp end of optical fiber [18] is coated with a metal. Corning 50/125 multimode optical fiber (Figure 3.4) and Jonard JIC-375 Three Hole Fiber Optic Stripper (Figure 3.5) are used as fabrication tools.

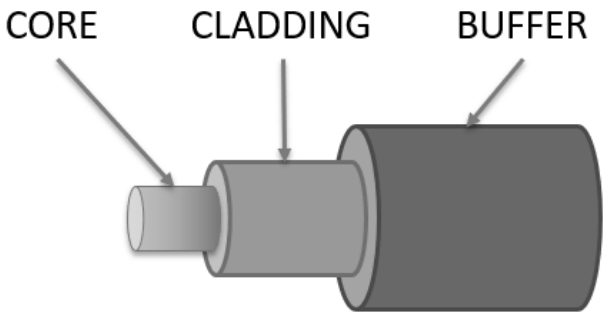

Figure 3.4: Corning 50/125 multimode optical fiber configuration



Figure 3.5: Jonard JIC-375 optical fiber stripping tool

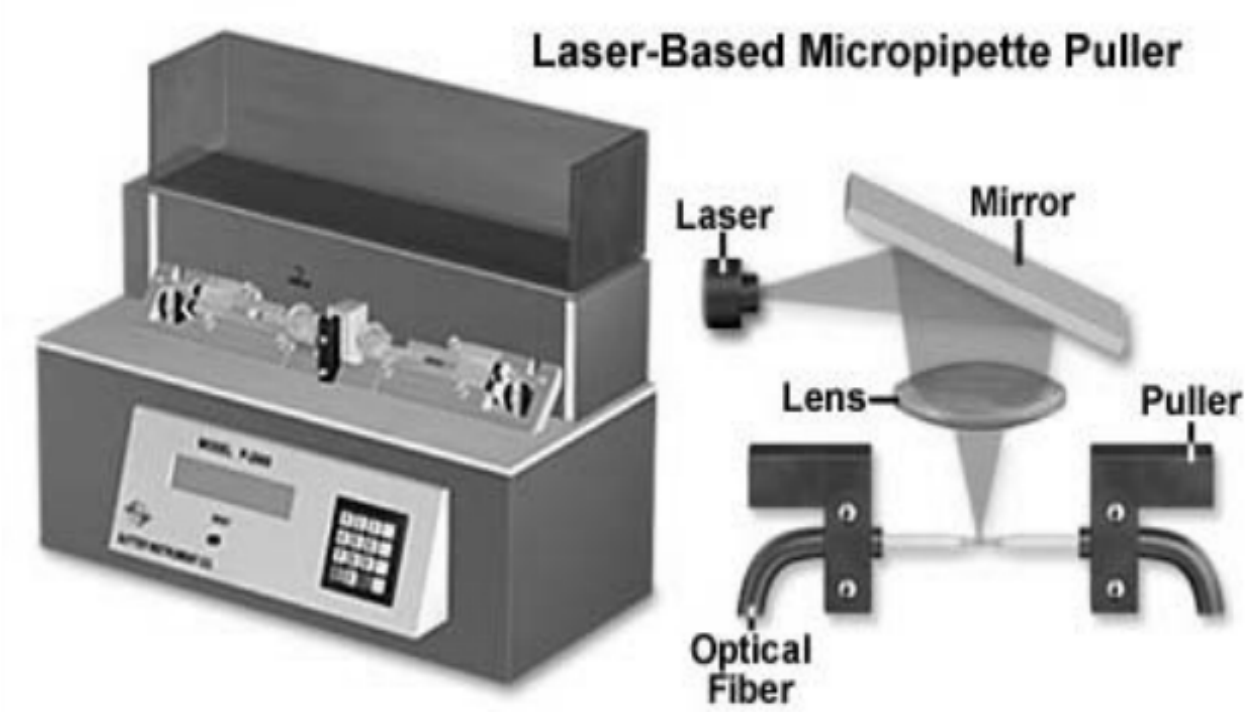

Figure 3.6: P-2000 Micropipette puller schematic. Source: Sutter Instruments

Buffer and cladding of the optical fiber is stripped using a optical fiber stripper, it is then cleaned with IPA wipe. Optical fiber is then loaded in a micropipette tip puller [15] (P-2000 by Sutter Instruments) which uses focused CO_2 laser to heat the fiber core and simultaneously pulls the fiber from both sides that results in long sharp fiber with end diameter being as small as 30 nm. Optical fiber end of varying geometries can be fabricated by varying following parameters of a tip puller.

1) Heat- The HEAT setting will affect the length and tip size of the fiber
2) Delay- The DELAY controls the amount of time the fiber has to cool before the pull begins
3) Pull- This controls the amount of force with which fiber is puller, hard pull will result in blunt and cracked fibers and soft pull will generally result in more uniform fiber ends
4) Rest of the two parameters(FIL and VEL) should be kept constant for optical fiber pulling

Following parameters were used to fabricate tip with sharp ends i.e. with tip diameter being 20-30 nm

Heat: 275
Delay: 127
Pull: 242

Slight deviation from these values will result in different tip geometries which could be useful to image surfaces of various topologies e.g. it will be advantageous to have a sharper tip if high lateral resolution is desired and a flat tip will give less resolution but will collect more signal. Following steps should be followed to get sharp and smooth tips:

1. Cut three feet of fiber or more if needed
2. Strip the middle of the fiber with the stripping tool, this removes the protective cover
3. Clean with alcohol (wipe off the stripped section)
4. Put fiber in the P-2000 puller. It is very important to put the fiber into the puller carefully. If it is not aligned properly the laser in the puller will not hit the fiber, use the groves in the puller to line the fiber up
5. Set the parameter for the tip puller
6. Start pull (push pull button) The fiber should break in 0.15 sec or less
7. Look at the tip under a microscope to make sure they are of desired geometry

Once fiber tips with desired sharpness have been made, next step would be to coat them with a metal. Several fibers are loaded on a fiber holder that is loaded in a coating chamber to coat 50 nm of gold. This would result in plasmonic probe/s ready to be loaded in a scanner head.



Figure 3.7: JDSU 1100 series HeNe laser and power supply

3.3 Laser for Exciting Surface Plasmons

JDSU 1100 continuous wave (Figure 3.7), low noise, 7 mW HeNe laser [Wikipedia] was used to excite surface plasmons on gold film which was deposited by AJA Orin magnetron sputtering system. Wavelength of laser was 632.8 nm, beam diameter was 0.81 mm, output power being 7 mW in TEM_{oo} mode with 500:1 polarization. Plane of polarization of an electromagnetic wave is taken to be the plane containing the electric field vector E , and the direction of propagation, K. Coherent linearly polarized light is described by the equation:

$$E = E_{o,x} \cos(kz - \omega t)x \tag{3.1}$$

This equation represents a wave of amplitude $E_{o,x}$, wavelength $\lambda = 2\pi/k$, propagating in the z-direction polarized in the (x,z) plane.

Surface plasmons [25] needs to be excited in a resonant manner. Surface plasmons can be excited either by bombarding electrons or by coupling light beam whose momentum matches to that of plasmons. There are more than one ways by which momentum of incoming light

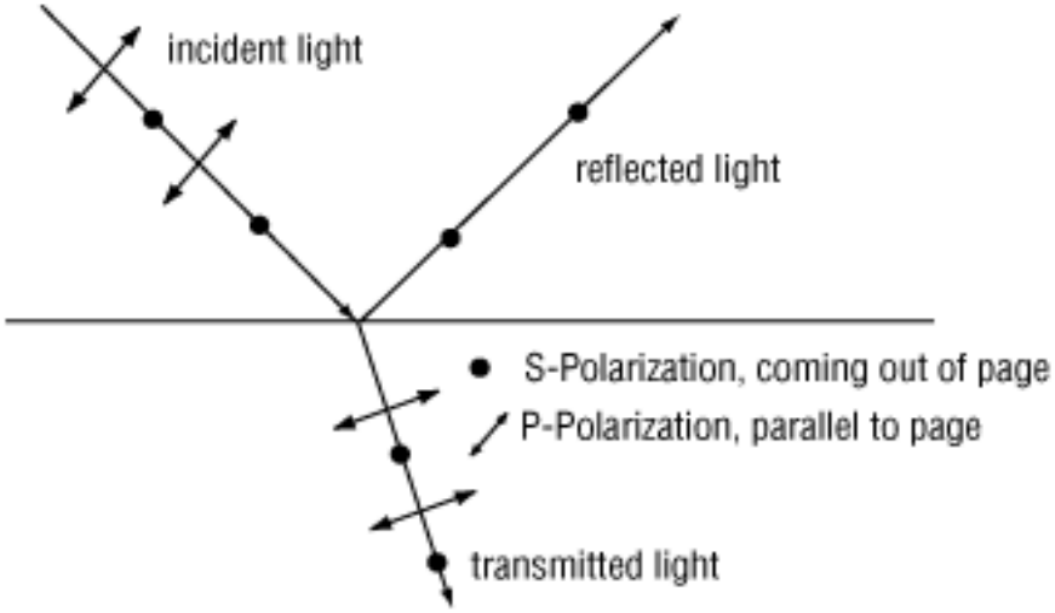

Figure 3.8: S and P polarization

beam can be matched to plasmons, most common being kretchman's configuration [12] and otto's configuration. Both configuration uses metal film on a prism, in case of former light is incident at metal dielectric interface with metal being infinitely large compared to glass and in latter case metal is thin as compared to infinite dielectric medium (Figure 3.9). Glass is used to increase the wavenumber of photon. S-polarized light (Figure 3.8) (polarization occurs perpendicular to the plane of incidence) cannot excite electronic surface plasmons due to momentum mismatch. It is important to use a focusing lens to reduce the laser beam spot size to match to the sample size e.g. in this case a lens of focal length 200 mm was used, which reduced beam spot to about 100 micrometer is diameter.

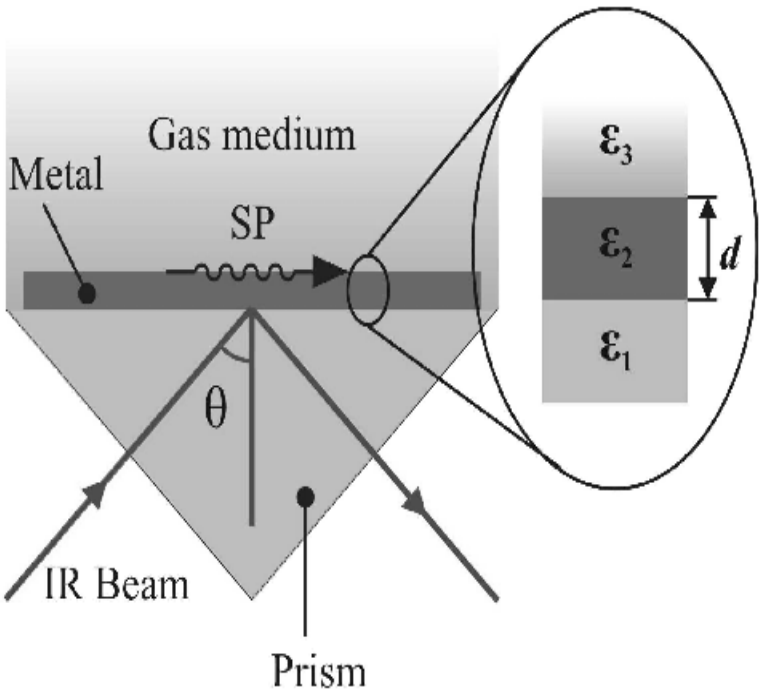

Figure 3.9: Kretschmann configuration

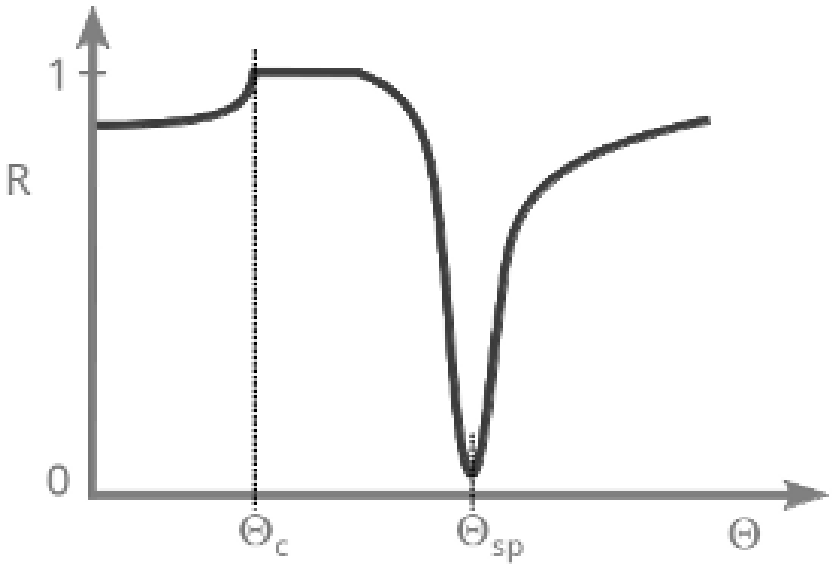

Figure 3.10: Surface Plasmon Resonance angle (θ_{sp})

3.4 Microscope Head

3.4.1 Scanner head construction

Microscope's scanner head consists of two piezoceramic tubes [47] connected by finely machined macor (Figure F.1). Piezoceramic tube actuators are monolithic actuator which can contract axially as soon as voltage is applied across the tubes i.e. between outer and inner electrode. Uniform alignment of dipole moments in piezoelectric material produces strain(hence motion) when voltage is applied. This is possible due to a process called poling of piezoelectric tubes (Figure 3.11), this process is a part of fabrication process during which scanners are heated to about 200°C to free the dipoles, and a DC voltage is applied to the scanner, application of DC voltage makes dipoles to align as per the applied electric field. Piezoelectric tubes are then cooled to freeze the dipoles in their aligned state. Piezoelectric tubes are coated with metal (gold) inside and outside, this coating acts as an electrode, wires from contacts are soldered directly to the surface of piezoelectric tube to transmit voltage from Nanoscope controller to the piezoelectric tubes. Outer surface (metal coating) of xy tube is segmented so that different electric potentials can be applied to different sections of tube which allows it to move in different directions.

Polarized piezoelectric material is characterized by many coefficients. However, these relationships can be simplified for small signal values i.e. for small electrical and mechanical amplitudes.

$$S = S^E \times T + d \times E \tag{3.2}$$

$$D = d \times T + \epsilon^T \times E \tag{3.3}$$

Where

D= Electric flux density

T= Mechanical stress

E= Electric field

S= Mechanical strain

d= Piezoelectric charge coefficient

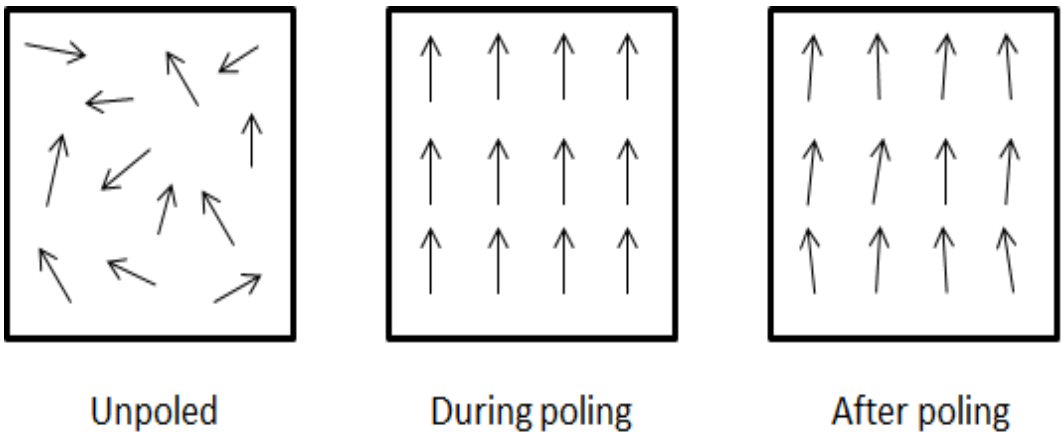

Figure 3.11: Possible orientation of piezoelectric crystal domains

ϵT= Permittivity

sE= Elasticity coefficient

Tube away from the fiber end can move radially in xy direction and tube closer to fiber end can extend and contract axially. Base of the scanner head has six electrodes (contact metal pins), one for each direction. Hypo-tubing passes through the axis of the scanner head, this hollow cylindrical tube holds the optical fiber, one side of which is fabricated as nanoscale plasmonic probe to collect signal and other end is coupled to photomultiplier tube. It is important to remove water from the piezoelectric tubes as it can damage electrical isolation hence, complete scanner head was baked at 90°C for 1 hour and was allowed to cool slowly. It is important to not exceed baking temperature more than 100°C. Baking piezo tubes at higher temperature can lead to de-poling (Figure 3.11). It was then coated with a thin layer of polymer to avoid hydration. Polymer was prepared by dissolving Styrofoam in chloroform, once mixture was ready scanner head was dipped in the solution for a few seconds and then was kept in the ambient to allow chloroform to evaporate leaving Styrofoam coating on the scanner head.

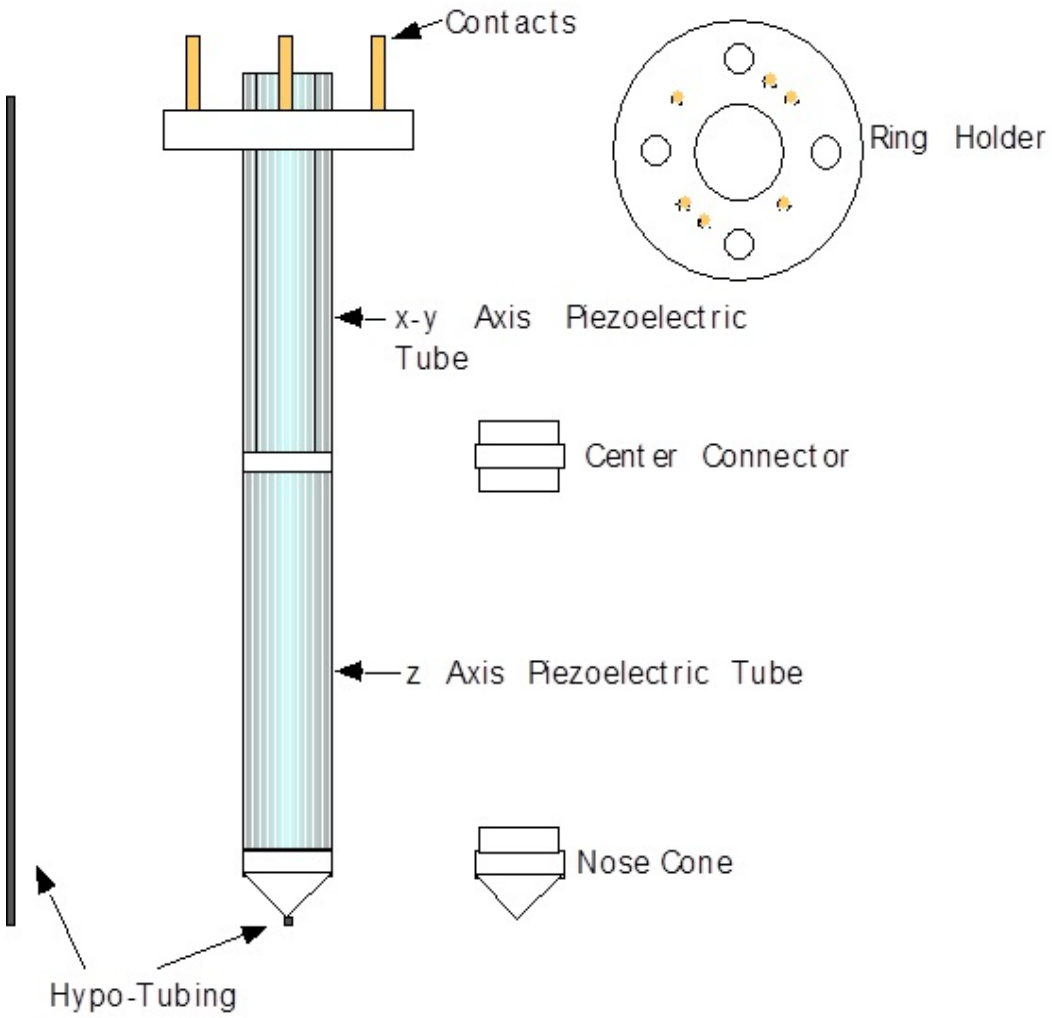

Figure 3.12: Piezoelectric tubes in scanner head

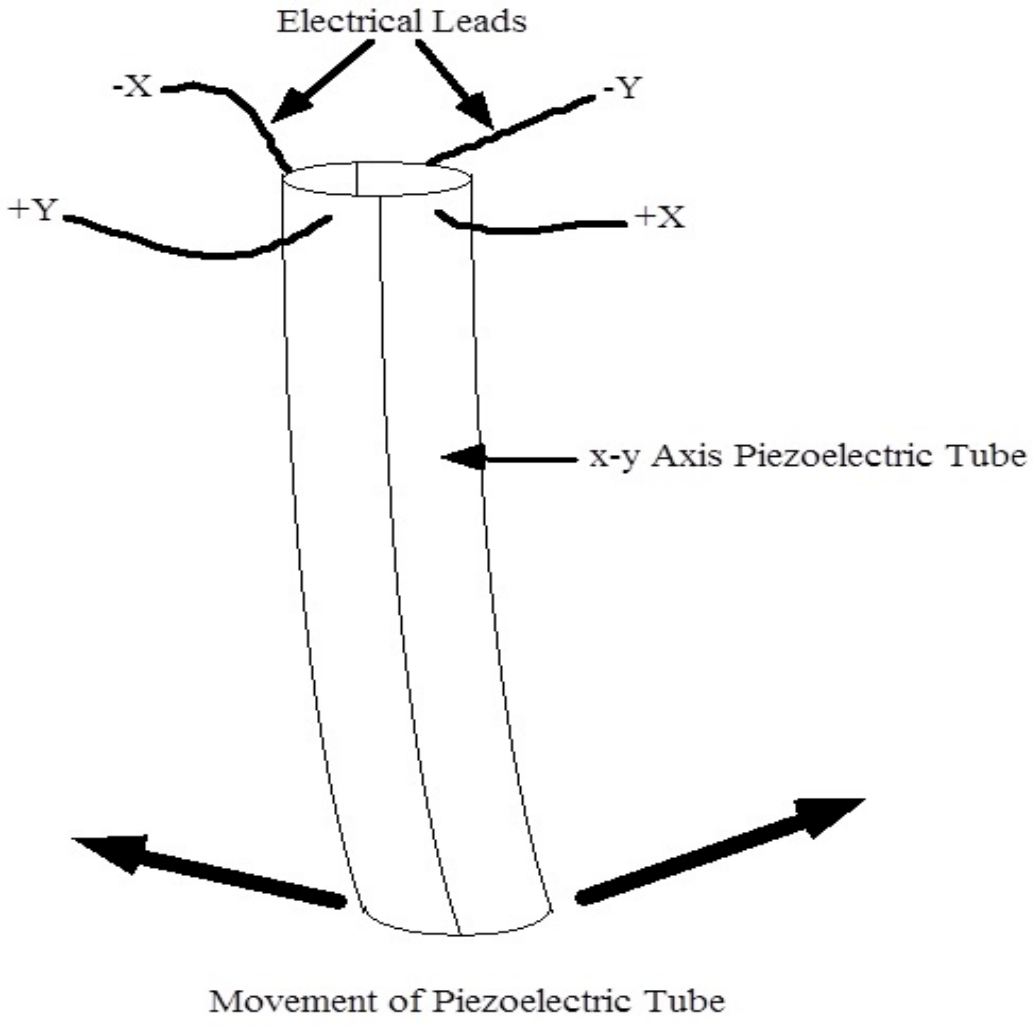

Figure 3.13: XY piezoelectric tube

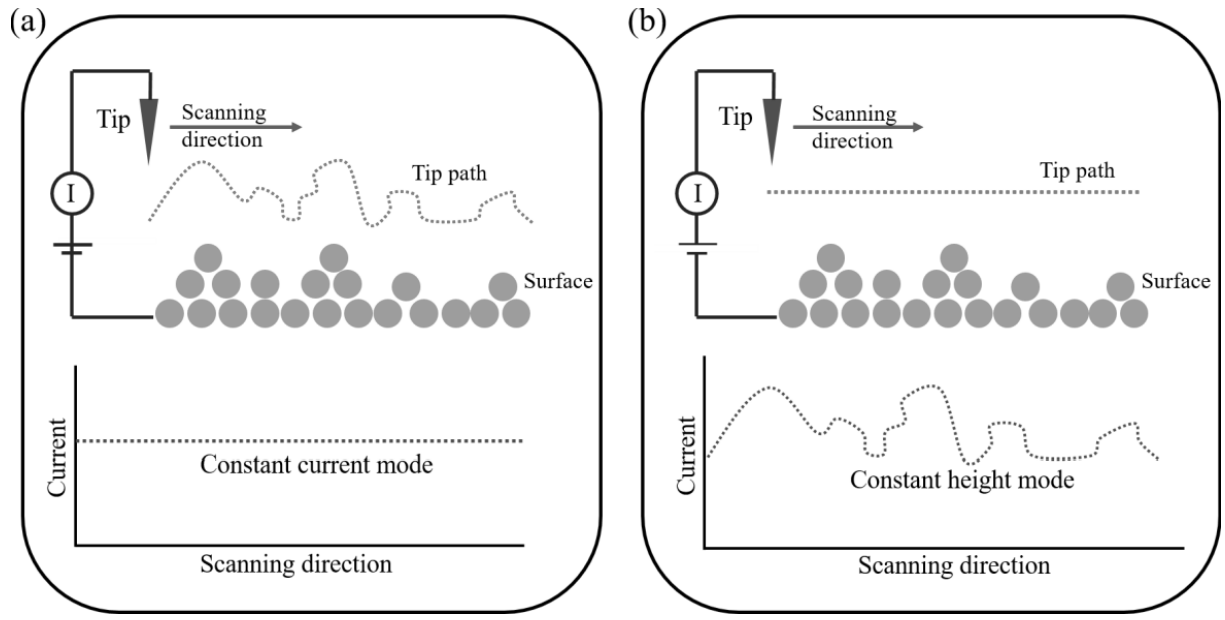

Figure 3.14: Scan modes: a) Constant current mode b) Constant height mode

3.4.2 Nanoscope IIIA Controller

Nanoscope IIIA was used to control the scanner head and to collect data. It comes with inbuilt software similar to the one used for STM. Apart from having various features to process data/images it can be used to scan in two modes (Figure 3.14) i.e. constant height and constant current mode. In constant current mode tunneling current remains constant, this is achieved by varying the voltage to the z piezoelectric tube which makes the tube to alter its length as it scans a sample. In constant height mode, there is no alteration in z tube's length and tip scans the area without any variation across z direction, image in this case is plotted as a variation of tunneling current.

Computer with this software is connected to the Nanoscope controller which has six op-amps (Figure E.1) to drive xy and z tube. Each op-amp (Figure E.2) drives piezotube in a direction by producing 100 to 200 Volts. Nanoscope controller also collects analog signal from current amplifier and converts to digital signal for the software to process.

Optical signal collected by optical fiber is converted to electrical signal by PMT which in turn is connected to current amplifier. PMT being a current source provides current in mA range, current amplifier converts it to voltage and that is fed to Nanoscope controller. Below is the schematic which explains connection between various components explained above

3.5 Signal Detection Assembly

3.5.1 Photomultiplier tube

Photomultiplier tubes (PMTs) (Figure 3.16) are used to detect faint optical signals from weakly emitting sources. Photomultipliers are contained within a glass tube that maintains a vacuum within the device. There are three main electrodes within a photomultiplier:

1)Photocathode
2)Dynodes
3)Anode

Within the envelope of the photomultiplier, there is one photocathode, one anode and several dynodes. Photons enter the photomultiplier tube and strike the photocathode. When this occurs, electrons are produced as a result of the photoelectric effect.

Once the electrons have been generated they are directed towards an area of the photomultiplier called the electron multiplier. As the name suggests, this area serves to increase or multiply the number of electrons by a process known as secondary emission. Each incoming photon generates primary electrons, number of primary electrons emitted by an incoming photon depends on the energy of incident photons. Focusing electrodes are present right after first dynode to ensure that all primary electrons reach next dynode and there is minimum loss of signal during amplification process. These primary electrons are then accelerated by nearest dynodes (Figure 3.15) and they in turn produce more electrons, this amplification process continues until last dynode. There are several factors that contribute to net amplification like spectral response, quantum efficiency, sensitivity and dark current determines overall reponse of a photomultiplie to incident photons. As photomultipliers do not store charge and respond to changes in input light fluxes within a few nanoseconds, they can be used for the detection and recording of extremely fast events.

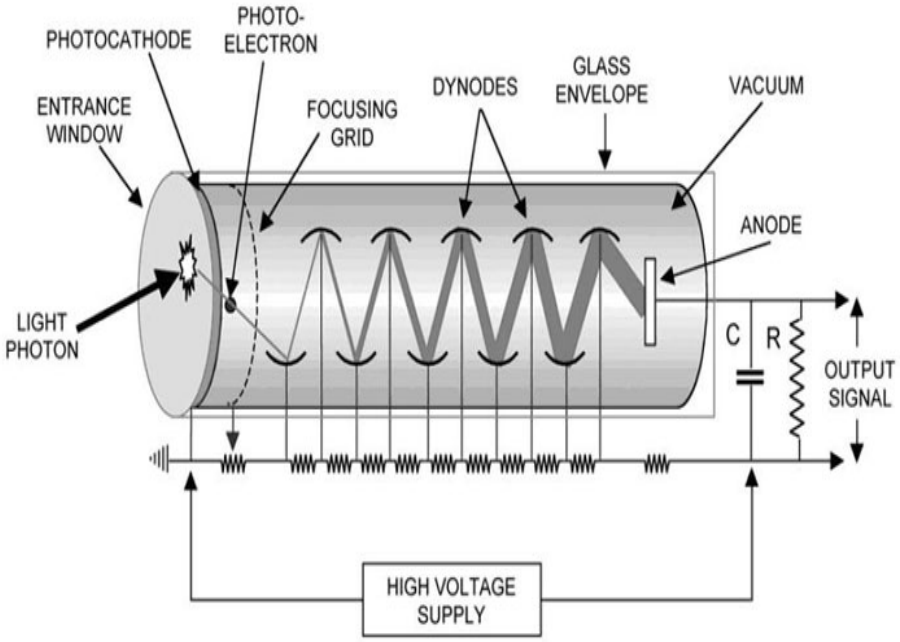

Figure 3.15: Photomultiplier tube schematic. Source: www.hamamatsu.com



Figure 3.16: Photomultiplier tube IP28

The electron multiplier is made up from a number of electrodes, called dynodes. These dynodes have different voltages on them, each one is more positive voltage than the previous one to provide the required environment to produce the electron multiplication effect. This operates by pulling electrons progressively towards the more positive areas in the following way. The electrons leave the photocathode with the energy received from the incoming photon. They move towards the first dynode and they are accelerated by the electric field and they arrive with much greater energy than they left the cathode. When they strike the first dynode more low energy electrons are released, and these are in turn attracted by the greater positive field of the next dynode, and these electrons are similarly accelerated by the greater positive potential of the second dynode, and this process is repeated along all the dynodes until the electrons reach the anode where they are collected.

The geometry of the dynode chain is carefully designed so that amplification effect occurs along its length with an ever increasing number of electrons being produced at each stage. When the anode is reached, the accumulation of charge results in a sharp current pulse for the arrival of each photon at the photocathode.

The detected current depends on two factors; the number of electrons ejected from the cathode (which in turn depends on the number of incoming photons and on their energy), and the gain of the photomultiplier. The gain is defined as the number of electrons collected at the anode relative to the number of electrons ejected from the cathode. Let g be the number of electrons liberated at any one dynode when a high energy electron strikes it (the dynode gain) and N be the number of dynodes of the photomultiplier.

Then the overall gain of the PMT is equal to g^N. For example, if $g = 2$ and $N = 10$ (a ten stage tube) then the gain is $\sim$1,000. However this gain is strongly dependent on the applied voltage. If the voltage is raised then the accelerating fields are stronger. That means the the energy of an electron as it strikes a dynode is also increased, and more electrons are released from the dynode. Suppose that the applied voltage is raised to make $g = 4$. Then the PMT gain becomes $\sim$105,000,0. Adjusting the gain of the photomultiplier tube by changing the voltage is commonly used to adjust the strength of the signal to accommodate both strong and weak light sources. To calculate the current we also need to know the number of electrons ejected from the cathode, which depends on two factors. First, the number

of incoming photons per second, also called the quantum efficiency, defined as the average number of electrons released from the cathode by the photoelectric effect per photon.

Let us suppose that 1 pW of light of wavelength 500 nm falls on a cathode whose quantum efficiency is 15 %. Then energy of one photon will be

$$\frac{h}{\nu} = \frac{hc}{\lambda} = \frac{6.62 \times 10^{-34} \times 3 \times 10^{8}}{5 \times 10^{-7}} = 3.98 \times 10^{-19} \text{ Joule} \tag{3.4}$$

Number of photons ejected from the cathode will be

$$\frac{10^{-12}\text{W}}{3.98 \times 10^{-19}\text{J}} = 2.5 \times 10^{6} \text{ photons/second} \tag{3.5}$$

Assuming gain of the photomultiplier tube to be 2×10^{6}, number of electrons then arriving at the anode would be

$$2.5 \times 10^{6} \times 2 \times 10^{6} = 5 \times 10^{12} \text{ electrons/second} \tag{3.6}$$

This will giave a current of

$$5 \times 10^{12} \times 1.6 \times 10^{-19} C = 8 \times 10^{-7} \text{ Amperes} \tag{3.7}$$

PMT is a current source, current amplifier should be set as per the current range being fed to it by PMT.

3.5.2 Current to Voltage Amplifier

A transimpedance amplifier (TIA) converts current to voltage. As photomultiplier tube is current source, its current response is more linear than voltage response. TIA offers low impedance to photomiltiplier tube and isolate it from output voltage of operational amplifier [1]. TIA is a commonly used amplifier for photodiodes, accelerometer and other types of sensors which are current sources. TIAs uses a resistor to dissipate current and used operational amplifier to for amplification.

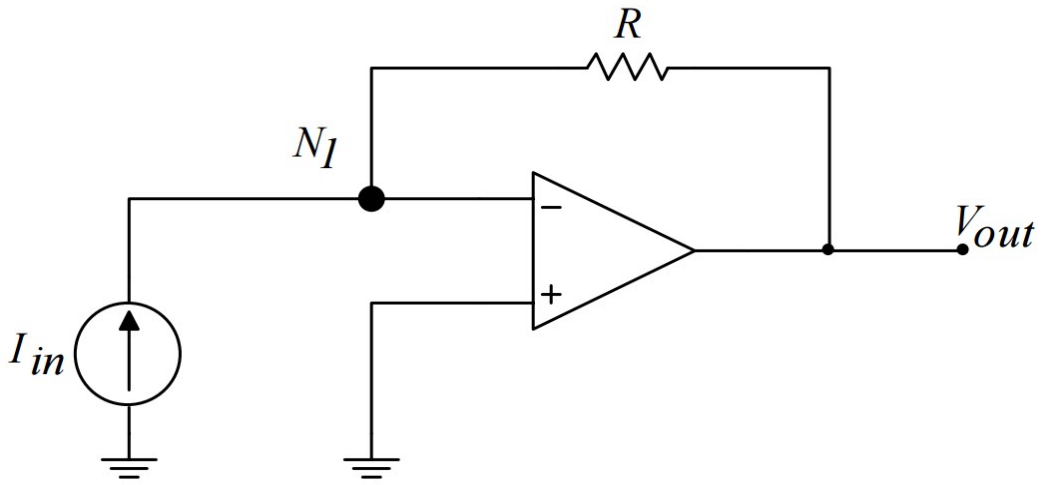

Figure 3.17: Current to voltage amplifier

(Figure 3.17) below represents a simplified diagram of current amplifier, I_{in} is current from PMT, R is sensitivity of the amplifier. Assuming that no current flows into op-amp, sum of current flowing into and out of Node N_1 is zero and V_{out} can be written as

$$I_1 + (V_{out} - 0/R) = 0 \tag{3.8}$$

$$V_{out} = -RI_1 \tag{3.9}$$

In some cases high sensitivity is required, in those cases high ohmic feedback resistor is replaced by three low ohmic resistors which are arranges like a 'T' hence the name 'T feedback network' (Figure 3.18). In this case part of amplified output is taken from input so that gain is controlled more by feedback network and less by open loop gain as shown below.

Voltage output is then given as:

$$V_{out} = -(1 + R_2/R_1 + R2/R)I_1 \tag{3.10}$$

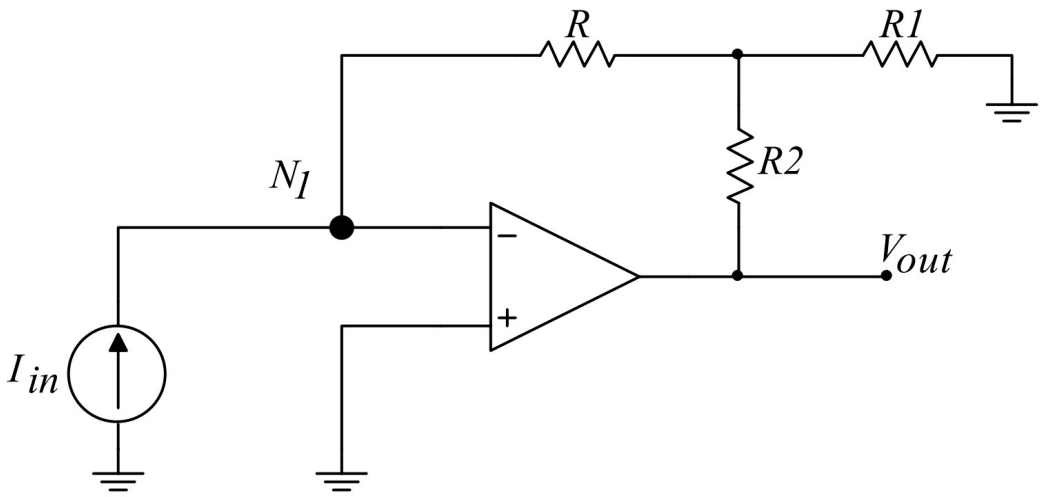

Figure 3.18: Current to voltage amplifier schematic for higher sensitivity

3.6 Apparatus Check: Step by step process to run Nanoscope Software

Nanoscope controller software (Figure 3.19) is provided by Digital Instruments Inc. and is designed to control STMs and AFMs. Homescreen of the software has interface for controlling the scan, feedback control, channel control and other controls. In the toolbar there are options to customize the software, most of the settings should be set to default. Piezoelectric tube calibration values should be entered and saved. Below are the steps to position the tip in evanescent region of the sample, once the tip is this region it can then be used to image.

1) In toolbar of home screen go to panels and enter x, y, z calibration values

2) Go to 'view' and click 'STS i(s) plot' this will provide constant bias voltage to piezo tubes and current vs tip height data is acquired, note that feedback at this point is disabled

3) Resolution of this z scan be controlled by entering 'number of samples' in 'Main Controls' window

4) Range of z scan can be adjusted by entering 'Ramp size' in 'Main Controls' window

5) Adjust screws on the microscope head to move the tip away and close to sample this is coarse adjustment of tip height

6) Tip can also be moved by changing the 'setpoint' value is STS plot, higher the setpoint closer the tip is to the sample. It is advisable to do coarse adjustments by screws on microcopic head and setpoint can be used for fine adjustments

7) Once a desired setpoint is reached, click 'scan' in 'view' and scan will start with the desired setpoint in constant height mode. Scan parameters(e.g. xy range, scan rate etc.) should be set before starting STS i(s) scan

8) Click camera icon at any point to save the scan, if this icon is clicked prior to starting the scan then data will be saved once scan is finished. It is possible to save partial scan by clicking it at any point. However, it is not possible to save data once scan is finished.

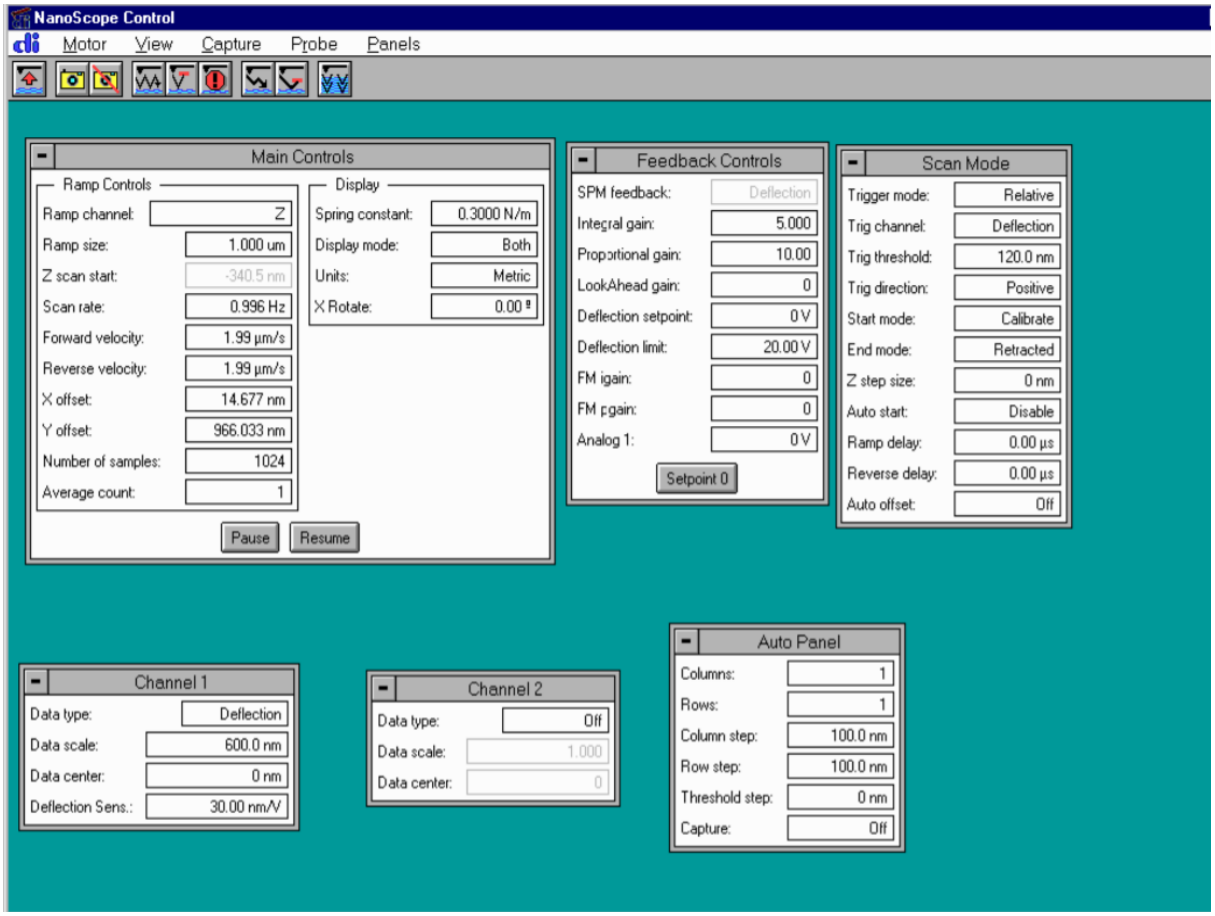

Figure 3.19: Home page of nanoscope software

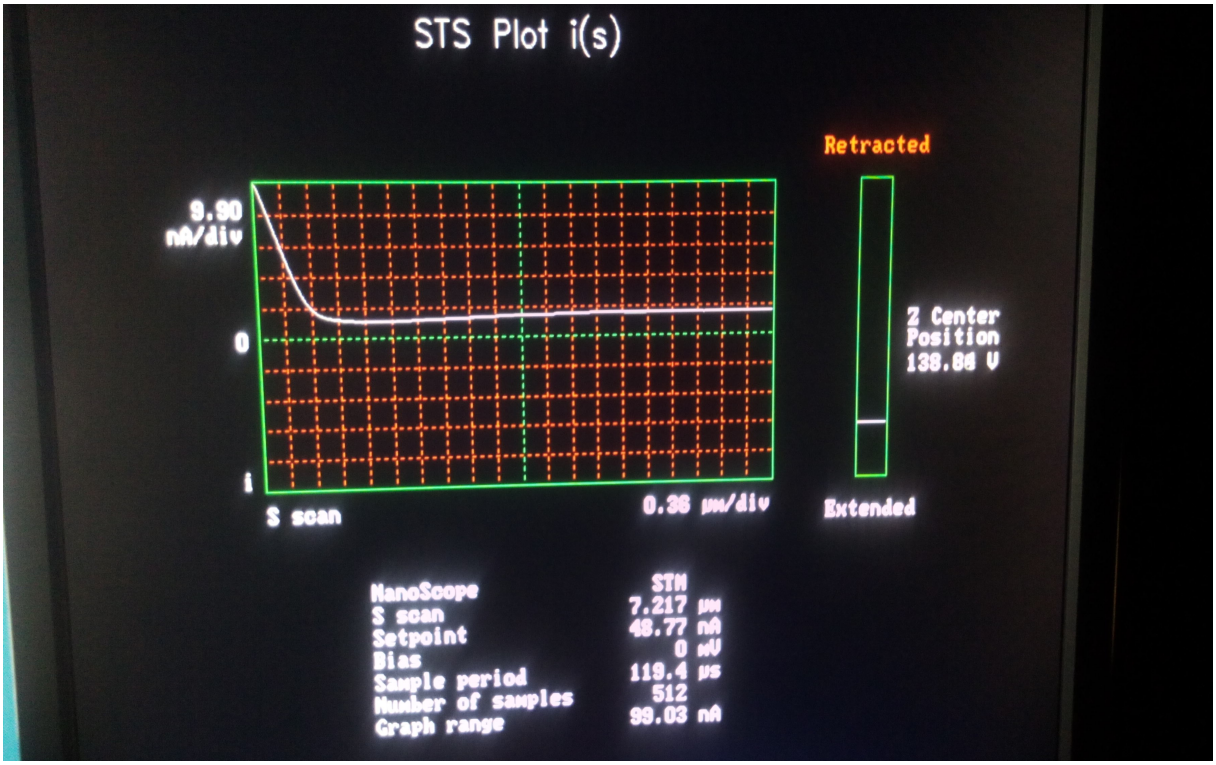

Figure 3.20: Signal strength vs distance plot

Figure 3.20 is a typical STS i(s) plot with tunneling signal strength on y axis and distance from sample on x axis. It is possible to change the scale of plot, number of samples, setpoint, z range in real time. Figure below was taken over a bare prism with the tip extending and retracting in direction perpendicular to the sample. Sample in this case is a bare prism and the incident beam is at an angle greater than the critical angle such that light is totally internally reflected. It is important to observe the surface of the prism while incident beam is totally reflected. Ideally, during TIR, beam spot on the surface of the prism should not be visible with bare eyes. However, practically it is not possible to get a perfectly clean and flat surface hence, there will always be some scattering of light from the top surface of the prim and beam spot may be visible due to light being scattered by imperfections/particles of the prism surface.

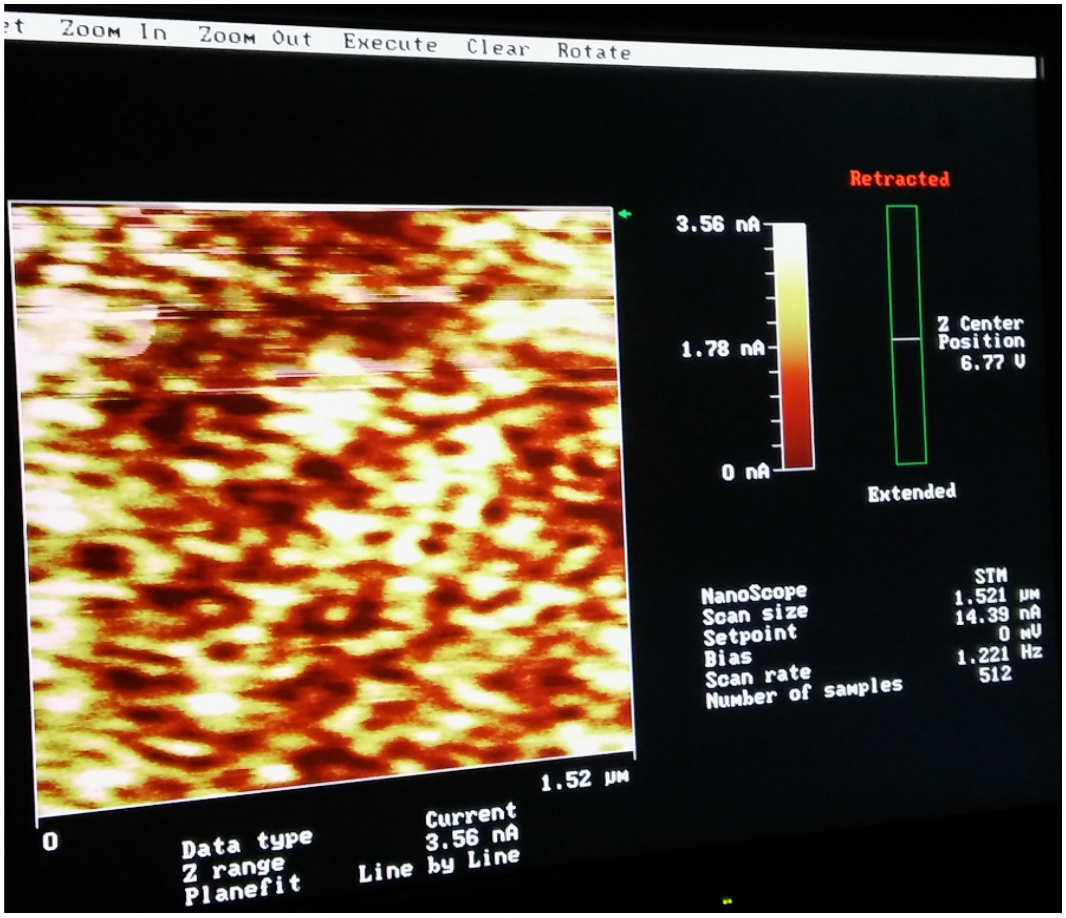

Figure 3.21: A test image of bare prism surface

Figure 3.21 is a test image of a bare prism obtained after a desired height (setpoint) was found using STS i(s) plot as in Figure 3.20. This image was obtained by raster scanning the tip over a bare prism. Scanning parameters such as scan size, scan rate, number of samples etc. are displayed along the image.

3.7 Sample Preparation

3.7.1 Gold film deposition by sputtering

Sputtering (Figure 3.22) is the process whereby atoms or molecules of a material are ejected from a target by the bombardment of high-energy particles. To obtain sputtering as a useful coating process a number of criteria must be met. Firstly, ions of sufficient energy must be created and directed towards the surface of a target to eject atoms from the material.

Secondly, ejected atoms must he able to move freely towards the object to be coated. This is why sputter coating is a vacuum process, low pressures are required to maintain high ion energies and to prevent too many atom-gas collisions after ejection from the target. It is important to consider mean free path here, it is the average distance that an atom can travel before hitting another atom.

RF Sputtering [33] runs an energetic wave through an inert gas in a vacuum chamber which becomes ionized. The target material or cathode which is to become the thin film coating is bombarded by these high energy ions sputtering off atoms as a fine spray covering the substrate to be coated. RF Magnetron sputtering uses magnets behind the negative cathode to trap electrons over the negatively charged target material so they are not free to bombard the substrate, allowing for faster deposition rates. Over time, positive ions are produced which accumulate on the surface of the target face giving it a positive charge. At a certain point this charge can build up and lead to a complete secession of sputtering atoms being discharged for coating. Gold was deposited on quartz coated slide using e-beam evaporator.

3.7.2 Plasma Glow Discharge

A gas plasma may form when gas is exposed to an electric field. If the field is strong enough, atoms fromm the gas will emit electrons and gas becomes ionized. So as to excite plasma, low current is passed through the gas as gas becomes ionized current flow increases but applied voltage remains same. Eventually, there are enough ions and charges for the plasma to be self-sustaining. When these ions collide with surface atoms of target, energy trasfer caused atoms to come off the surface and this is how deposition of target occurs.

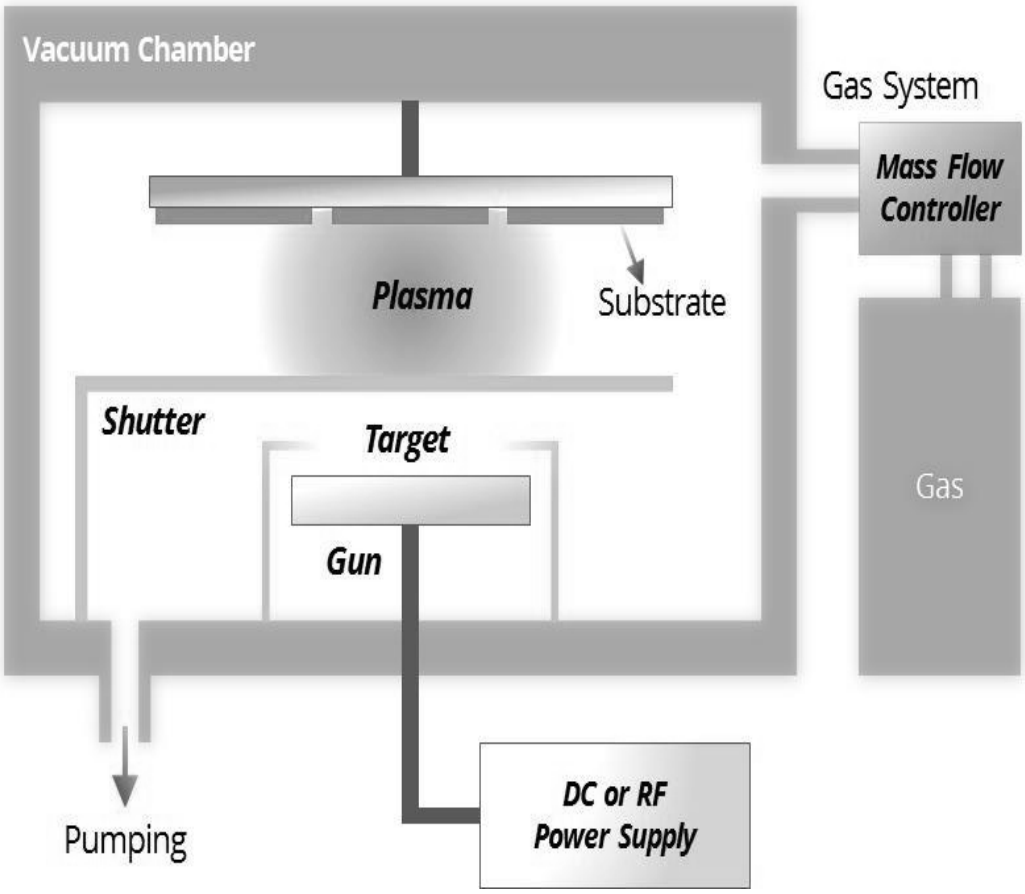

Figure 3.22: RF sputtering schematic

3.7.3 MoS_2 Exfoliation and Transfer over Gold Film

Molybdenum disulphide and transition metal dichalcogenides in general demonstrate affinity for gold [40]. It has been shown that strong van der Waals (vdW) interaction exists between gold and top most layer of bulk MoS_2. This property has been exploited to obtain thin MoS_2 flakes by mechanical exfoliation (Figure 3.23). Bulk crystal is gently pressed on scotch tape and scotch tape is repeatedly pressed against itself multiple times. This repeated exfoliation results in thinner flakes and scotch tape is pressed against final substrate (gold) where thinner flakes are desired. A fresh, smooth and clean substrate will have better adhesion and there is greater probability of large area thin flakes will adhering to it.

Gold coated quartz slide was first cleaned using acetone, IPA and DI water followed by plasma cleaning. Sonification in this case should be avoided as it can decrease adhesion of gold to quartz slide and can cause metal to come off resulting in non uniform thickness and a rough surface. So as to transfer thin MoS_2 flakes on gold, bulk MoS_2 was first exfoliated on scotch tape and scotch tape was then gently pressed against gently heated 40^oC gold coated slide. After tape being in contact with gold for about 30 seconds it was then gently peeled off. Slide was then examined under optical microscope to identify thin and large exfoliated MoS_2 flakes, these flakes were later identified by markers made around it. These markers would then be used to land plasmonic tip over the desired flake/s gold film exposed to ambient environment for extended duration decreases its affinity and results in poor yield. Freshness of metal film plays an important role in exfoliating large area thin flakes hence it is essential to exfoliate MoS_2 as soon as gold film is deposited. It is important to minimize area of contact between tape and metal layer, large contact area or excess glue may peel off gold layers during the process. It is advised to have most of the Nitto tape covered by exfoliating material so as to minimize the possible damage glue may cause.

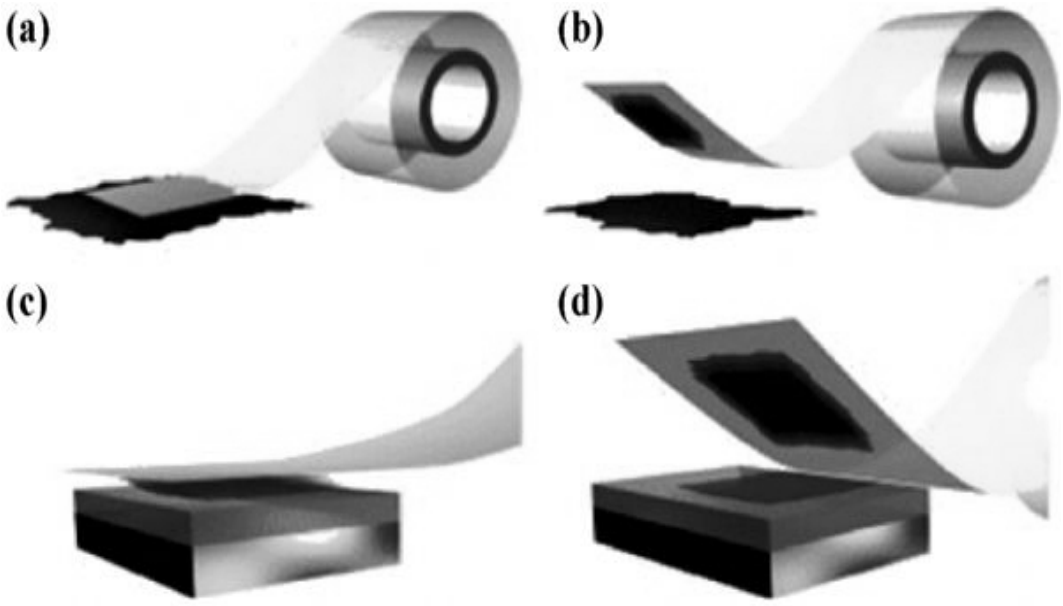

Figure 3.23: MoS_2 exfoliation using Nitto tape. Source: Slideshare.net/mechanical exfoliation

Chapter 4

Results and Discussion

4.1 Plasmonic Probe tips

The probe tip is a vital component of any scanning probe microscope. For SPSTM it is important to have optical fiber tips fabricated for maximum throughput of the tunnelled signal. There is a compromise between resolution and signal strength, a sharp tip provides better lateral resolution but signal tunneled is low in intensity, a dull tip will collect more signal but will decrease resolution. Thin metal layer on the tip not only makes it sturdy but also causes field enhancement (Figure 2.7) thus amplifying the signal. Metal coating also prevents scattered light from entering the fiber.

Corning 50/125 fiber was cut from the fiber roll, one end of the fiber was cleaned with IPA wipe and plastic coating along with cladding was stripped off using fiber stripper. Stripped fiber was loaded in a tip puller (Figure 3.6) and a sharp tip was pulled with the very end of the tip being about 100 nm, it was then coated with 50 nm of gold using magnetron sputterer (Figure 3.22). Tip puller will generate two identical tips in each pull. Fabricated tip are examined under optical for microscope for its desired gometry, optical images of plasmonic tips are shown in Figure 4.1, Figure 4.2, Figure 4.3 and Figure 4.4.

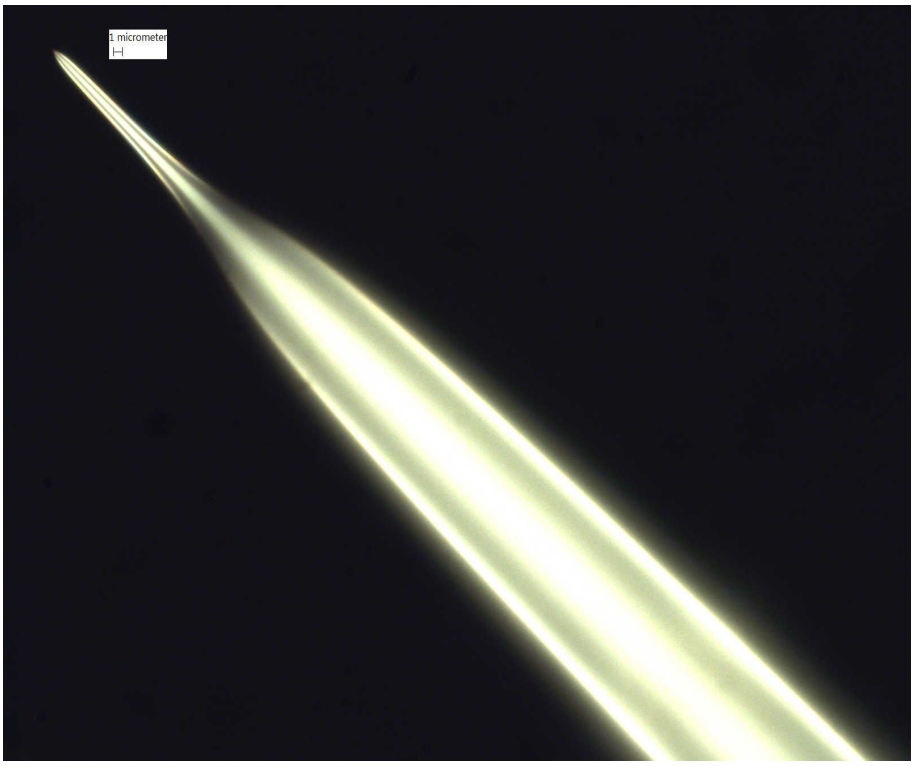

Figure 4.1: An optical image of metal coated tip: geometry 1

It is common for tips to crash while imaging and sometimes it happens even before data collection starts. Hence, imaging a tip after data collection becomes important. While imaging a sample with SEM charging effect should be avoided, since tip is coated with metal we need to ensure smooth passage of electrons from tip to SEM sample holder. Metal coated tips are hence loaded in metal tubes which are glued to holder with carbon tape as shown in (Figure 4.5). If tips are found crashed after scans then its advised to check sample for contamination by possible debris from crashed tip. SEM images of tips post data collection are shown in Figure 4.6, Figure 4.7 and Figure 4.8. Figure 4.8 shows a low resolution SEM scan of the tip held in a metallic holder, using a silver paste to hold metal coated tip to the holder will ensure smooth electrical path to SEM holder.

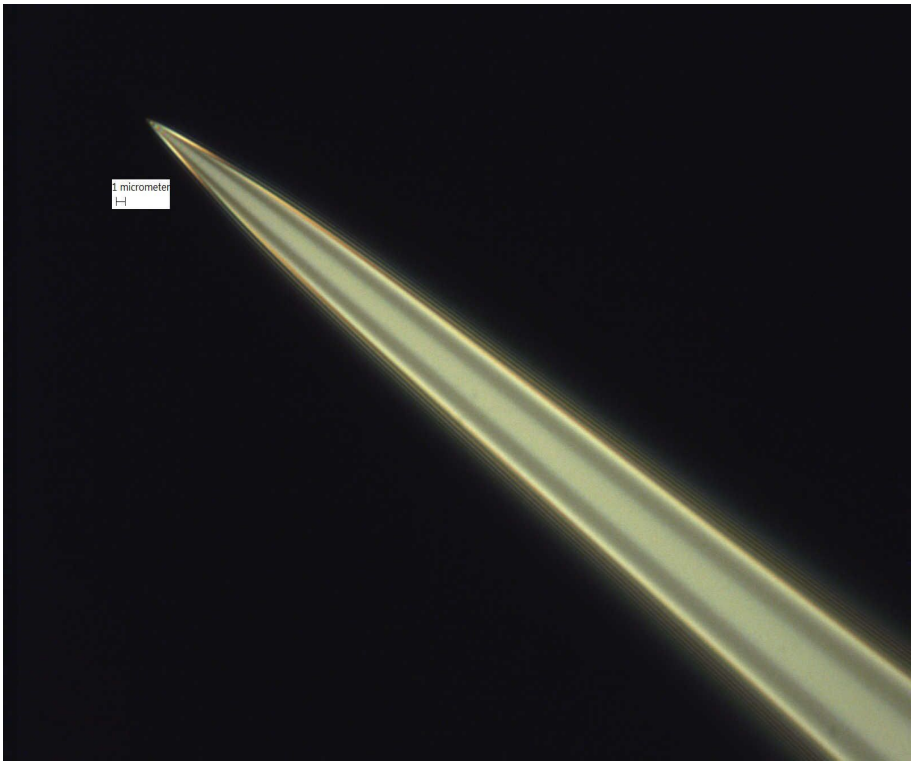

Figure 4.2: An optical image of metal coated tip: geometry 2

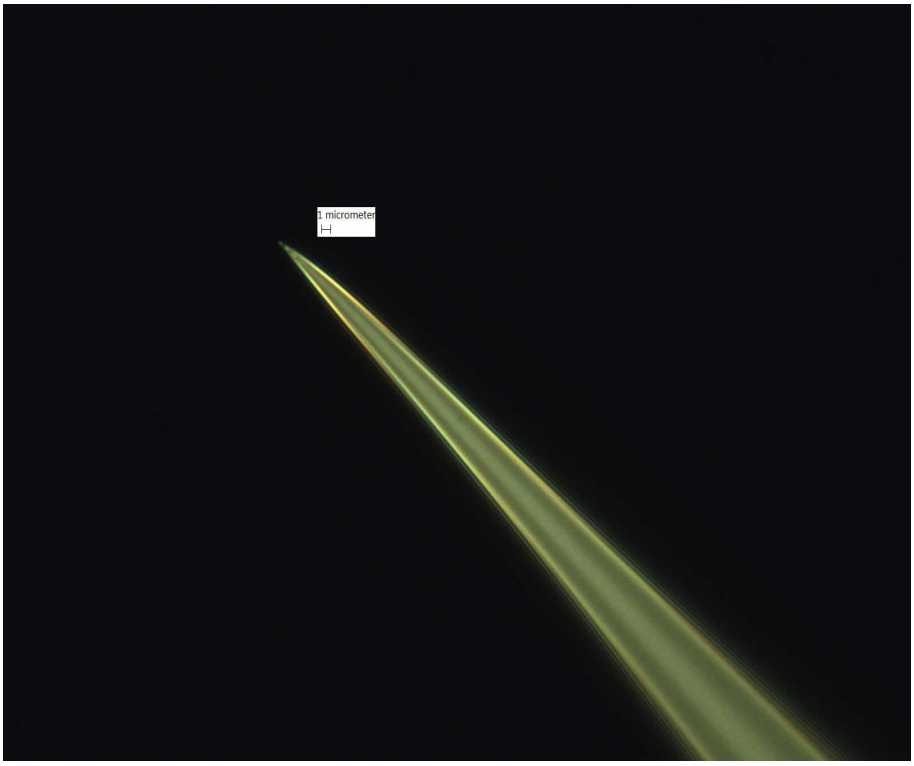

Figure 4.3: An optical image of metal coated tip: geometry 3

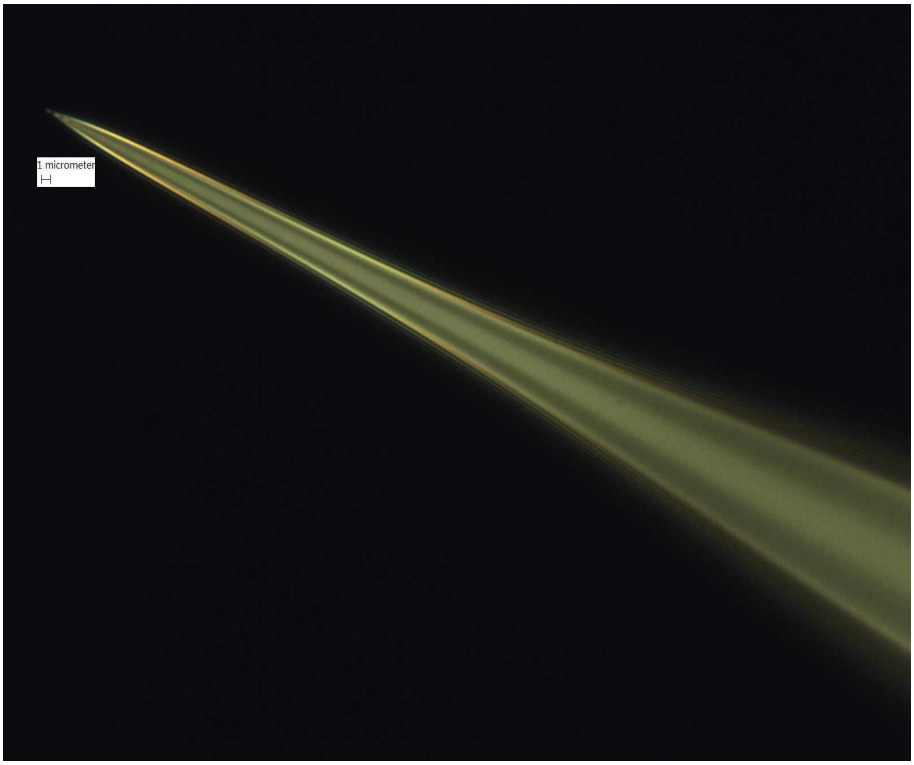

Figure 4.4: An optical image of metal coated tip: geometry 4

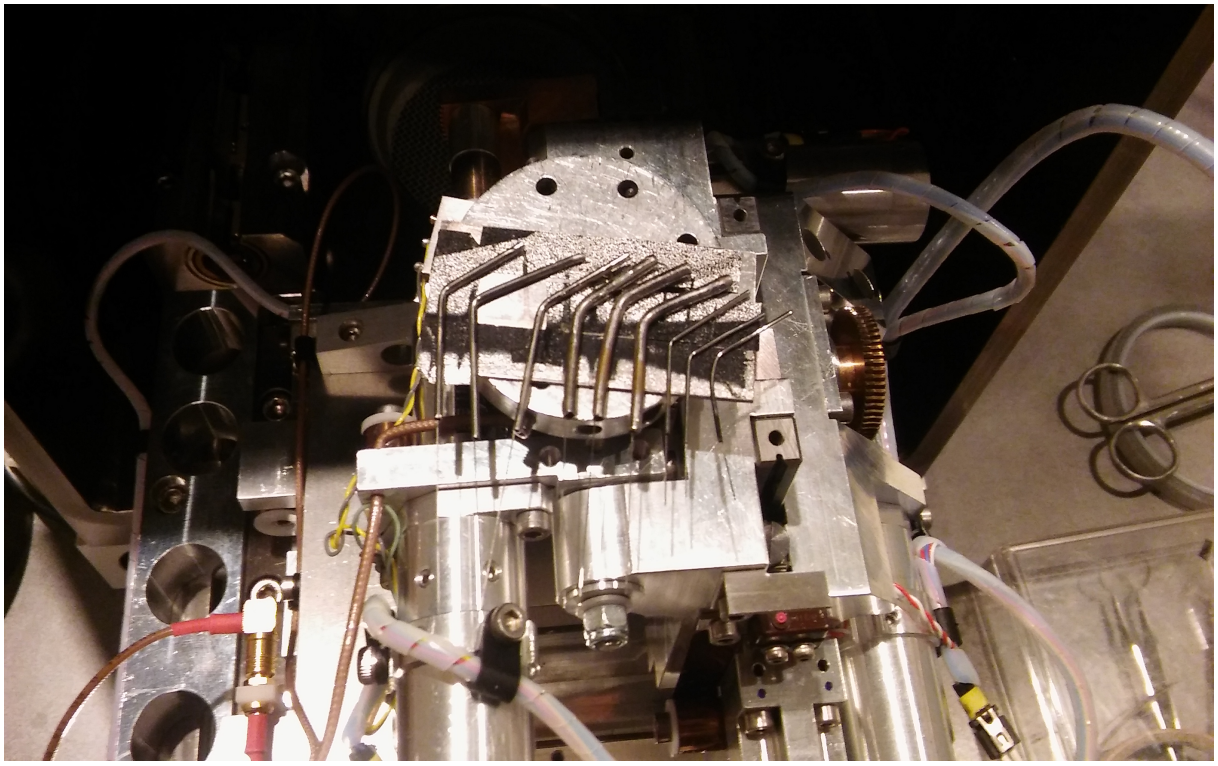

Figure 4.5: Fiber holder for SEM

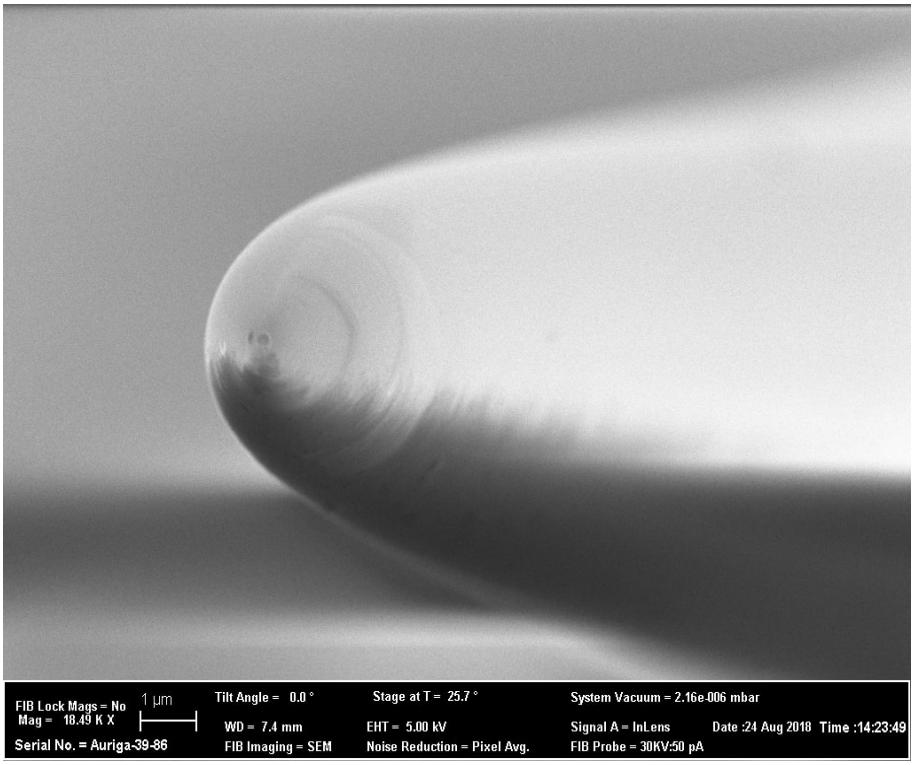

Figure 4.6: SEM image of the metal coated tip: view 1

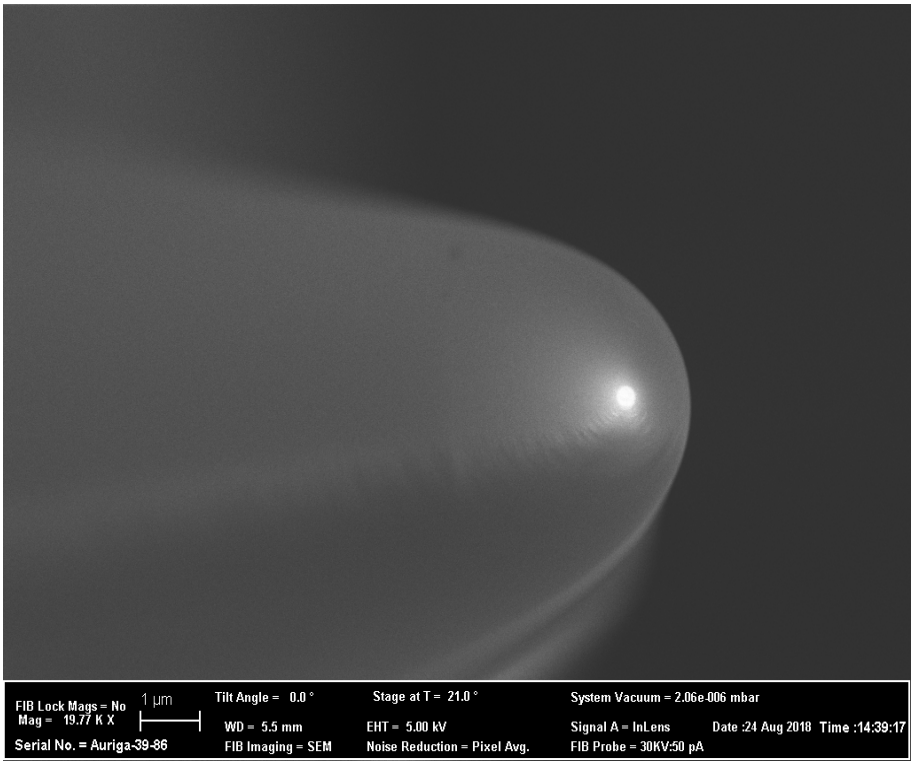

Figure 4.7: SEM image of the metal coated tip: view 2

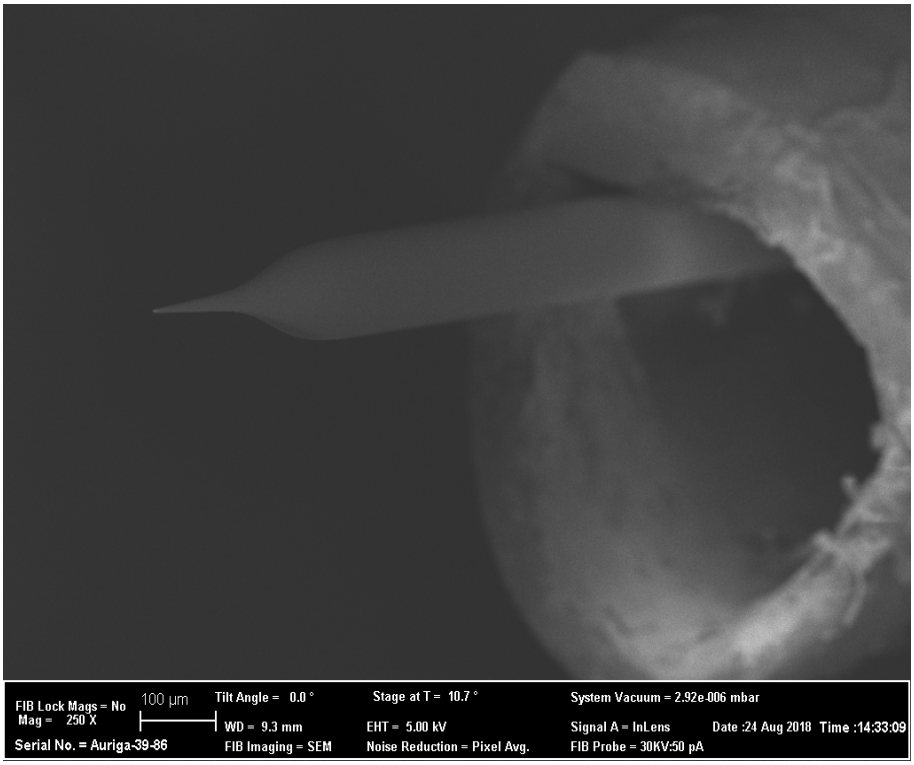

Figure 4.8: SEM image of the metal coated tip in metallic holder

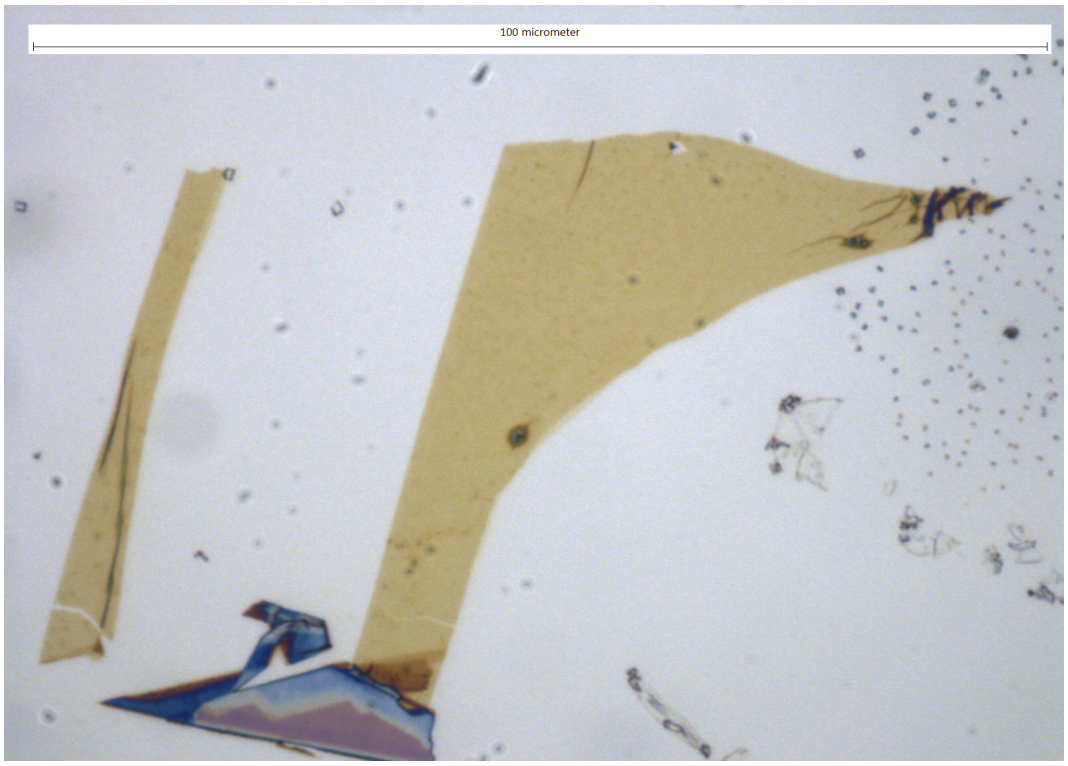

Figure 4.9: Optical image of MoS_2 flake 1

4.2 Sample Flakes: Optical and AFM images

MoS_2 and Sulphur containing transition metal dichalcogenides in general demonstrate strong affinity for gold. Molybdenum disulphide was chosen as the material to demonstrate working of SPSTM. Bulk MoS_2 was exfoliated on a Nitto tape and 50 nm of gold was deposited on a cleaned quartz slide. Small portion of a Nitto tape was chosen such that most of it is covered by MoS_2, it was then cut and isolated from rest of the tape. Nitto tape was then gently pressed on a fresh gold coated coated quatrz slide and was rubbed with a Q-tip to provide better contact, it was then slowly lifted off the slide. Primary identification of thin flakes was done optically and thickness of the flakes was then confirmed using AFM. Figure 4.9 is an optical image of MoS_2 flake after exfoliating on a gold coated slide. Figure 4.10 and Figure 4.2 are AFM scans of the same flake to measure its thickness. Figure 4.12 and Figure 4.13 are AFM scans of another MoS_2 flake.

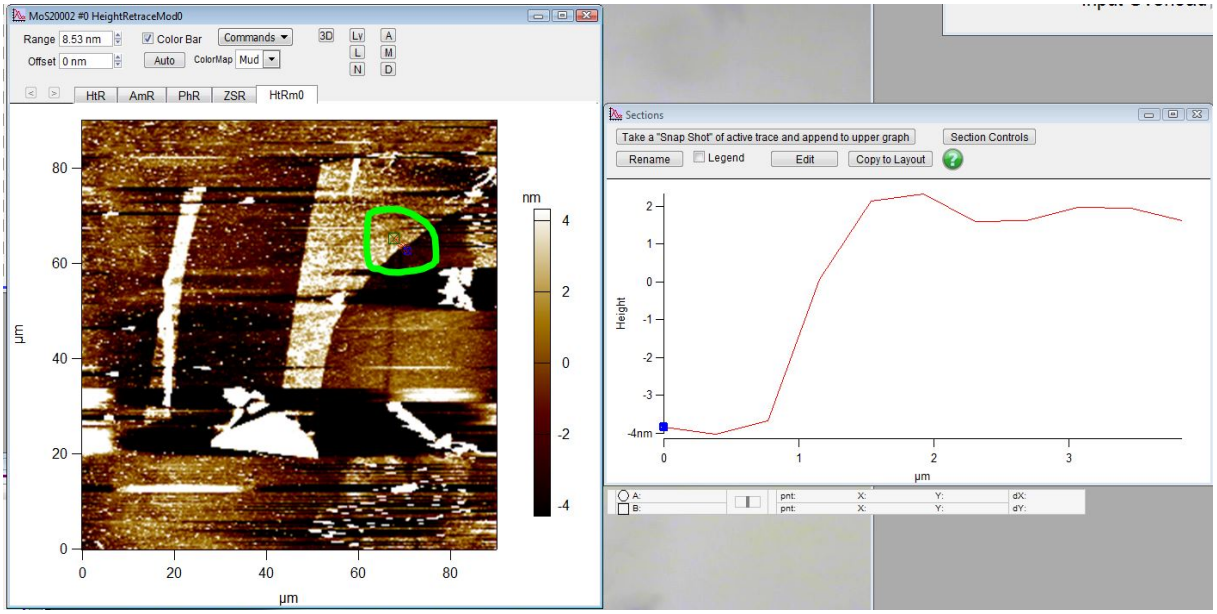

Figure 4.10: An AFM scan of MoS_2 flake 1: Area 1

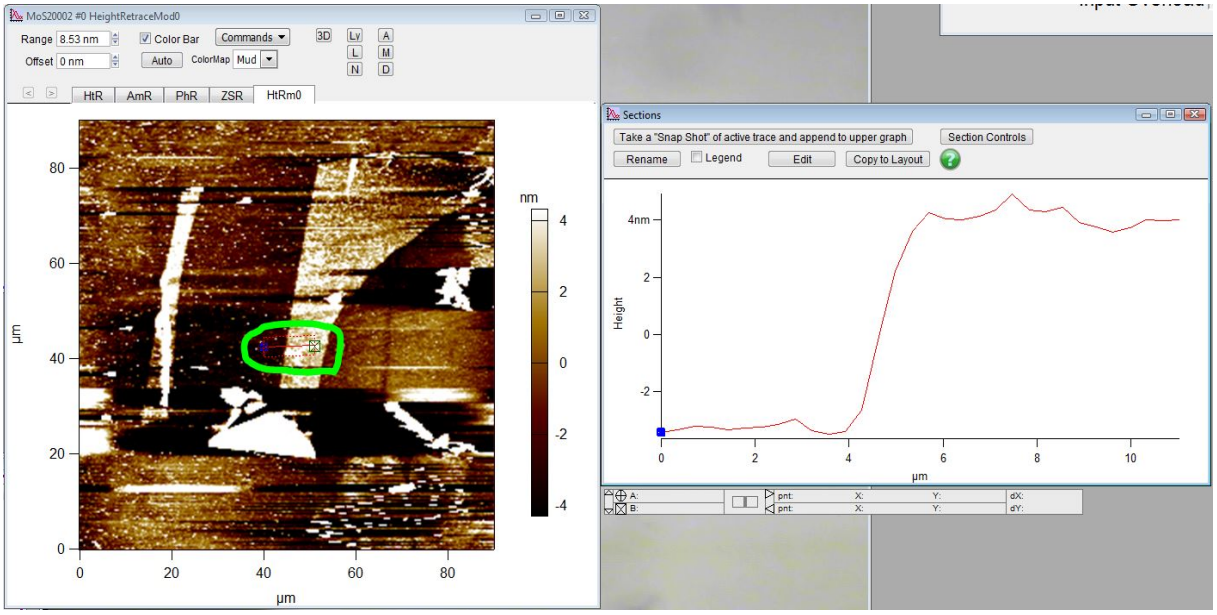

Figure 4.11: An AFM scan of MoS_2 flake 1: Area 2

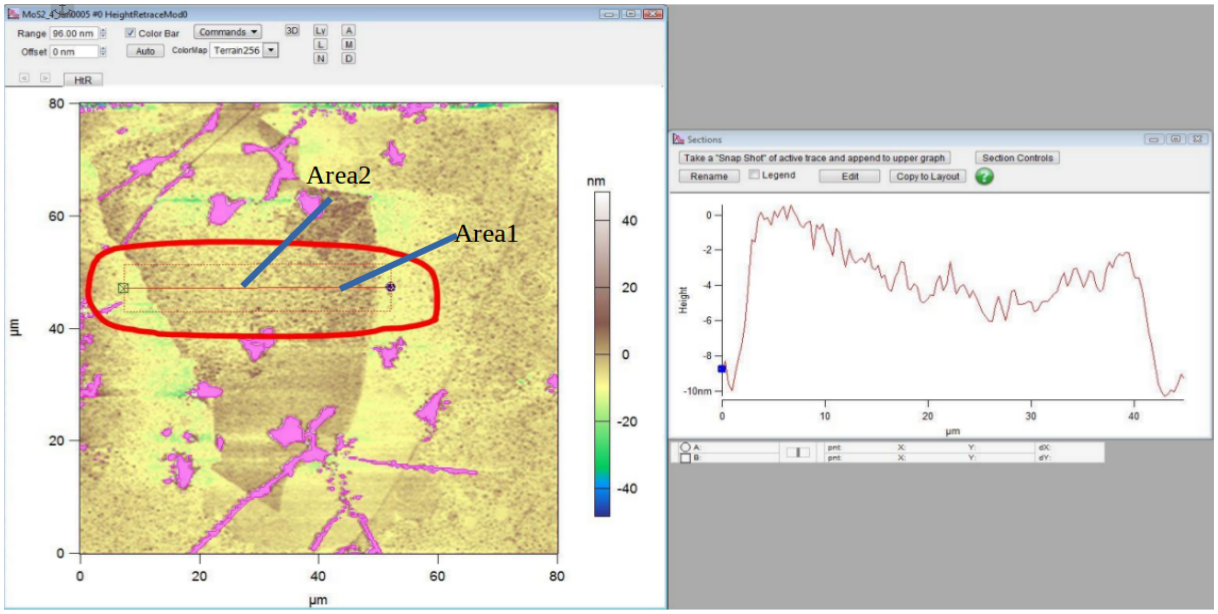

Figure 4.12: An AFM scan of MoS_2 flake 2: Area 1

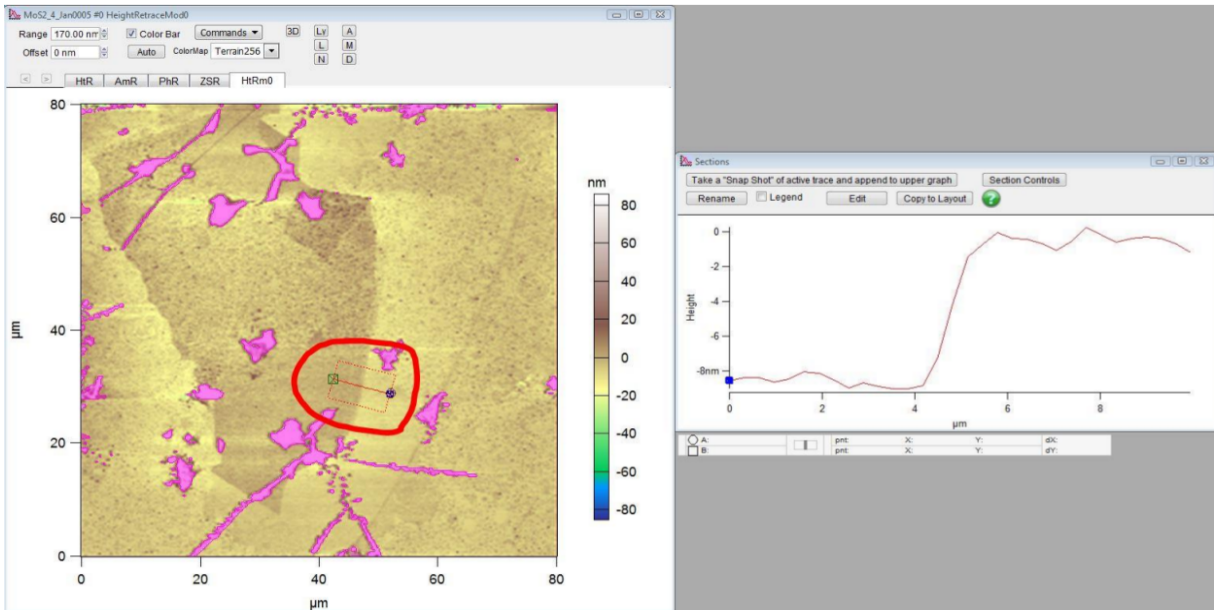

Figure 4.13: An AFM scan of MoS_2 flake 2: Area 2

4.3 Exponential Dependence of Probe Signal Intensity on Probe Height

The envisioned nanoscale imaging capability of SPSTM stems from the exponential decay of the evanescent field of plasmon modes, expected to manifest itself as the exponential decrease in the detected optical signal intensity with increasing probe height. Therefore, experimental verification of the exponential dependence of probe signal intensity on probe height is a crucial demonstration of the working principle of SPSTM.

A thin MoS_2 flake was peeled over SPSTM sample holder i.e. over 50 nm thick gold film on a quartz slide. SPSTM sample holder was then placed over cylindrical lens with index matching fluid between the flat cylindrical lens surface (top surface) and the uncoated surface of sample holder (bottom surface). Incident angle of the HeNe laser beam was then varied while laser beam spot remained fixed on the area of gold surface where sample is not present, incident angle was fixed when surface plasmons were excited i.e. when intensity of reflected beam minimized. At this point, nanoscope software was initiated in STS i(s) mode and plasmonic tip was brought closer to the beam spot on the gold surface. STS i(s) plot was saved when exponentially decaying signal was detected. Sample holder was then gently moved such that now MoS_2 flake covers the beam spot, at this point angle of incident was again adjusted so as to minimize the reflected beam, this indicated that surface plasmon angle (hence surface plasmons) was established for modified surface (i.e. for MoS_2 over gold film) and STS i(s) plots were recorded over two areas of different MoS_2 thicknesses as in Figure 4.12.

Figure 4.14 shows decaying surface plasmons signal in z direction measured by the plasmonic tip in SPSTM over three different areas of the sample holder i.e. over the gold surface and over the MoS_2 flake at two different thicknesses. Since full range of the signal (Figure 4.14) has non-exponential part at both the ends, Figure 4.15 shows natural log of the exponential portion in original data.

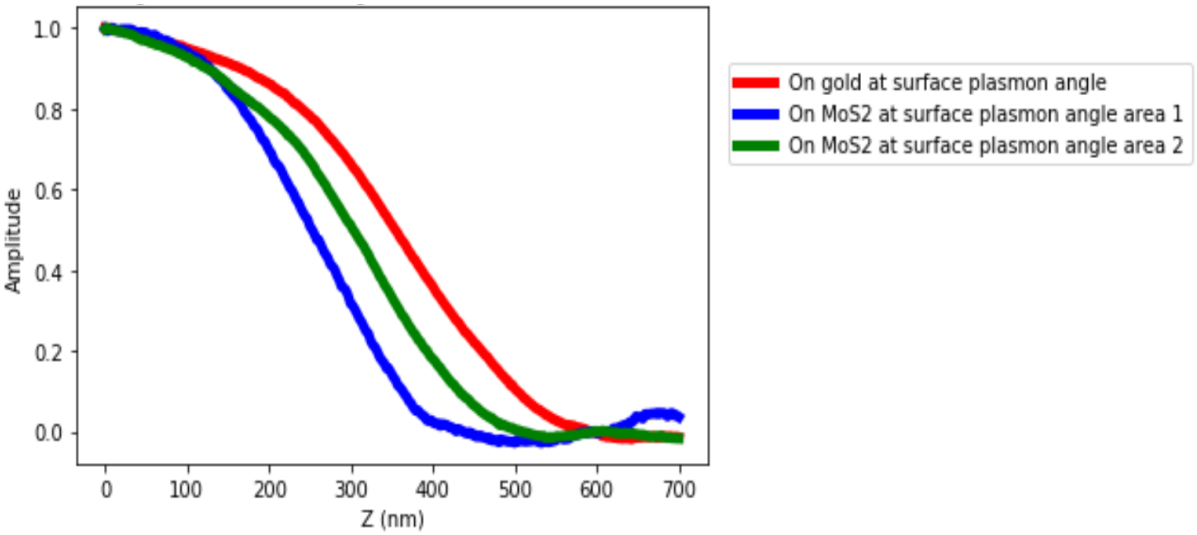

Figure 4.14: Decaying surface plasmons over modified surfaces: Modified by MoS_2

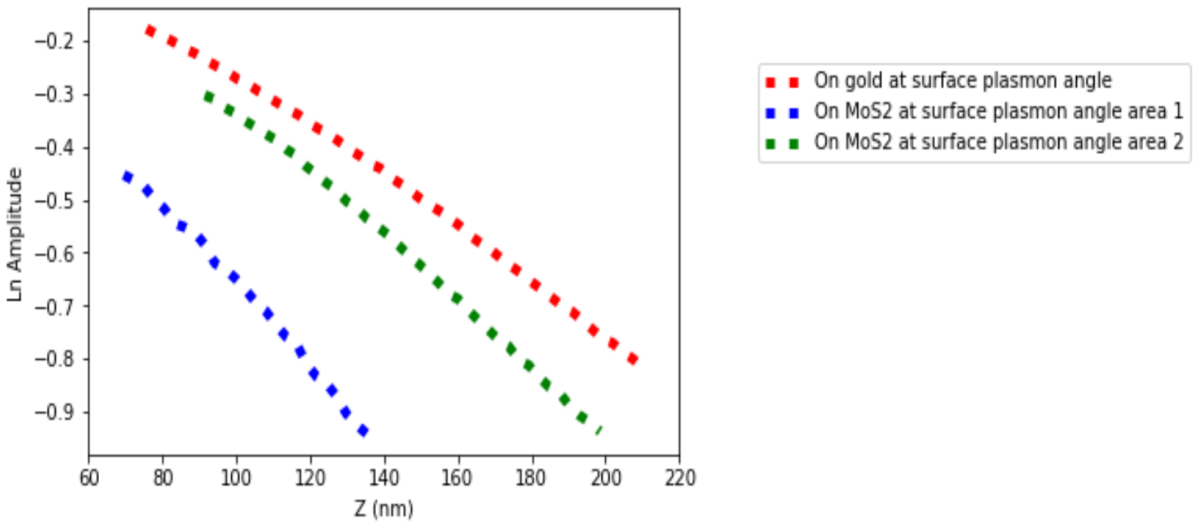

Figure 4.15: Log plot of exponential region

4.4 Discussion

The decay length plots demonstrates working principle of SPSTM. Further experiments needs to be done to explore SPSTM to its full potential e.g. imaging this flake with a sharper plasmonic tip will reveal optical properties and chemical structure, it can be used to study a sample with spatially varying chemical composition. An addition of a split fiber and a spectrophotometer will help to perform surface plasmon assisted spectroscopy at nanometer scale, an addition of a chemical map over a topographical image would be a unique feature of SPSTM as it is capable of performing spectroscopy and surface imaging simultaneously. It would also be interesting to examine more exotic samples e.g. examining optical properties of boundaries in heteroepitaxially grown two-dimensional materials. SPSTM can prove to be a versatile tool in surface science research of thin films.

Bibliography

[1] Allen, P. E. and Holberg, D. R. (1987). Cmos analog circuit design. *Oxford university press*. 53

[2] Aspnes, D. and Studna, A. (1975). High precision scanning ellipsometer. *Applied Optics, Optical Society of America*, 14(1). 8

[3] Betzig, E., Lewis, A., Harootunian, A., Isaacson, M., and Kratschmer, E. (1986). Near field scanning optical microscopy (nsom): development and biophysical applications. *Biophysical journal, Elsevier*, 49(1). 13

[4] Binnig, G., Quate, C. F., and Gerber, C. (1986). Atomic force microscope. *Physical review letters, APS,*, 56(9). 11

[5] Binnig, G. and Rohrer, H. (1987). Scanning tunneling microscopyfrom birth to adolescence. *Reviews of modern physics, APS*, 59(3). 11

[6] Binnig, G., Rohrer, H., Gerber, C., and Weibel, E. (1982). Surface studies by scanning tunneling microscopy. *Physical review letters, APS*, 49(1). 11

[7] Bloembergen, N. and Pershan, P. (1962). Light waves at the boundary of nonlinear media. *Physical review, APS*, 128(2). 23

[8] Braat, J. J. (1997). Abbe sine condition and related imaging conditions in geometrical optics. *Fifth International Topical Meeting on Education and Training in Optics, International Society for Optics and Photonics*, 3190(59). 1

[9] Cheong, W.-F., Prahl, S. A., and Welch, A. J. (1990). A review of the optical properties of biological tissues. *IEEE journal of quantum electronics, IEEE*, 26(12). 7

[10] de Fornel, F., Goudonnet, J.-P., Salomon, L., and Lesniewska, E. (1989). An evanescent field optical microscope. *Optical Storage and Scanning Technology, International Society for Optics and Photonics*, 1139. 13

[11] Decca, R., Drew, H., and Empson, K. (1997). Investigation of the electric-field distribution at the subwavelength aperture of a near-field scanning optical microscope. *Applied physics letters, AIP*, 70(15). 33

[12] Dornhaus, R., Benner, R. E., Chang, R. K., and Chabay, I. (1980). Surface plasmon contribution to sers. *Surface Science, Elsevier*, 101(3). 43

[13] E.Hecht (1987). Optics, 2nd ed. *Addison-Wesley*, California. 1

[14] Erts, D., Lohmus, A., Lohmus, R., and Olin, H. (2001). Instrumentation of stm and afm combined with transmission electron microscope. *Applied Physics A, Springer*, 72(1). 13

[15] Flaming, D. and Brown, K. (1982). Micropipette puller design: form of the heating filament and effects of filament width on tip length and diameter. *Journal of neuroscience methods, Elsevier*, 6(1). 40

[16] Gabor, D. (1948). A new microscopic principle. *Nature Publishing Group*. 5

[17] G.Binning, H. (1982). Scanning tunneling microscopy. *Helv.Phys.Acta.*, 55(726). 11

[18] Giallorenzi, T. G., Bucaro, J. A., Dandridge, A., Sigel, G. H., Cole, J. H., Rashleigh, S. C., and Priest, R. G. (1982). Optical fiber sensor technology. *IEEE transactions on microwave theory and techniques, IEEE*, 30(4). 39

[19] Griffith, J., Grigg, D., Vasile, M., Russell, P., and Fitzgerald, E. (1992). Scanning probe metrology. *Journal of Vacuum Science Technology A: Vacuum, Surfaces, and Films, AVS*, 10(4). 11

[20] H. non, S. and Meunier, J. (1991). Microscope at the brewster angle: Direct observation of first-order phase transitions in monolayers. *Review of Scientific Instruments*, 62(4). 2

[21] Hartley, W. G. (1993). The light microscope: its use and development. *Senecio*. 2

[22] Hawkes, P. W. and Spence, J. C. (2008). Science of microscopy. *Springer Science Media*. 2

[23] Heavens, O. S. (1991). Optical properties of thin solid films. *Courier Corporation*. 7

[24] Homola, J., Yee, S. S., and Gauglitz, G. (1999). Surface plasmon resonance sensors. *Sensors and Actuators B: Chemical, Elsevier*, 54. 34

[25] Hutter, E. and Fendler, J. H. (2004). Exploitation of localized surface plasmon resonance. *Advanced materials, Wiley Online Library*, 16(19). 42

[26] Newton, I. (1952). Opticks. *Dover*, New York. 2

[27] Nicholls, E. A. G. (1972). Super resolution aperture scanning microscope. *Nature*, 237(512). 9

[28] P.J. Leqrgans, A.F. Turner, R. R. (1986). Frustrated total internal reflection: A demonstration and review. *American Journal of Phys.*, 54(7). 15

[29] Pohl, D. W. and Courjon, D. (2012). Near field optics. *Springer Science Media*, 242. 11

[30] Pritchard, A. and Goring, C. (1840). Microscopic illustrations of living objects: Most eligible methods of constructing microscopes, and instructions for using them. *Whittaker*. 2

[31] Querry, M. R. (1969). Direct solution of the generalized fresnel reflectance equations. *Josa, Optical Society of America,*, 59(7). 25

[32] R.C. Reddick, R. W. and Ferrell, T. (1989). A new form of scanning optical microscopy. *Phys Rev B*, 39(767). 13

[33] Rossnagel, S. and Hopwood, J. (1994). Metal ion deposition from ionized mangetron sputtering discharge. *Journal of Vacuum Science Technology B: Microelectronics and Nanometer Structures Processing, Measurement, and Phenomena, AVS*, 12(1). 59

[34] Rothen, A. (1945). The ellipsometer, an apparatus to measure thicknesses of thin surface films. *Review of Scientific Instruments, AIP*, 16(2). 8

[35] Seiler, H. (1983). Secondary electron emission in the scanning electron microscope. *Journal of Applied Physics*, 54(11). 5

[36] Sheppard, C. and Mao, X. (1988). Confocal microscopes with slit apertures. *Journal of Modern Optics*, 35(7). 3

[37] Stroscio, J. A. and Kaiser, W. J. (1993). Scanning tunneling microscopy. *Academic Press*, 27. 9

[38] Synge, E. (1928). Phil. mag. *6*, 356. 9

[39] Van Zuylen, J. (1981). The microscopes of antoni van leeuwenhoek. *Journal of microscopy*, Wiley Online Library(121-3). 1

[40] Velicky, M., Donnelly, G. E., Hendren, W. R., McFarland, S., Scullion, D., DeBenedetti, W. J., Correa, G. C., Han, Y., Wain, A. J., Hines, M. A., et al. (2018). Mechanism of gold-assisted exfoliation of centimeter-sized transition-metal dichalcogenide monolayers. *CS nano, ACS Publications*, 12(10). 61

[41] Weber, W. H. and Ford, G. (1981). Optical electric-field enhancement at a metal surface arising from surface-plasmon excitation. *Optics letters, Optical Society of America,*, 6(3). 33

[42] Wickramasinghe, H. K. (1989). Scanned-probe microscopes. *Scientific American, JSTOR,*, 261(4). 9

[43] Wiesendanger, R. and Roland, W. (1994). Scanning probe microscopy and spectroscopy: methods and applications. *Cambridge university press*. 9

[Wikipedia] Wikipedia. Helium-neon laser. 42

[45] Williams, D. B. and Carter, C. B. (1996). Transmission electron microscopy. *Springer*, 3(17). 5

[46] Yee, K. (1966). Numerical solution of initial boundary value problems involving maxwell's equations in isotropic media. *IEEE Transactions on antennas and propagation*, 14(3). 22

[47] Zhang, Q., Wang, H., and Cross, L. (1993). Piezoelectric tubes and tubular composites for actuator and sensor applications. *Journal of materials science, Springer*, 28(14). 45

[48] Zhu, S., Yu, A., Hawley, D., and Roy, R. (1986). Frustrated total internal reflection: a demonstration and review. *American Journal of Physics, AAPT*, 54(7). 15

Appendices

Appendix A

Tip Fabrication by Meniscus Etching

Fiber etching to produce sharp tips of varying geometries in terms of taper length, cone angle is an area of study in its own. It is possible to produce variety of tip shapes by etching core of fiber with Hydrofluoric Acid (HF) solution under an organic protective layer Figure A.2. Several factors like etching rate, meniscus distortion, etching time etc plays an important role in final geometry of tip.

Figure A.1 was used for HF meniscus etching. HF was collected in a plastic container kept on manual vertically moving stage, an optical fiber with cladding removed was held by a tip with core submerged in HF. It is important to keep full setup on vibration free environment and vibration damping cushions should be used. After keeping the fiber dipped for over an hour, stage should be lowered slowly and optical fiber should be examined under microscope.

NOTE: HF is a powerful contact poison and is highly corrosive. Fluoride ion readily penetrates the skin, causing destruction of deep tissue layers, including bone. If HF is not rapidly neutralized, tissue destruction may continue for days and result in limb loss or death



Figure A.1: HF etching setup

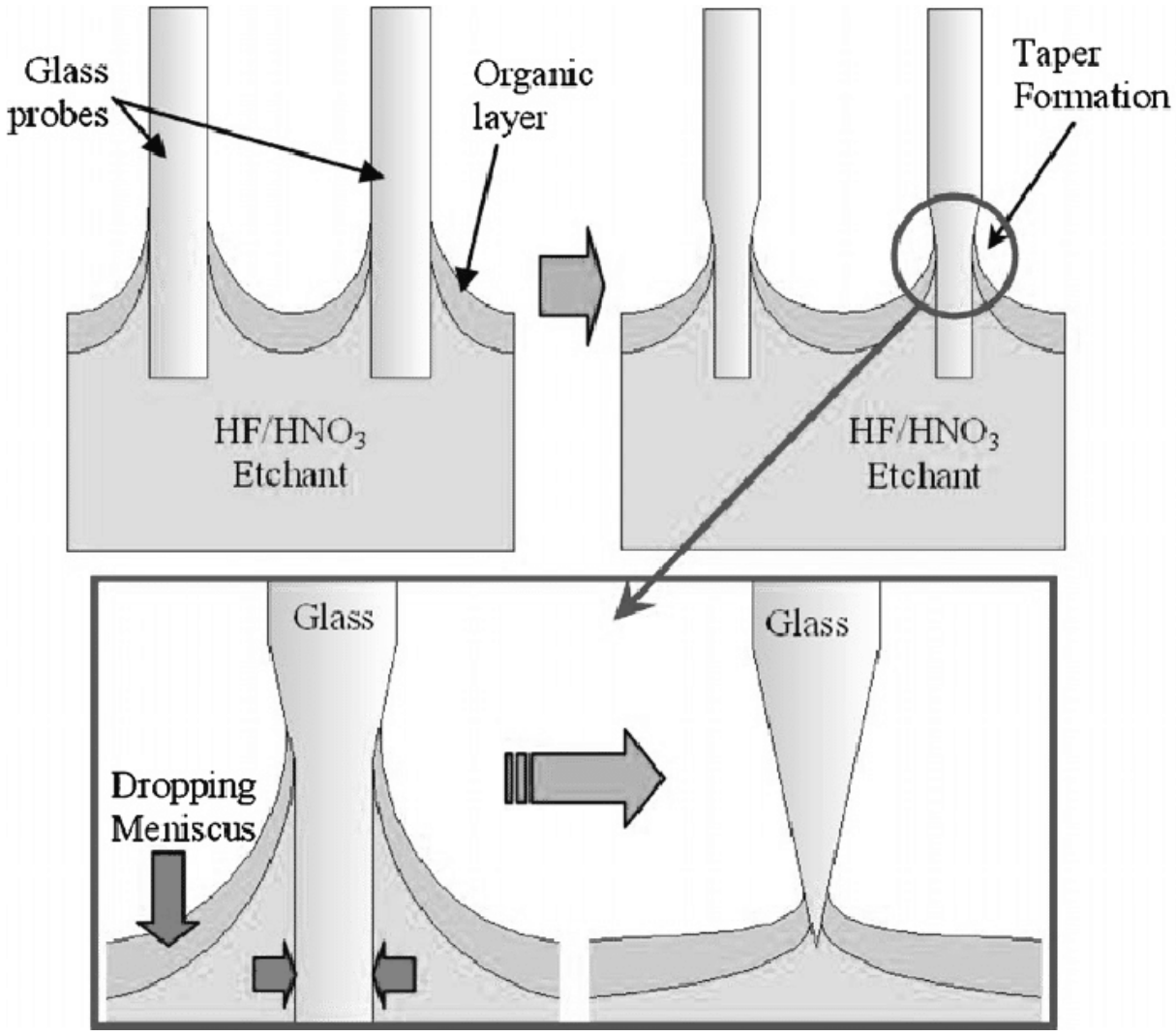

Figure A.2: Meniscus etching. Source: www.researchgate.net

Appendix B

PMT Casing

Photomultiplier tubes are several orders of magnitude more sensitive than any other detector, care must be taken to eliminate stray light. Also, PMT have very low noise levels and current generated can be amplified to detect individual photons. Hamamtsu IP-128 PMT was used in this setup, this tube was enclosed in a metal casing Figure B.1 whose interior was coated with black fiber sheet which absorbs any scattered light within the case, it has feed-though ports for optical fiber and electrical connections. Optical fiber holder was aligned such that optical fiber end was right in front of PMT photocathode/dynodes. PMT's response to light depends on it's operating voltage hence, it should always be operated at right voltage which in this case is 400 Volts.



Figure B.1: PMT casing



Figure B.2: PMT power supply socket

Appendix C

Nanoscope Pin Connections

Nanoscope controller has two ports that acts as an interface with the computer Figure C.3 and with the microscope head Figure C.1, Figure C.2. Interface for computer is located at the back panel and interface for the miscroscope head is on the front panel as shown in Figure C.1, C.2 and C.3. For the purpose of operating SPSTM head, only piezo tubes and signal from PMT needs to be connected to NS controller. Since SPSTM is a modified version of STM not all 37 pins of NS controller are used. Nonoscope only needs to power piezo tubes and should be able to collect analog signal from current amplifier. These connections were made using Figure C.4 which was provided by Mr. Smith from ASMicro.

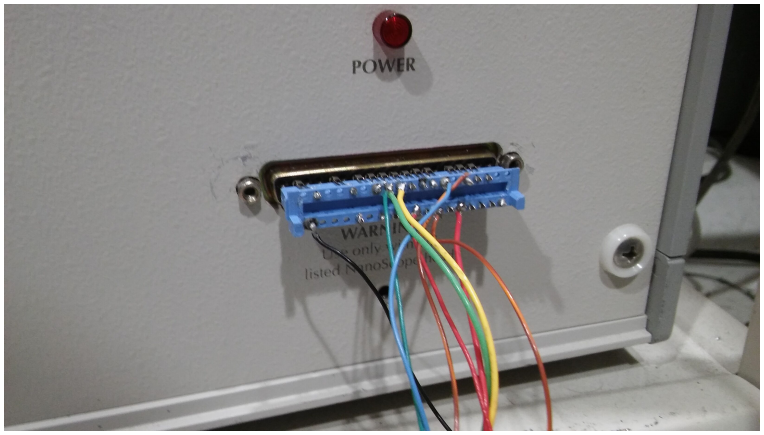

Figure C.1: 37 pin connector on Nanoscope controller

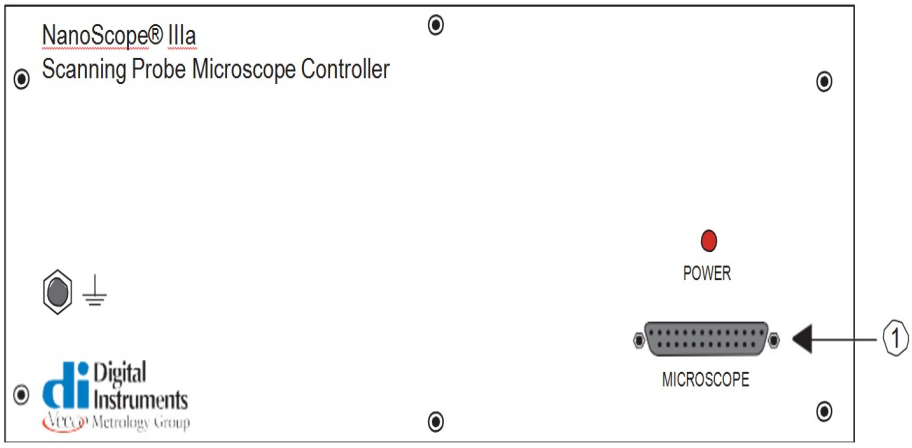

Figure C.2: Nanoscope front panel: pin connections for microscope

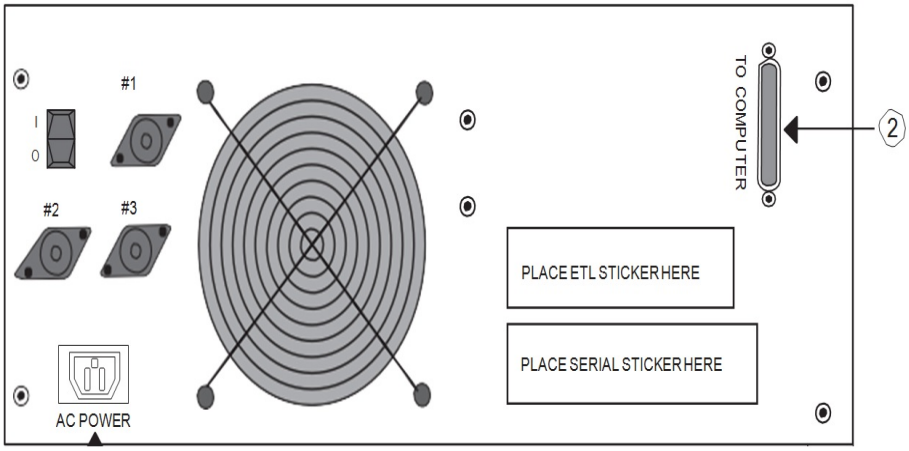

Figure C.3: Nanoscope rear panel: slot for computer cable

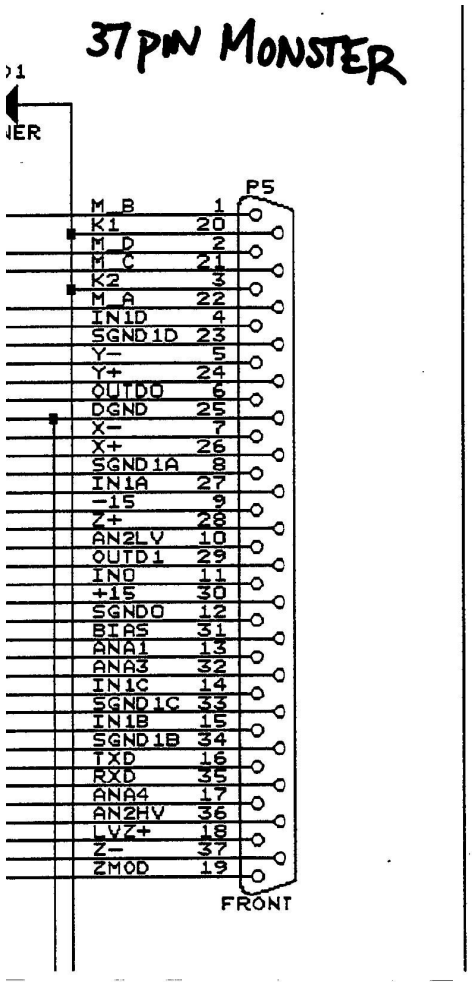

Figure C.4: 37 pin connector: pin labels

O-ring type center macor acts as an interface between power cords from Nanoscope head and power cords from piezotubes. Metallic pins in Figure C.5 embedded in center macor are connected on both ends by cords from NS controller and cords from piezo tubes. Figure C.5 is top view of cords from NS controller being soldered to metallic pins embedded in center macor.

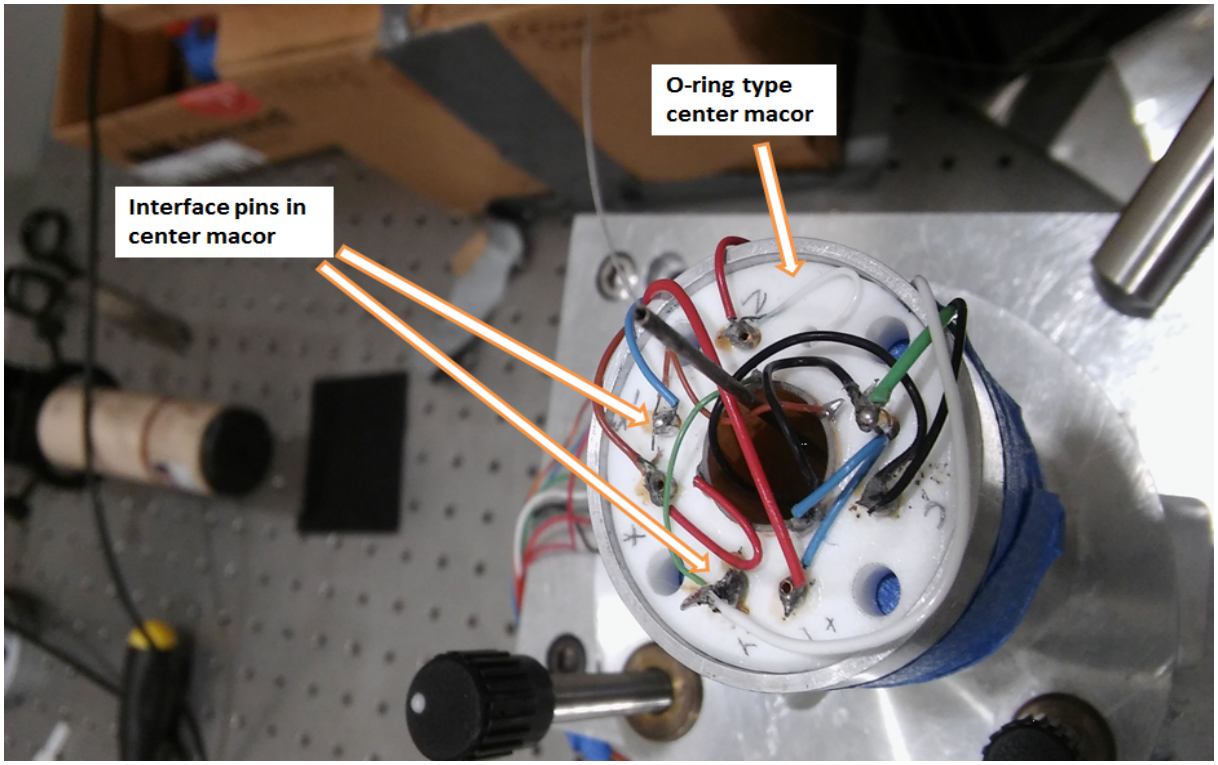

Figure C.5: Top view of center macor and interface pins embedded within

Appendix D

Optical Fiber Holder

Optical fibers needs to be metal coated after cladding has been removed by the fiber stripper. A customized holder Figure D.1 was built to load fibers in chamber. It consists of two microscope glass slides held by clips. Kepton tape is first applied on glass slide and optical fibers are loaded on it, second glass slide holds fibers firmly against the first slide, both slides are held together by clips as shown in the image below. After fibers were coated, clips are removed followed by second glass slide. Coated fibers are then pulled off the kepton tape one by one using tweezers. Microscope glass slides and clips must be cleaned with acetone and IPA to avoid contamination of vacuum chamber.

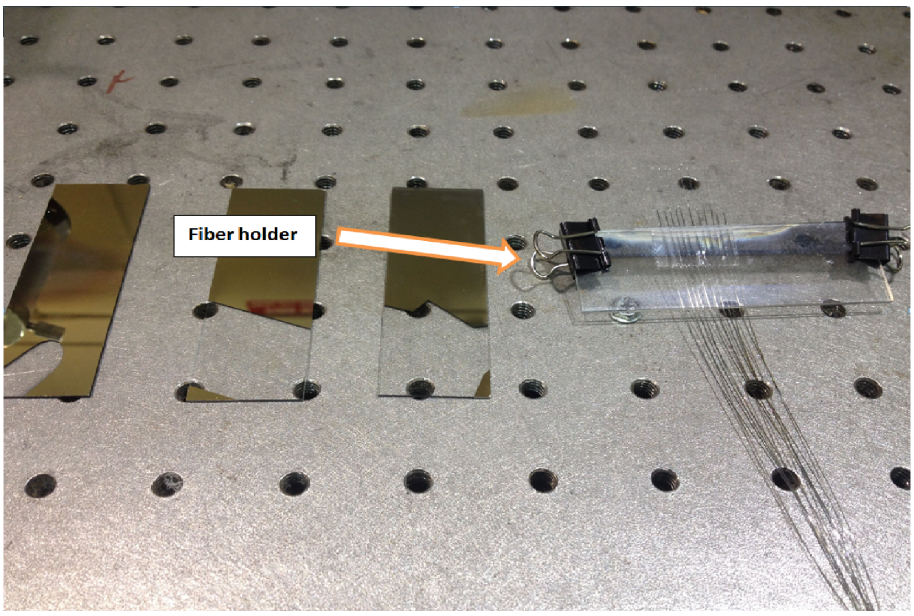

Figure D.1: Fiber holder for coating

Appendix E

Nanoscope Cards

Nanoscope controller houses two cards Figure E.1, Figure E.2 that provides power to xy piezo tubes and z piezo tubes. There are two op-amps Figure E.3 that drives piezo tubes in each direction. Proper electrical insulation of connections terminating on contact pins in scanner head must be ensured at all times to ensure safe working these op-amps. These are low current and high voltage power sources.

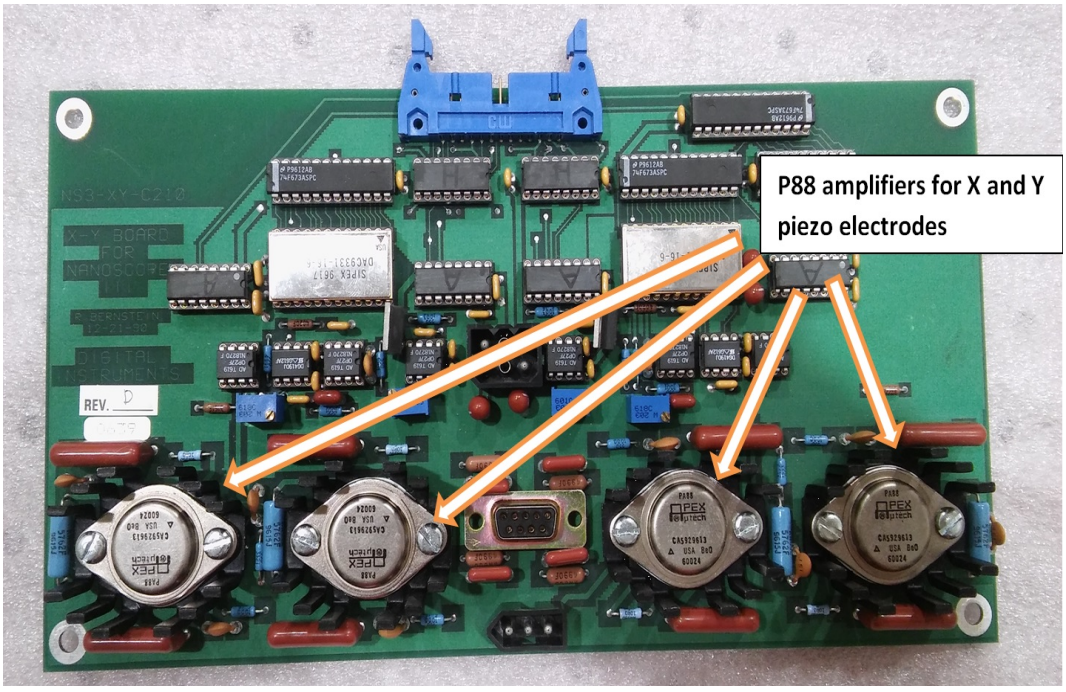

Figure E.1: xy cards

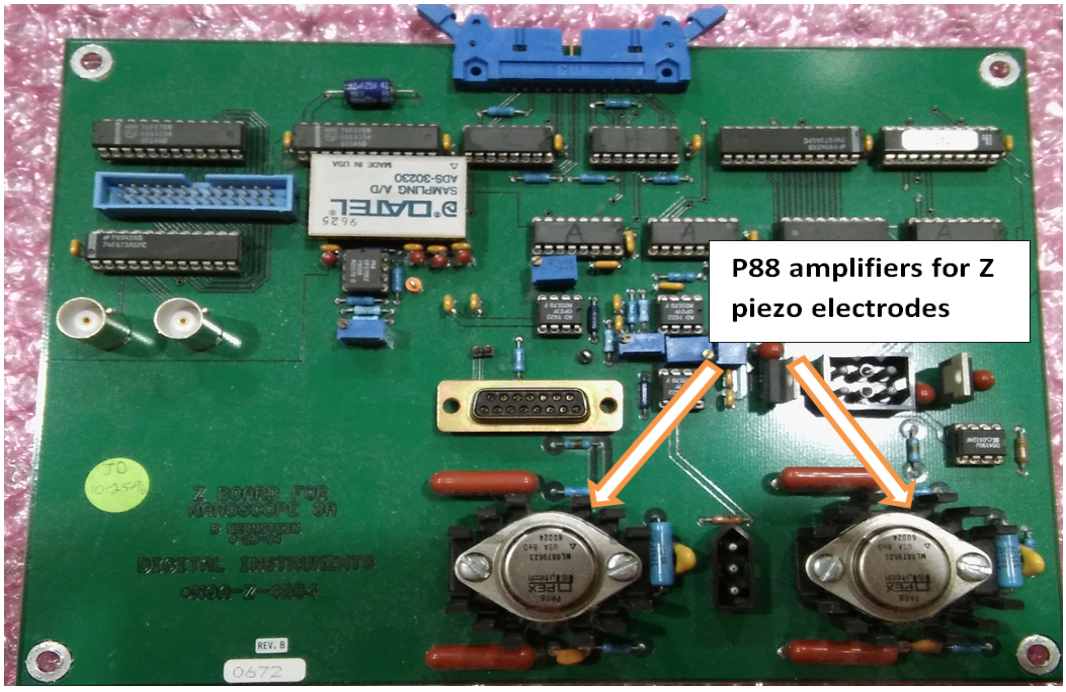

Figure E.2: z card

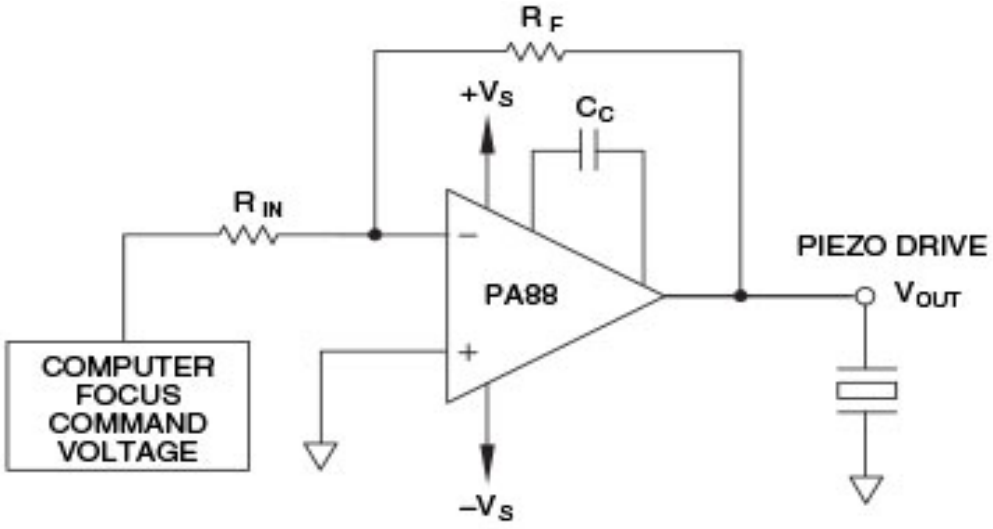

Figure E.3: P88 high voltage low current power amplifier in NS xy and z cards

Appendix F

Scanner Head Macor Drawings

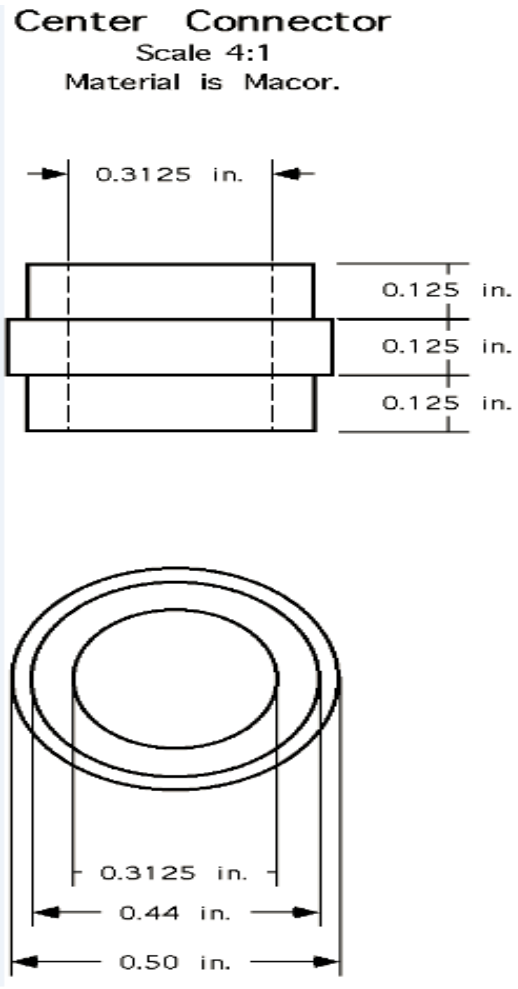

Figure F.1: Center macor

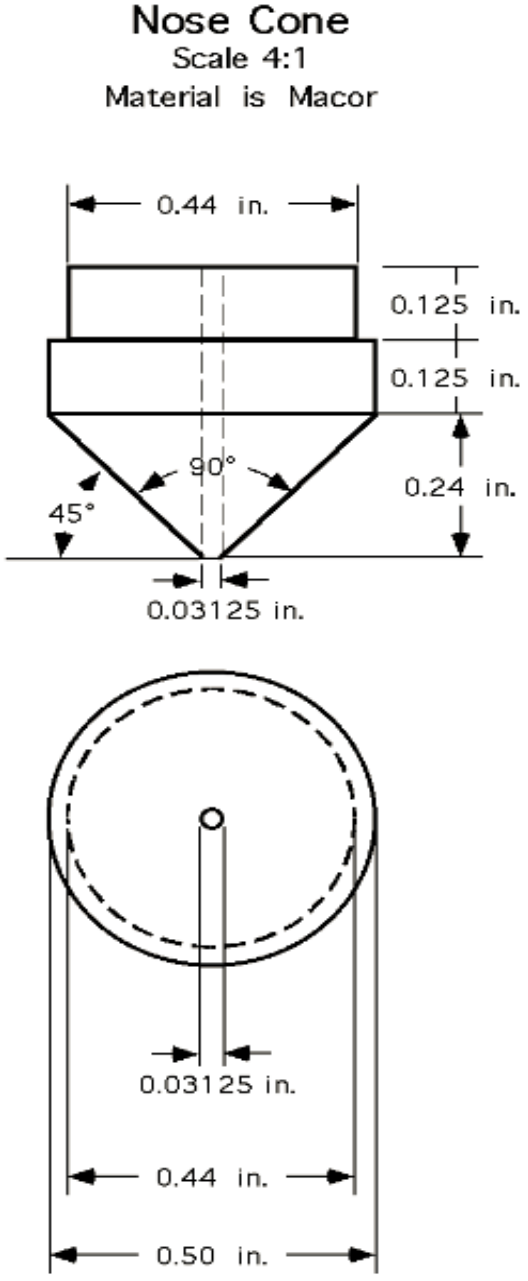

Figure F.2: Nose cone

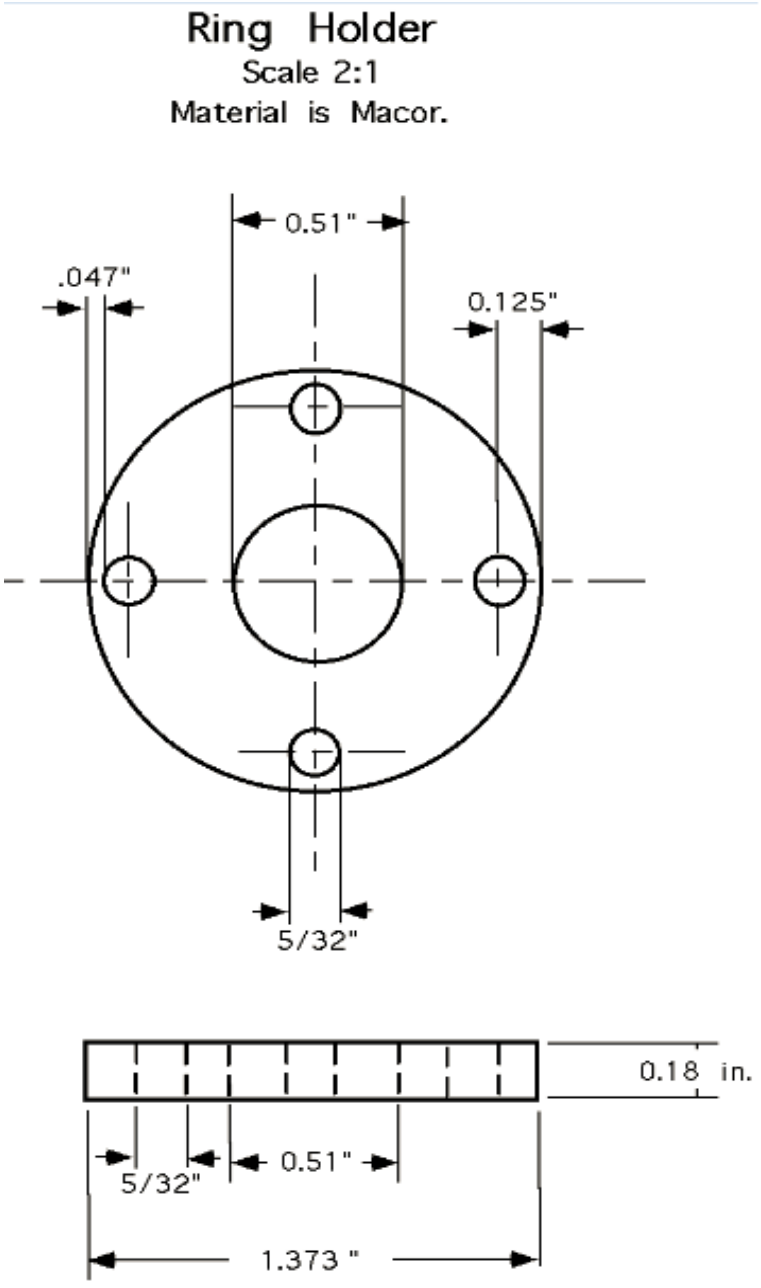

Figure F.3: Ring holder

Vita

Vineet Khullar hails from a small town in North West of India. Vineet joined PhD at department of Electrical Engineering and Computer Science (EECS) at University of Tennessee (UT), Knoxville in 2015. He earned Masters in Physics from UT in 2014.

Vineet worked closely with Dr. Thomas Ferrell (from Physics department) in field of optics and engineering physics. He had opportunities to work with collaborators in field of crystal growth, 2D materials and near-field optics.